ULTRAVIOLET ABSORPTION CROSS-SECTIONS FOR ATMOSPHERIC GASES

by

G.N. Haddad B.Sc. (Hons.)
Department of Physics

A thesis submitted for the degree of
Doctor of Philosophy
in the
University of Adelaide
May, 1967

CONTENTS

SUMMARY

This thesis describes the measurement of total absorption cross sections for molecular oxygen and molecular hydrogen in various regions of the ultraviolet spectrum.

Total absorption cross sections for molecular oxygen have been measured for the region 1050-2350Å with a spectral resolution of approximately 1Å. The dispersing instrument was a ½ metre Seya-Namioka monochromator fitted with a gas discharge tube as a light source. The discharge tube was operated with either hydrogen, giving the characteristic spectrum of many lines, or with argon, which emits a continuous spectrum for part of this region. A number of detectors and a variety of cell lengths and gas pressures were used to cover the entire spectral range.

The region containing the Schumann-Runge bands (1750-2000Å) has been investigated thoroughly. In this region the rotational lines are too narrow to be completely resolved by the instrument leading to an observed cross section which does not obey Beer's law. These results have been analysed using simple theoretical models. The "window" region, the Schumann-Runge

continuum and the region containing the Herzberg I continuum (2000-2350Å) have also been investigated. Particular attention has been given to absorption at wavelengths corresponding to those of strong solar lines, and in particular, to the window in the absorption spectrum falling at the wavelength of the intense solar Lyman-α line.

The results for molecular oxygen are discussed with reference to composition studies of the terrestrial atmosphere which use observations of the solar spectrum from high altitude rockets.

Accurate absolute absorption cross sections have been measured for molecular hydrogen in the region 1060-1130Å using, as the dispersing instrument, a 1 metre near normal incidence monochromator with a best resolution of 0.1Å. The instrument was fitted with a high pressure argon light source and the installation of the instrument and associated differential pumping equipment is described. Detection and data handling techniques have been refined for this experiment in order to measure the relatively low integrated cross sections to the required accuracy; this equipment is described.

The absorption cross sections of the individual

rotational lines in molecular hydrogen have been measured and a curve of growth analysis, (described in terms of various models) has been used to determine absolute integrated cross sections for rotational lines in the first four vibrational bands of the Lyman series.

The simplest method of detecting molecular hydrogen in interstellar space is to detect absorption in the Lyman bands, particularly in the region from 950Å to 1130Å. The present data are used to compute the expected absorption by interstellar molecular hydrogen under a variety of assumptions.

PREFACE

This thesis contains no material which has been accepted for the award of any other degree or diploma in any University. To the best of the author's knowledge and belief it contains no material previously published or written by another person, except where due reference is made in the text.

G. N. Haddad
May, 1967

ACKNOWLEDGEMENTS

The work on molecular hydrogen was done in association with Mr. A.J.D. Farmer and the absorption measurements on molecular oxygen between 1050 and 1250Å were made with Mr. A.J. Blake.

The author would like to thank Dr. K.H. Lokan most sincerely for his enthusiasm, help and encouragement during the experiments on molecular hydrogen and also for his many helpful suggestions during the writing of this thesis.

Thanks are also due to Mr. E.J. Connock and the staff of the Physics Department workshop for their assistance in building the apparatus involved in this work.

Finally the author would like to thank his supervisor, Professor J.H. Carver, for his help and encouragement during this work.

CHAPTER I

Introduction

The experimental study of the absorption of vacuum ultraviolet radiation by gases is reviewed and it is pointed out that these studies have led, in particular, to investigations of the composition of the upper atmosphere.

There have been many determinations of the absolute wavelength of absorption lines but relatively few measurements of absolute absorption coefficients.

This thesis presents absolute absorption coefficients for molecular oxygen from 1050-2350Å and for molecular hydrogen from 1060-1130Å.

The relevance of these measurements to the terrestrial atmosphere and to the interstellar medium is discussed.

1.1 Experimental vacuum ultraviolet spectroscopy

One of the earliest measurements of absorption by gases in the vacuum ultraviolet region was made by Schumann (Lyman, 1928) who showed that strong absorption in air set in at wavelengths less than 1850Å. In 1901 Kreusler (Kreusler, 1901) made an investigation of the

absorption of air at 1860Å and 1930Å. Kreusler (1901) also followed the lead of Schumann (Lyman, 1928) in his early work on some individual gases, namely molecular oxygen and molecular nitrogen. Lyman (1908) made valuable contributions to early work on both these gases and included measurements on ozone, helium, hydrogen and water vapour. Many other gases including nitrous oxide, nitric oxide, nitrogen peroxide, ammonia and methane were later studied by Leifson (1926).

Most of the measurements during this period (Lyman, 1928) were made with either fluorite optics or grating instruments; a variety of sources was employed to cover the range 140-3000Å. These early results obtained from 1896 to 1928 were largely qualitative surveys but led to an understanding of absorption in the terrestrial atmosphere and established the range of wavelengths for which each constituent gas was important.

The technology of vacuum ultraviolet spectroscopy developed rapidly from this time with advances in the efficiency of gratings, better vacuum systems, more intense continuous light sources and advances in photo-electric methods for detecting ultraviolet radiation.

A review of the work in this field up to 1957 has been given by Watanabe (1958). Over the period from

1928 to 1957 many gases were studied in great detail and the features in the absorption spectra of most of them understood in terms of the energy levels of the molecules. Molecular oxygen, molecular nitrogen, nitric oxide, ozone, water vapour, nitrous oxide, carbon dioxide, methane, ammonia, carbon monoxide, hydrogen and the rare gases are some species which have been studied and the absorption cross-sections which have been measured for each of them are given in the review by Watanabe (1958).

Most investigators have used vacuum spectrographs and photographic photometry. Preston (1940) and Watanabe et al (1953) improved the experimental techniques by using photoelectric photometers for various wavelength regions. Curtis (1954) and others (Aboud et al 1955) have extended the range of wavelengths with photoelectric techniques down to 100Å. Hinteregger (1953) has developed a double beam type of photoelectric detector.

Later reviews of the absorption spectroscopy of gases have been given by Weissler (1959), Schultz et al (1962) and Cook and Ching (1965).

There have been many high dispersion measurements (e.g. Tilfordetal, 1965; Herzberg and Howe, 1959; Monfils, 1965) of the energies of absorption lines for

some of the gases mentioned above which have enabled the molecular constants to be calculated for these molecules. There have, however, been relatively few sound measurements of absolute absorption coefficients which are independent of both the instrument used and the optical path length of the absorbing gas. This is because it is difficult to measure absolute absorption coefficients with an instrument limited to a finite resolution; in this case the measured absorption coefficient generally depends on the layer thickness of the absorbing gas.

This thesis gives the results of an investigation of the methods of determining absolute absorption coefficients when using an instrument limited in resolution. The absorption over the spectral line is presented as a function of layer thickness in a manner which is independent of the instrument resolution and permits evaluation of the absorption cross-section absolutely.

Determinations of the absorption cross sections for the atmospheric gases, besides giving valuable information about the molecules themselves (see section 1.2.1), can be used to interpret measurements of the attenuation of the solar flux in the atmosphere, to give

number densities of certain constituent gases as a function of height (see section 1.4). One of the species which is an important absorber in the atmosphere is molecular oxygen and the determination of its absorption cross-section is important from this aspect.

1.2 Molecular Spectroscopy

1.2.1 Oscillator Strengths

Frequently experimental data are expressed in terms of the oscillator strength f^{nm} which represents the ratio of the quantum theoretical to the classical value of the transition strength where the classical value is calculated on the assumption of a single oscillating electron of frequency C ν_{nm}. That is, the oscillator strength is defined by the relation (Herzberg, 1950)

$$f^{nm} = \frac{8\pi^2 \mu C \nu_{nm}}{3he^2} |\underline{R}^{nm}|^2$$

where μ and e are the mass and charge of an electron and

$$R^{nm} = \int \psi_n^* \underline{r} \psi_m \, d\tau$$

is the matrix element for the transition between the two states m (initial) and n (final).

The transition probabilities per unit time for absorption between two such states can be related to the

absorption coefficient k_ν which is defined by the relation

$$I_\nu = I_\nu^o \; e^{-k_\nu \Delta x}$$

where I_ν and I_ν^o are the intensities of the radiation incident on and transmitted through a column of gas of length Δx, with the gas at 0°C and 1 atmosphere pressure. It can be shown that (Herzberg, 1950)

$$\int k_\nu d\nu = \frac{N_m \; 8\pi^3 \; \nu_{nm}}{3hc} \; |\underline{R}^{nm}|^2$$

where $\int k_\nu d\nu$ is the integrated absorption coefficient over the line N_m is the number of particles in the lower state and ν_{nm} is the wave number of the transition.
Therefore we have

$$f^{nm} = \frac{\mu c^2}{\pi e^2 N_m} \int k_\nu d\nu \; .$$

Oscillator strengths for atoms or molecules obey the Thomas-Reiche-Kuhn sum rule according to which the sum of the oscillator strengths for all possible transitions from one initial state is numerically equal to the number of electrons in the system (Bethe and Salpeter, 1957). Sum rules for higher order multipole transitions also exist (Dalgarno and Lynn, 1957).

1.2.2 Quantum mechanics of molecules

In order to make calculations of the oscillator strengths for molecular transitions the wave functions for the system must be known. Unfortunately wave functions for molecular systems cannot be calculated exactly and one is forced to use an approximation of some kind.

The simplifying feature which is the basis of all molecular approximations is the large ratio of nuclear mass to electron mass. Born and Oppenheimer (1927) were able to show that an approximate solution of the complete wave equation for a molecule can be obtained by first solving the wave equation for the electrons alone with the nuclei regarded as fixed, and then solving a wave equation for the nuclei alone, in which a characteristic energy value of the electronic wave equation, regarded as a function of internuclear distance, was used as a potential function. The nuclear motions may then be classified into translations and rotations of the "rigid" equilibrium arrangement and internal vibrations of the nuclei about equilibrium. Thus the molecular energy levels can be classified into electronic, vibrational and rotational types.

The complete wave equation for a molecule may be written in the form

$$\left(- \frac{\hbar^2}{2m} \sum_{i=1}^{n} \nabla_i^2 - \sum_{j=1}^{N} \frac{\hbar^2}{2M_j} \nabla_j^2 + V \right) \psi = E\psi$$

where there are n electrons and N nuclei and V is the sum of the electrostatic interactions between all pairs of particles. The principle result of Born and Oppenheimer's treatment, then, is that an approximate solution of this wave equation can be written as

$$\psi(\underline{r}_i, \underline{R}_j) = \psi_e(\underline{r}_i, \underline{R}_j) \cdot \psi_{vr}(\underline{R}_j).$$

The functions $\psi_e(\underline{r}_i, \underline{R}_j)$ are the electronic wave functions depending on the electronic coordinates $\underline{r}_i$ and on the nuclear coordinates $\underline{R}_j$. These functions are solutions of the wave equation for the electrons alone - namely

$$\left[- \frac{\hbar^2}{2m} \sum_{i=1}^{n} \nabla_i^2 + V_e(\underline{r}_i, \underline{R}_j) \right] \psi_e(\underline{r}_i, \underline{R}_j) = E^{el}(\underline{R}_j) \cdot \psi_e(\underline{r}_i, \underline{R}_j).$$

The potential function V_e depends on the internuclear coordinates so that ψ_e and E^{el} are also functions of the values selected for the internuclear coordinates

$\underline{R}_j$. If this wave equation is solved for all possible configurations of the nuclei to give the electronic energy $E^{el}(\underline{R}_j)$ as a function of the nuclear coordinates $\underline{R}_j$, the nuclear wave functions $\psi_{vr}(\underline{R}_j)$ can be obtained. Born and Oppenheimer have shown that the nuclear wave equation is

$$\left[- \Sigma \frac{\hbar^2}{2M_j} \nabla_j^2 + E^{el}(\underline{R}_j) \right] \psi_{vr}(\underline{R}_j) = E.\psi_{vr}(\underline{R}_j)$$

where the values of E are the characteristic energy values for the entire molecule. This procedure provides a good approximation (Born and Oppenheimer, 1927) at least for the lower vibrational and rotational excited states. If greater accuracy is required it is necessary to consider the coupling between electronic and nuclear motions (e.g. Wolniewicz, 1966).

For the special case of diatomic molecules it has been found that the potential energy functions for the lowest electronic states can be represented quite accurately by a function (Morse, 1929) of the form

$$E^{el}(r) = D \{1 - e^{-a(r-r_e)}\}^2$$

where r is the internuclear distance

r_e is the equilibrium internuclear distance

and D and a are adjustable parameters.

The so-called Morse potential is shown in figure 1.1 together with the curve for the ground state of the hydrogen molecule drawn according to Rydberg's data (Herzberg, 1950).

1.3 Diatomic Molecules

1.3.1 Resolution of the total eigenfunction

The eigenfunction ψ_{vr} of a vibrating rotator can, in first approximation, be expressed as the product (Schiff, 1955)

$$\frac{1}{r} \psi_v \psi_r$$

where $\frac{1}{r} \psi_v$ is the vibrational eigenfunction of a linear oscillator depending only on the change of internuclear distance $(r-r_e)$ and ψ_r is the rotational eigenfunction depending only on the orientation of the molecule in space. Thus in a first approximation the total eigenfunction for a diatomic molecule is given by

$$\psi = \psi_e \cdot \frac{1}{r} \cdot \psi_v \cdot \psi_r$$

1.3.2 Resolution of the total energy

In the discussion of diatomic molecules the minimum value of the potential energy function (see figure 1.1) of a given stable state is considered as

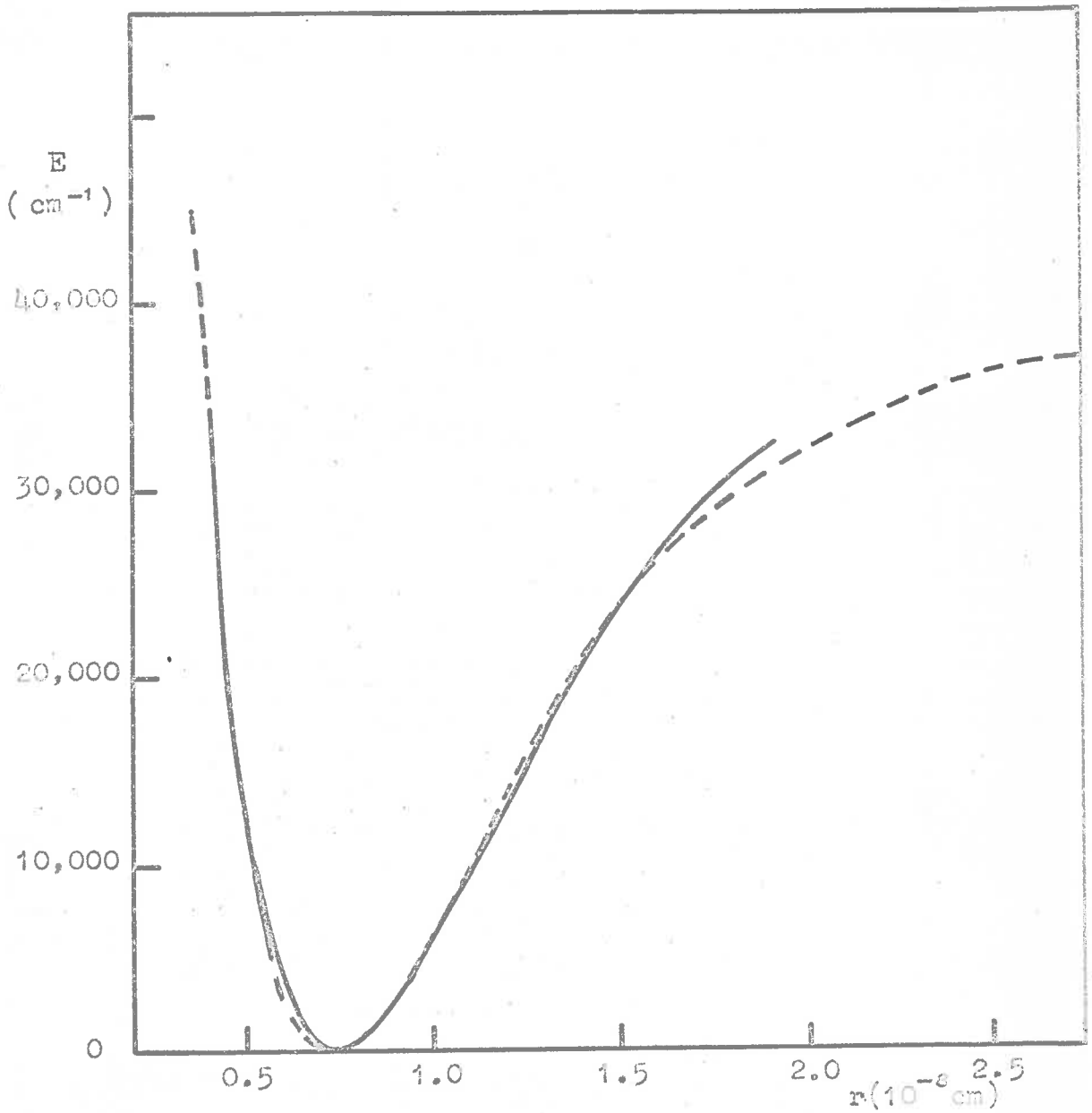

Figure1.1. Potential curve of the H_2 ground state. The full curve is drawn according to Rydberg's data. The broken curve is a Morse curve.(after Herzberg,1950)

the electronic energy of the state E_e. In addition the molecule may have vibrational energy E_v and rotational energy E_r; thus the total energy of the molecule may be written as

$$E = E_e + E_v + E_r.$$

The relative orders of magnitude for these terms are

$$E_e \approx 100E_v \text{ and } E_v \approx 100E_r$$

Figure 1.2 represents a typical energy level diagram for an idealized diatomic molecule and a typical vacuum ultraviolet transition is shown. This particular transition involves a change in electronic, vibrational and rotational states.

1.3.3 Resolution of the total matrix element

It follows from section 1.3.1 that the total matrix element for a given rotational and vibrational transition of a band system may be written as

$$\underline{R} = \underline{R}_e^{nm} \cdot \underline{R}_{vib}^{v'v''} \cdot \underline{R}_{rot}^{J'J''}$$

and similarly the oscillator strength may be written as

$$f^{nm} = f_e \cdot f_v \cdot f_r$$

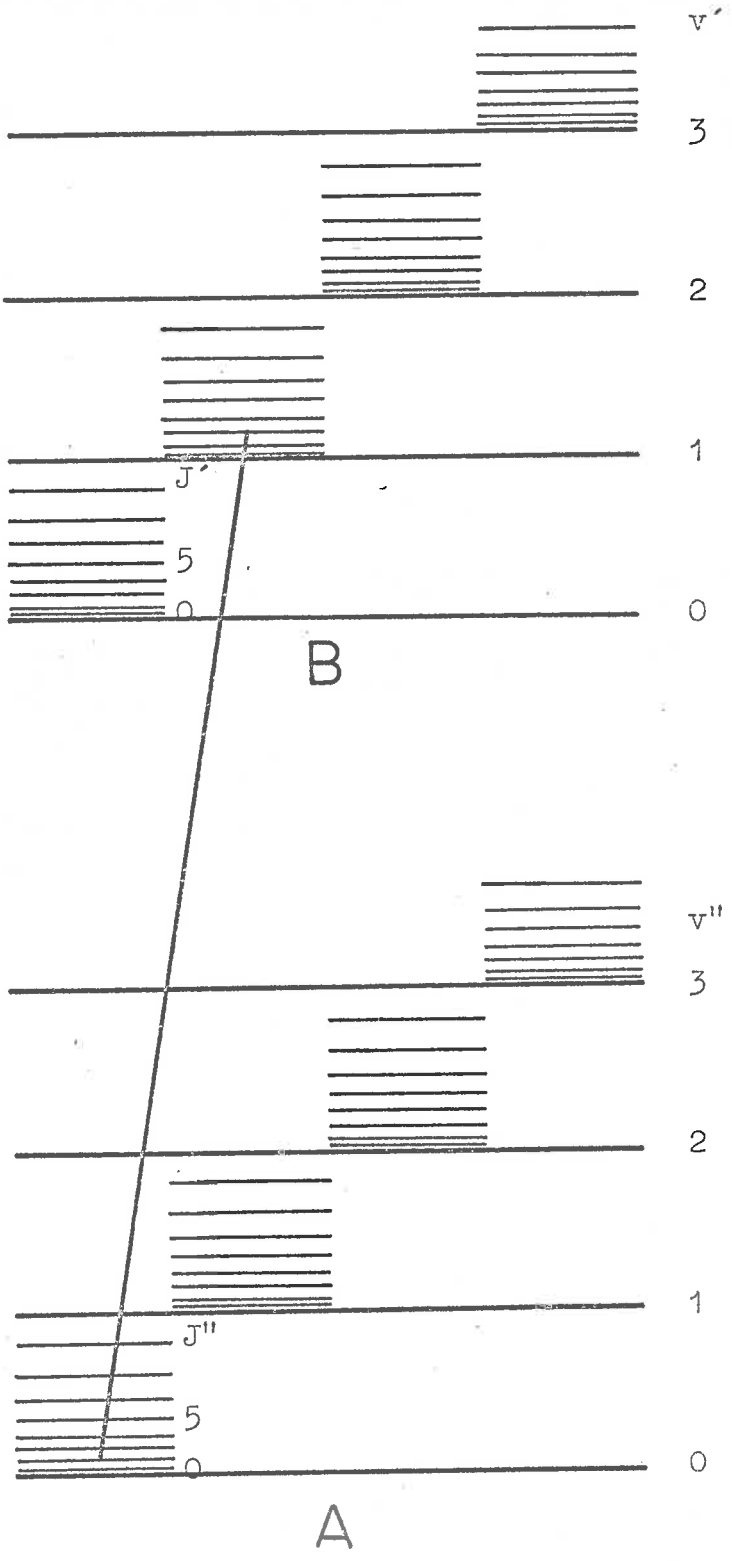

Figure 1.2. Vibrational and rotational levels of two electronic states A and B of a diatomic molecule (schematic), showing a typical vacuum ultraviolet transition.

where fe is the oscillator strength for the electronic transition and fv and fr are vibrational and rotational line strength factors depending on the vibrational and rotational quantum numbers in the upper (v′,J′) and lower (v′′,J′′) states.

1.3.4 Calculation of Oscillator Strengths

In order to calculate oscillator strengths for transitions in diatomic molecules the wave functions must be known. The calculated values of oscillator strength depend on the overlap integral and are therefore extremely sensitive to the choice of potential function; much more so than are the calculated values of the eigenenergies.

One of the aims of the work reported in this thesis was to measure accurately the absolute oscillator strengths for molecular hydrogen, a simple diatomic system, and to compare them with those calculated by Nicholls (1965) and Patch (1964).

1.4 Atmospheric Absorption processes

It has been pointed out (section 1.1) that vacuum ultraviolet spectroscopy is relevant to the study of the composition of the upper atmosphere as well as being extremely useful in giving information about the molecules themselves.

The absorption of the solar vacuum ultraviolet radiation has been used by many workers (e.g. Byram et al, 1955; Friedman et al, 1964; Smith et al, 1965) to investigate the composition of the atmosphere over heights ranging from 10-180km. With the aid of sounding rockets measurements have been made of the attenuation of the solar flux as a function of height at particular wavelengths in the vacuum ultraviolet region. Determinations of the variation of this attenuation with height and wavelength, together with a knowledge of the absorption cross-sections of atmospheric gases, provide estimates of the number densities of particular constituents of the atmosphere. (Jursa et al 1959, 1963, 1965; Chubb et al, 1958; Kupperian et al, 1959). Rockets are more applicable than satellites to this type of work since they remain within the atmosphere during flight.

Figure 1.3 shows the altitude at which solar radiation at wavelengths in the range from 0-3000Å has decreased to $\frac{1}{e}$ of its intensity outside the atmosphere with an overhead sun (Friedman, 1960; Watanabe, 1958). This is the level at which solar radiation undergoes its maximum rate of absorption in the atmosphere. The

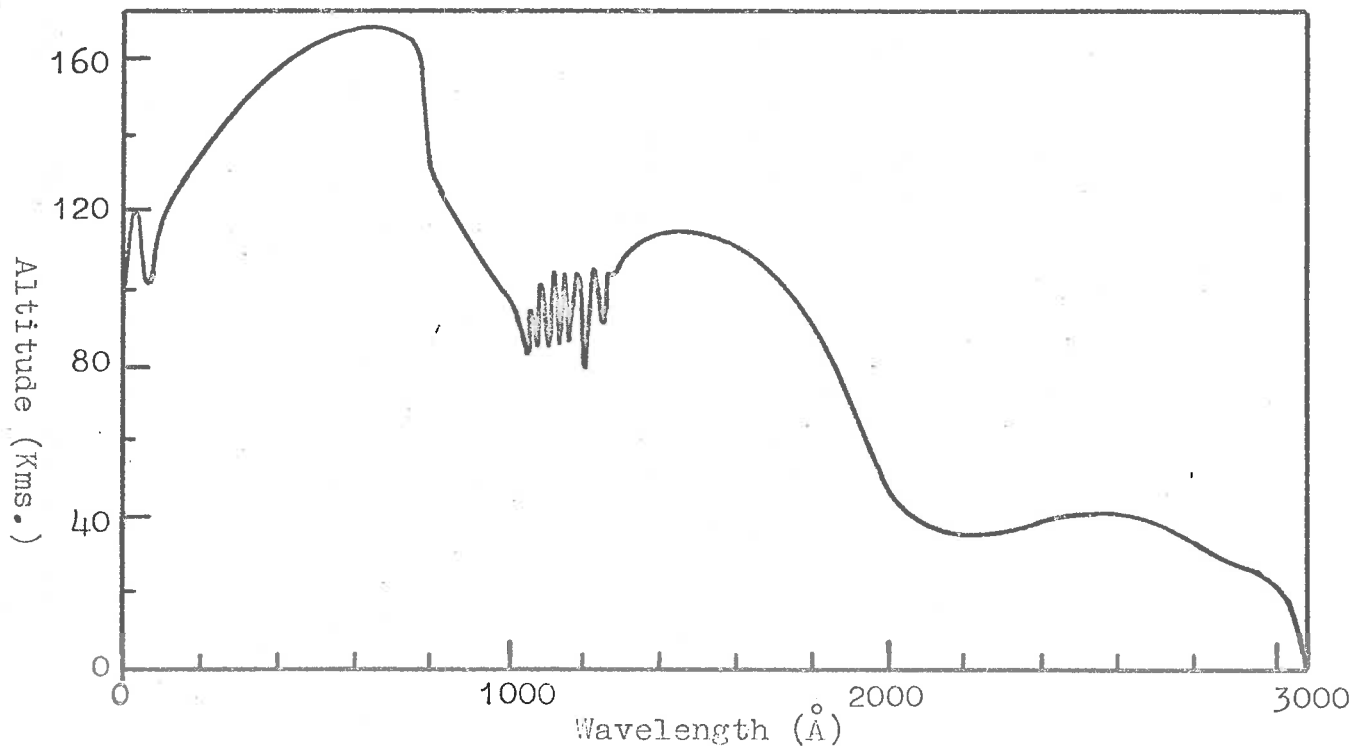

Figure 1.3 Penetration of solar radiation through the atmosphere. The curve indicates the level at which the intensity has decreased by a factor of e^{-1}.

absorption features of this diagram may be identified with the absorption spectra of particular atmospheric species.

Over the range of wavelengths from 2100-3000Å the absorption of radiation by the atmosphere may be attributed entirely to ozone which has a maximum concentration at about 25km (Johnson et al, 1951; Johnson et al, 1952). The primary atmospheric absorber over the range from 1000-2000Å is molecular oxygen which dissociates in the absorption process (Friedman, 1960). The variation of the depth of penetration of solar radiation in this range shows the same features (figure 2.1) as the variation of the absorption coefficient of molecular oxygen at these wavelengths (c.f. section 3.4). From 1400Å to 1500Å, near the peak of the Schumann-Runge continuum, solar radiation penetrates no lower than about 110km. At shorter wavelengths there are several narrow deep minima in the absorption spectrum, one of which corresponds to the wavelength of the intense solar Lyman-α line of atomic hydrogen at 1215.7Å. These "windows" allow penetration of the solar radiation to about 80km and the window at Lyman-α allows this intense solar radiation to penetrate to approximately 75km. On the short wavelength side of 1000Å the atmosphere becomes

increasingly opaque as molecular nitrogen becomes important in absorbing the solar radiation. Finally below about 700Å the species O_2,N_2,O and N all contribute to the absorption.

The results of various workers measurements of molecular oxygen densities in the upper atmosphere are reviewed in section 3.5.

1.4.1 Molecular Oxygen

Molecular oxygen is one of the most important absorbers in the atmosphere and its distribution with height is shown in figure 3.20 from the results of various workers (section 3.5.1).

The measurements of the absorption coefficients of molecular oxygen presented in this thesis (see chapter 3) have been used by Carver et al (1964) to measure molecular oxygen distributions from Woomera. A detailed discussion of this work is presented in Chapter 3.

1.5 Interstellar Absorption

It has been suggested in recent years that molecular hydrogen forms a significant proportion of the mass of our Galaxy (c.f. section 5.1). There is as yet, no direct observational evidence for the existence

of molecular hydrogen in interstellar space and there exist widely different theoretical estimates of the expected abundance. (Gould et al, 1963; Gould and Salpeter, 1963; Lambrecht and Schmidt, 1964; Knapp et al, 1965).

If molecular hydrogen is present in sufficient quantities it can be detected by making use of its absorption bands in the vacuum ultraviolet region. In principle the observations are simple; a hot star (O or B) is used as a source of continuum radiation and the interstellar absorption lines are registered on this background. The observations must, of course, wait until they can be performed from outside the earth's atmosphere.

The results of the measurements of the oscillator strengths of molecular hydrogen presented in this thesis may be used to interpret the results of two experiments of this kind which are being planned (see section 5.2). The application of the results of these proposed experiments is discussed with reference to the present measurements in Chapter 5.

CHAPTER II

Curves of Growth

Measurements of the transmissivity of a gas in the vacuum ultraviolet are usually made with instruments whose resolution is inadequate to measure the true line shape of spectral lines. This leads to a measure of the transmissivity of the gas, at a frequency close to that of the centre of the line, which does not obey Beer's law.

The manner in which the integrated absorption over the spectral line varies with the amount of absorbing material is called the curve of growth for that particular line, and it is necessary to discuss the behaviour of curves of growth, for various types of lines in order to understand the meaning of any absorption measurement, made in a region in which lines appear in the spectrum.

2.1 Equivalent width

In general, the aim of any absorption measurement is to measure the oscillator strengths for various transitions; that is, the quantity to be measured is $\int k_\nu \, d\nu$ which then gives a value for the oscillator strength. The ideal situation for measuring the

integrated absorption across the spectral line is one in which the resolution of the instrument being used is infinitely high. This means that the measured line shape is then the true line shape. In fact, in the vacuum ultraviolet region, the instrument bandpass is generally much larger than the width of the actual lines so that the apparent absorption is no longer directly related to the absorption coefficient by Beer's law.

It is easy to see qualitatively that this must be so if the instrument transmits light over a range of frequencies large compared with the width of the absorption line: even when a strong line extinguishes the light at the line centre the apparent transmission is still greater than zero because light at other wavelengths within the instrument bandpass is still transmitted through the absorption cell. The departure from Beer's law clearly depends on the relationship between instrument resolution and line width. This difficulty which has long been recognized in the study of stellar atmospheres (e.g. Preston, 1961), is overcome by introducing a quantity which is independent of instrument resolution, namely the equivalent width.

Consider the case of an isolated absorption line of some as yet undetermined shape. The absorption at a particular frequency ν can be written as*

$$A_\nu = 1-T_\nu = 1 - \exp(-k_\nu a)$$

where a is the amount of material absorbing the radiation

k_ν is the absorption coefficient at frequency ν

and T_ν is the transmission at frequency ν.

The equivalent width W is given by

$$W(a) = \int_0^\infty A_\nu d\nu = \int_0^\infty 1-\exp(-k_\nu a)d\nu$$

and the relationship between W(a) and a is known as the curve of growth. The integrated absorption over the line is finite and this absorption area is known as the equivalent width because the absorption area is equal to that produced by a rectangular line which is a perfect absorber over the frequency range W.

If the resolution function of the instrument being used to measure the absorption is given by

$$\phi(\nu-\nu', \delta)$$

---

* The notation in this section is taken from Goody, 1964.

where δ is a parameter which defines the instrument resolution and the instrument is set at a frequency ν', then the measured absorption will be

$$A_{\nu'} = 1-T_{\nu'}$$

$$= \frac{1}{\beta\delta} \int_0^\infty [1-\exp(-k_\nu a)]_\circ \phi(\nu-\nu', \delta)d\nu$$

where

$$\int_0^\infty \phi(\nu-\nu', \delta)d\nu = \beta\delta \ .$$

If now the width of the line is small compared with the instrument width so that the intensity of the source can be considered constant over the line, ~~and if the situation is simplified by setting the line at $\nu=0$,~~ then

$$A_{\nu'} = \frac{1}{\beta\delta} \phi(\nu-\nu', \delta) . \int_0^\infty [1-\exp(-k_\nu a)]d\nu \ .$$

Thus

$$W'(a) = \int_0^\infty A_{\nu'} \, d\nu' = \int_0^\infty [1-\exp(-k_\nu a)]d\nu$$

$$= W(a).$$

Therefore the equivalent width of a spectral line is a quantity which is independent of the resolution function of the instrument provided that the resolution width

of the instrument is large compared with the width of the spectral line. This condition can be imposed on the experiment to allow a variable, which is independent of the instrument used, to be measured. This situation is somewhat paradoxical since if a resolution small compared with the line width cannot be achieved one must choose an instrument resolution large compared with the line width. The intermediate situation cannot be analysed unless the instrument profile is well determined.

2.2 Weak line approximation

In general, the curve of growth (that is the variation of W(a) with a) will depend on the shape of the absorption line k_ν as a function of frequency. The exception is that if $k_\nu a \ll 1$ the integrated absorption is independent of the line shape; this situation is known as the weak line approximation.

Let k_ν be written as $S.f(\nu-\nu_o)$ where S is called the line strength and $f(\nu-\nu_o)$ is a function defining the shape of the absorption line and is normalised such that

$$\int_{-\infty}^{\infty} f(\nu-\nu_o).d(\nu-\nu_o) = 1 \quad .$$

Introducing the dimensionless parameter $x = \frac{\nu-\nu_o}{\alpha}$ where α is the width of the shape function it follows that

$$f(x) = \alpha . f[\nu(x)]$$

where $\int_{-\infty}^{\infty} f(x)dx = 1.$

The expression for the equivalent width of a single line

$$W = \int_{-\infty}^{\infty} [1-\exp(-k_\nu a)]d\nu$$

now becomes

$$\frac{W}{\alpha} = \int_{-\infty}^{\infty} [1-\exp\left(-\frac{Sa}{\alpha}f(x)\right)]dx$$

which can be expanded as

$$\frac{W}{\alpha} = \frac{Sa}{\alpha}\int_{-\infty}^{\infty} f(x)dx - \left(\frac{Sa}{\alpha}\right)^2 \frac{1}{2!}\int_{-\infty}^{\infty} f^2(x)dx + \left(\frac{Sa}{\alpha}\right)^3 \frac{1}{3!}\int_{-\infty}^{\infty} f^3(x)dx.....$$

and if $\frac{Sa}{\alpha}$ is small (that is if $k_\nu a << 1$) this implies

$$W \rightarrow Sa .$$

Therefore if a measure of W can be obtained with $\frac{Sa}{\alpha}$ sufficiently small the line strength S can be measured directly. Unfortunately in practice when $\frac{Sa}{\alpha}$ is

made small enough to satisfy the approximation, W is no longer measurable and S cannot be obtained in this way.

In the present work, for example, where the instrument resolution is $\simeq 0.3\text{Å}$ and the line width is $\simeq 0.005\text{Å}$ (see section 2.6), the weak line approximation is only valid if the value of the absorption at the centre of the line $\lesssim 2\%$.

2.3 Single line of Lorentz Shape

In general, however, the curve of growth is not independent of the shape function $f(\nu-\nu_o)$. One case which has been thoroughly treated in the literature (e.g. Kaplan and Eggers, 1956; Schmidt, 1930) is the single line of Lorentz shape.

For this type of spectral line the shape function may be written as

$$f(\nu-\nu_o) = \frac{1}{\pi} \frac{\alpha_L}{(\nu-\nu_o)^2+\alpha_L^2}$$

and the expression for the equivalent width is integrable. Using the parameter $x = \frac{\nu-\nu_o}{\alpha_L}$ the shape function becomes $f(x) = \frac{1}{\pi(x^2+1)}$ and the expression for the equivalent width may be written as

$$W = \int_{-\infty}^{\infty} \left\{ 1 - \exp \left[- \frac{Sa}{\alpha_L} f(x) \right] \right\} dx ..$$

Using $\xi = \frac{Sa}{\alpha_L}$ the results of the integration can be conveniently expressed in terms of Bessel functions of the first kind with imaginary arguments. This gives (Ladenberg and Reiche, 1913)

$$\frac{W}{\alpha_L} = \xi e^{-\frac{\xi}{2\pi}} \left[I_o \left(\frac{\xi}{2\pi} \right) + I_1 \left(\frac{\xi}{2\pi} \right) \right] .$$

In the weak line limit where ξ is small this gives

$$\frac{W}{\alpha_L} \rightarrow \frac{Sa}{\alpha_L} \quad \text{as before.}$$

For large ξ it can be shown (Goody, 1964) from the asymptotic limits of the Bessel functions that

$$\frac{W}{\alpha_L} \rightarrow 2(\xi)^{\frac{1}{2}}$$

and this is known as the strong line (or square root) approximation.

The natural profile of any spectral line is Lorentzian with a width α_N given by

$$\alpha_N = \frac{1}{4\pi\tau}$$

where τ is the lifetime of the excited state of the molecule. Typically, however, natural widths of

spectral lines are negligible compared with line widths due to Doppler broadening at the sort of temperatures encountered in the laboratory or the atmosphere. This means that the pure Lorentz shape of the natural line is dominated by the Doppler shape and the expression for W given above cannot be used. The only case of interest is that of pressure broadened lines which are Lorentzian in shape and this case will be dealt with in a later section (c.f. sections 2.5; 2.6).

2.4 Doppler lines

Thermal motion of the molecules broadens the spectral lines because of the Doppler effect and the effect becomes increasingly important as the temperature is raised.

The shape function for a Doppler line may be shown to be (Goody, 1964)

$$f(\nu-\nu_o) = \left(\frac{mc^2}{2\pi kT\ \nu_o^2}\right)^{\frac{1}{2}} \exp\left[-\frac{mc^2(\nu-\nu_o)^2}{2kT\nu_o^2}\right]$$

where m is the mass of the molecule

T is the absolute temperature

k is Boltzmann's constant

and the line has a Doppler width*

---

* Strictly speaking this is not a full width as it is usually understood, but the $\frac{1}{e}$ half width of the Gaussian line profile.

$$\alpha_D = \frac{\nu_o}{c}\left(\frac{2kT}{m}\right)^{\frac{1}{2}} \quad \ldots\ldots \qquad 2.4.1$$

Molecular hydrogen at 25°C, for example has a Doppler width, calculated using this formula, of $\alpha_D = 0.0056\text{Å}$.*

At low pressures, where the effects of pressure broadening are unimportant and absorption in the remote Lorentz wings is negligible, a spectral line has a pure Doppler shape since the natural line width is small compared with the Doppler width.

Using the Doppler profile

$$f(\nu-\nu_o) = \frac{1}{\alpha_D\sqrt{\pi}} \exp\left[-\frac{(\nu-\nu_o)^2}{\alpha_D^2}\right]$$

and again using $x = \frac{\nu-\nu_o}{\alpha_D}$ with $\omega = \frac{Sa}{\alpha_D\sqrt{\pi}}$ the expression for the equivalent width W becomes

$$W = \alpha_D \int_{-\infty}^{\infty} [1-\exp(-\omega e^{-x^2})]dx.$$

This expression may be expanded in terms of ω and integrated term by term but the expression converges slowly for large ω. This treatment gives (Goody, 1964)

$$W = \sqrt{\pi}\,\omega\,\alpha_D \left\{1 + \sum_{n=1}^{\infty} (-1)^n \frac{\omega^n}{n!\sqrt{n}}\right\}.$$

* Although the Doppler width has been defined in terms of frequency it is more convenient to use α_D defined in terms of wavelength units since all the experimental work uses wavelengths rather than frequencies. Hence α_D is quoted in terms of $\alpha_D = \frac{\lambda_o}{c}\left(\frac{2kT}{m}\right)^{\frac{1}{2}}$ in units of wavelength (A°)

This, then, gives the shape of the growth curve for a real line under conditions where the shape function is determined solely by Doppler broadening. For large ω an asymptotic expansion has been developed (Goody, 1964)

$$W = 2\,\alpha_D\,(\ln\omega)^{\frac{1}{2}}\left[1 + \frac{0.2886}{\ln\omega} - \frac{0.1335}{(\ln\omega)^2} + \cdots\right]$$

2.4.2

These two expressions allow a calculation of the full Doppler curve of growth as shown in figure 2.1.

2.5 Doppler-Lorentz mixture

The combined Doppler-Lorentz line shape has been extensively treated in studies of stellar atmospheres (Woolley and Stibbs, 1953). The shape function is too complicated for an analytical solution and the expression for W must, in general, be evaluated numerically. Figure 2.2 shows, for the mixed profile, the behaviour of W with a for various values of d where d is a parameter proportional to the ratio between the Lorentz and Doppler widths.

If, however, the equivalent width of the line is considerably greater than both the Lorentz width α_L and the Doppler width α_D, there is an asymptotic expansion for W which was developed by Plass and Fivel, 1953

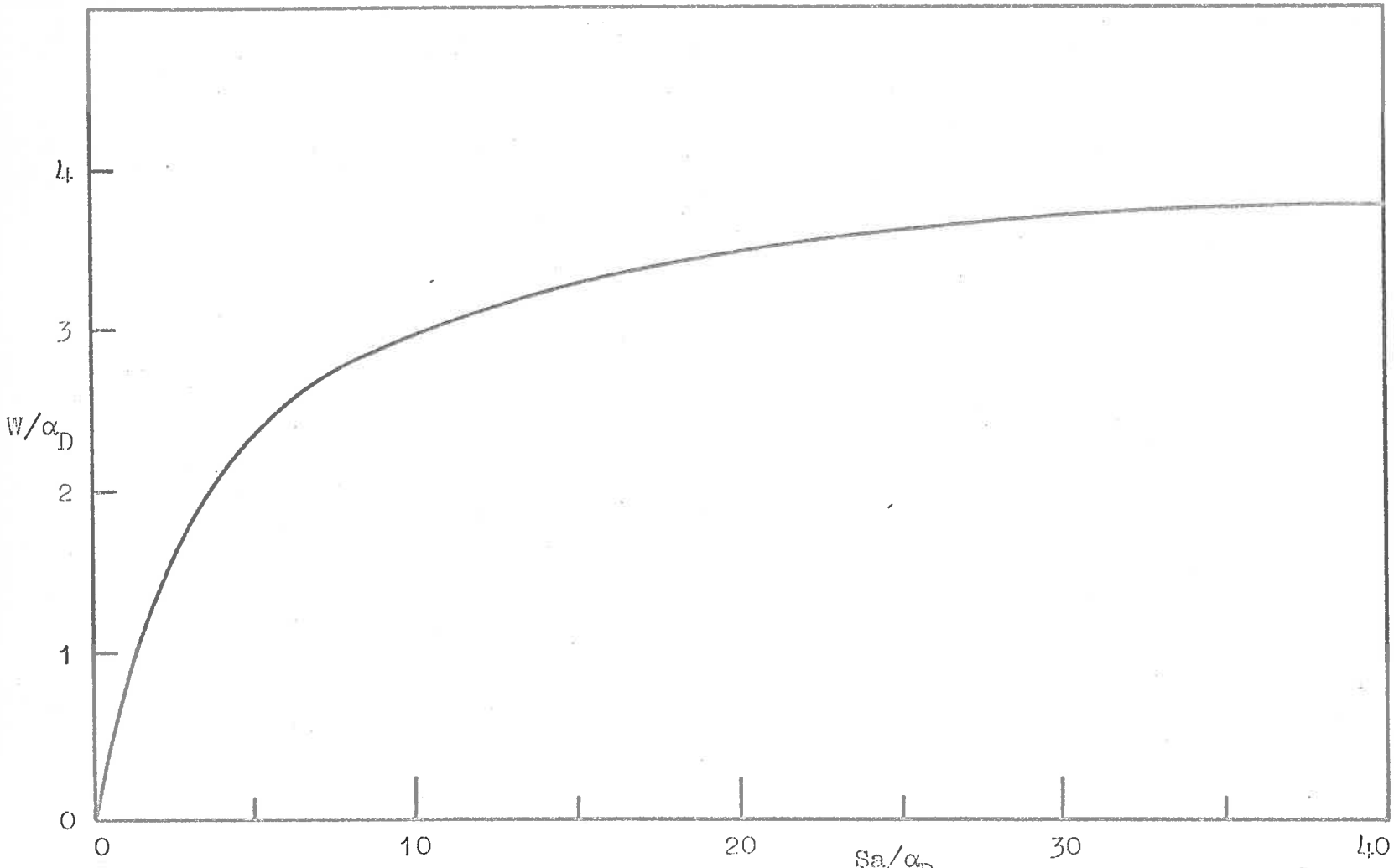

Figure 2.1 Theoretical curve of growth for a Doppler line.

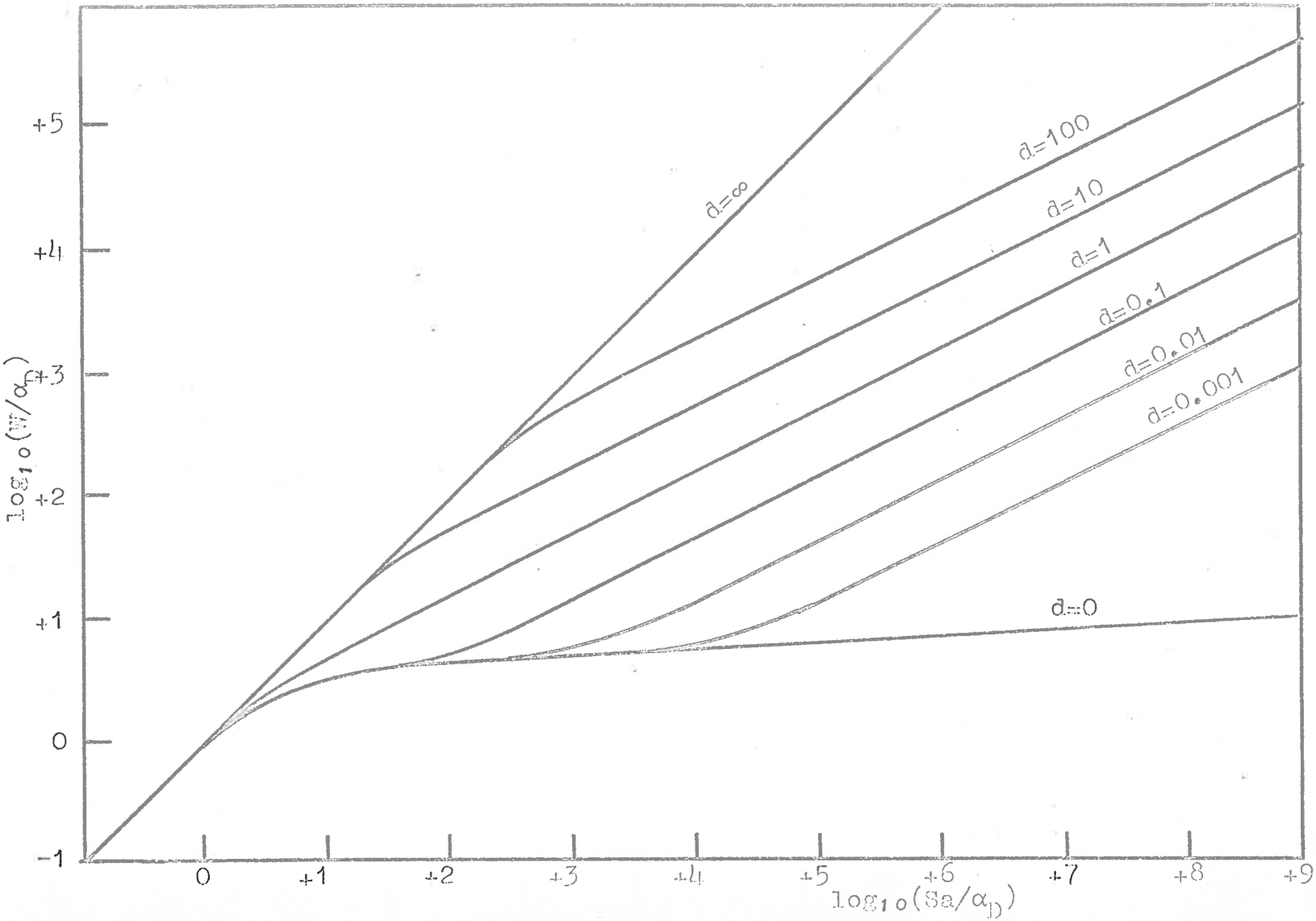

Figure 2.2. Curve of growth for a combined Doppler-Lorentz profile.

namely

$$W = \alpha_L \; \xi \, e^{-\frac{\xi}{2\pi}} \left[I_o\left(\frac{\xi}{2\pi}\right) + I_1\left(\frac{\xi}{2\pi}\right) \right] \cdot \left[1-(1-6d^{-2}) \left(\frac{4\xi}{\pi}\right)^{-1} \right] \qquad 2.5.1$$

where $d = \frac{2\alpha_L}{\alpha_D}$.

As mentioned previously (c.f. section 2.3) this combined profile is important in laboratory measurements owing to the fact that as the pressure is increased the collision frequency increases, and the lifetimes of the excited states are significantly shortened. This introduces, into the line profile, Lorentzian wings which are pressure dependent. At the same time the increased layer thickness extinguishes the centre of the line, which has a Doppler shape, so that eventually the curve of growth is entirely determined by the Lorentzian wings.

2.6 Experimental determination of a curve of growth

In the course of the present studies a detailed curve of growth exhibiting the characteristics of a mixed Doppler-Lorentz line was obtained for the isolated P_4 transition at 1074.26Å in the (3-0) band

of molecular hydrogen. The details of the experimental determination are discussed in Chapter 4.

The equivalent width of the line was measured accurately at room temperature as a function of pressure over a range of pressures from 10^{-2} torr to 30 torr with a constant cell length of 60cms. The results are presented in figures 2.3, 2.4, 2.5 and 2.6. At low pressures (up to $\simeq$ 0.2 torr) the contribution to W from the Lorentz wings is negligible and the curve of growth is characteristic of a pure Doppler line. The strength of this particular line is such that over this range of layer thicknesses ω is sufficiently large for the asymptotic expansion to be valid. Squaring the expression 2.4.2, and retaining the first two terms, one obtains

$$W^2 = 4\,\alpha_D^2 \ln \omega \left[1 + \frac{0.5772}{\ln \omega}\right]$$

$$= 4\,\alpha_D^2 \ln \omega + \text{constant}$$

$$= 4\,\alpha_D^2 \left[\ln p + \text{constant}\right]$$

where p is the pressure of the absorbing gas.
The experimental data are shown in figure 2.3 where W^2 is plotted as a function of ln p. The linear relationship between the two quantities is well displayed, establishing the Doppler character of the line. The slope of the line

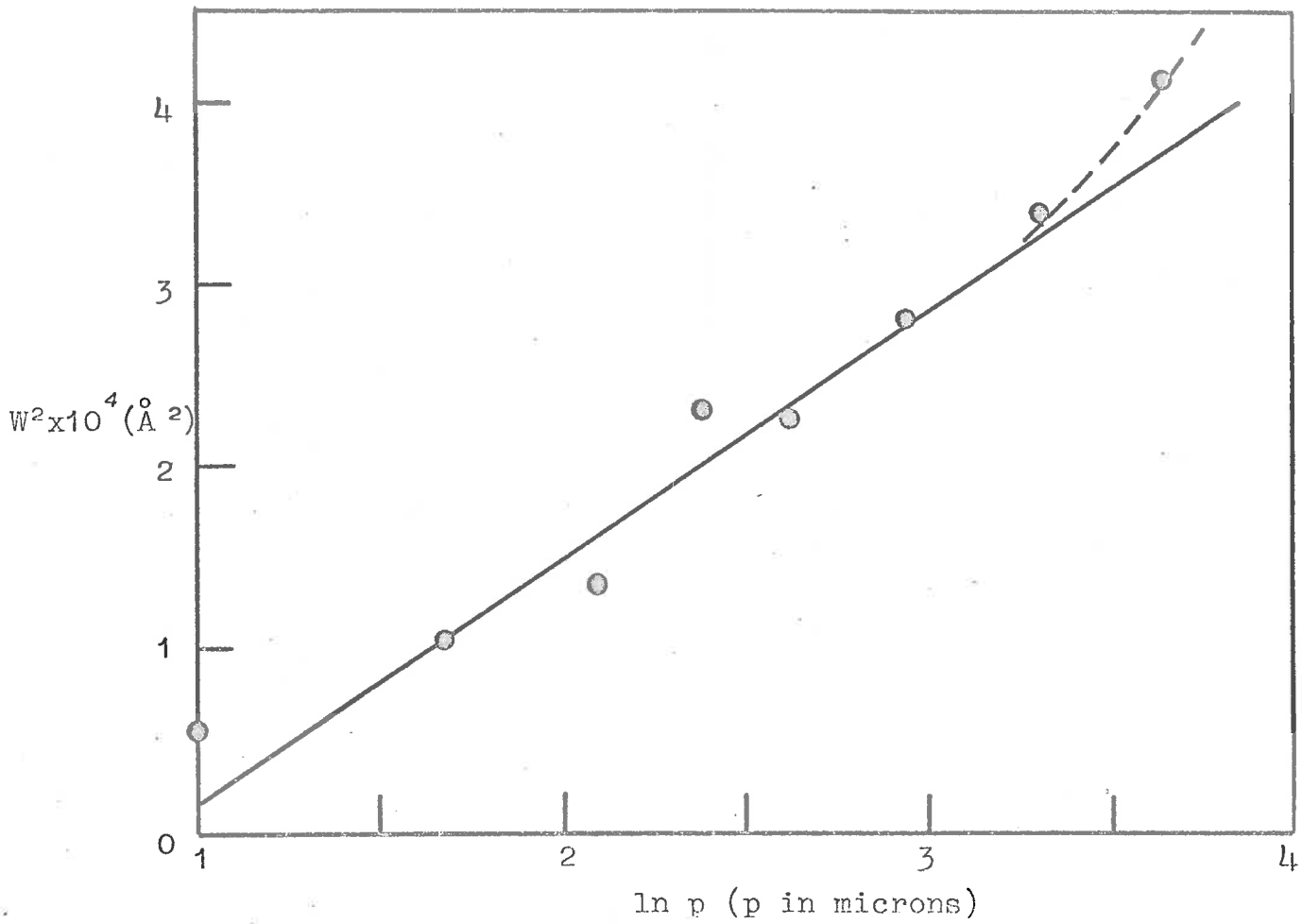

Figure 2.3 Curve of growth for the P_4 line in the 3-0 band of the Lyman series of molecular hydrogen shown in the region where W^2 is linearly related to ln p.

is $4\ \alpha_D^2 = 1.22\times10^{-4}$ Å^2 yielding a value for the Doppler width of 0.0055Å in excellent agreement with the value of 0.00556 at 298°K calculated from equation 2.4.1. Thus a line width of ≈ 0.006Å has been measured using an instrument resolution of ≈ 0.3Å and this in itself is a remarkable achievement.

In figure 2.4 the low pressure data are displayed together with the theoretical Doppler curves of growth for a Doppler width of 0.00556Å and assumed strengths of S = 8, S = 12 and S = 16. Below a pressure of ≈ 0.2 torr the curve for S = 12 fits the experimental data well and the other two curves indicate that the calculated growth curve is quite sensitive to a correct choice of S. Beyond a pressure of 0.5 torr the experimental points begin to diverge from the Doppler curve indicating the onset of significant pressure broadening.

Results for higher pressures are presented in figure 2.5. These results were corrected for a constant amount of absorption which underlies all the lines* to give a more accurate measure of the strength S. If the

---

* This is due to the fact that there are a large number of pressure broadened Lorentz lines overlapping in this region. At a pressure of 20 torr these contribute to an effective continuum of strength 0.03cm^{-1}.

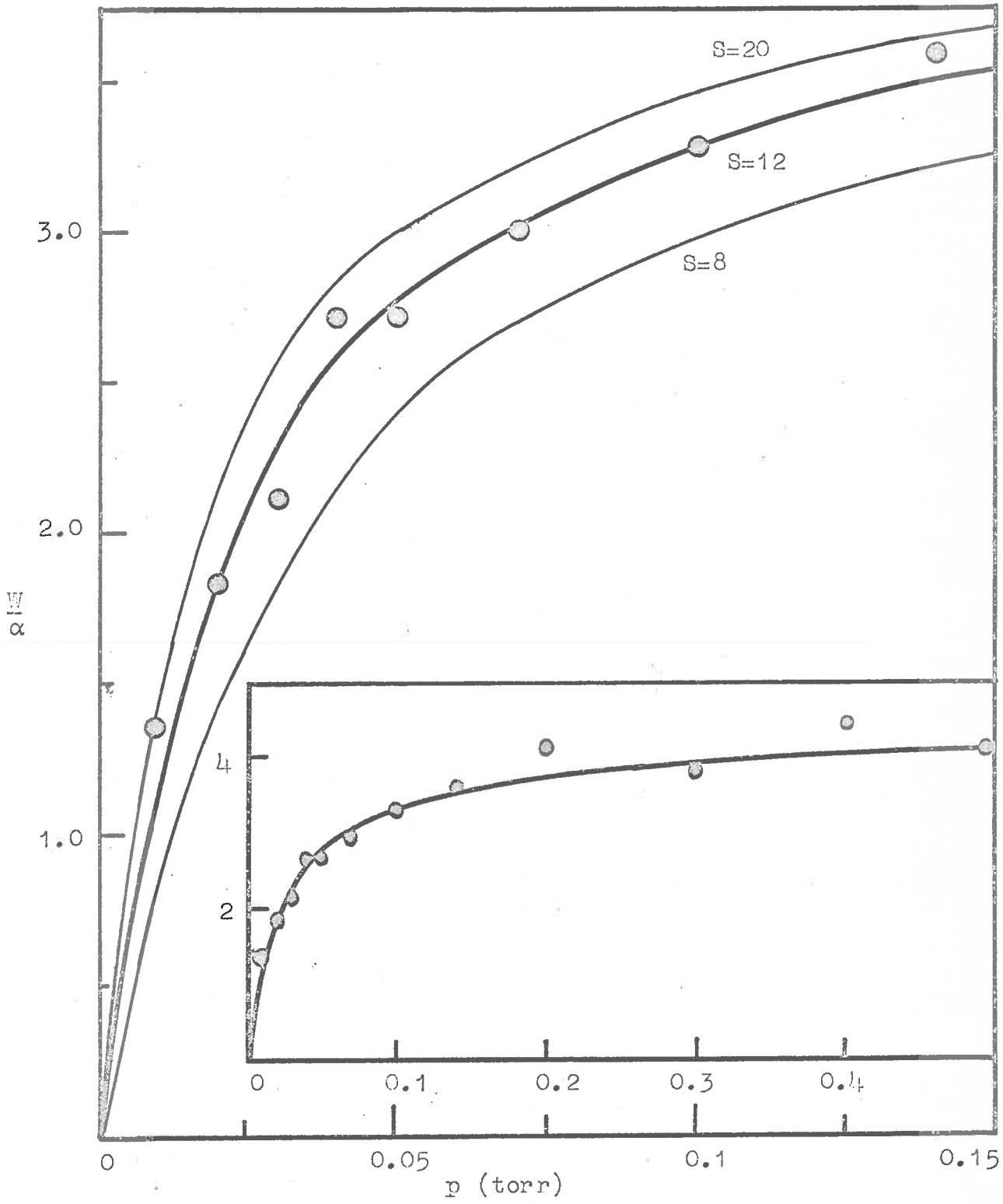

Figure 2.4 Curve of growth for the line $P_4(3\text{-}0)$ showing the experimental points compared with the theoretical curves for chosen values of line strength S=8, S=12, S=20. Inset: The extension of the curve for S=12 and the experimental points to higher pressures of absorbing gas.

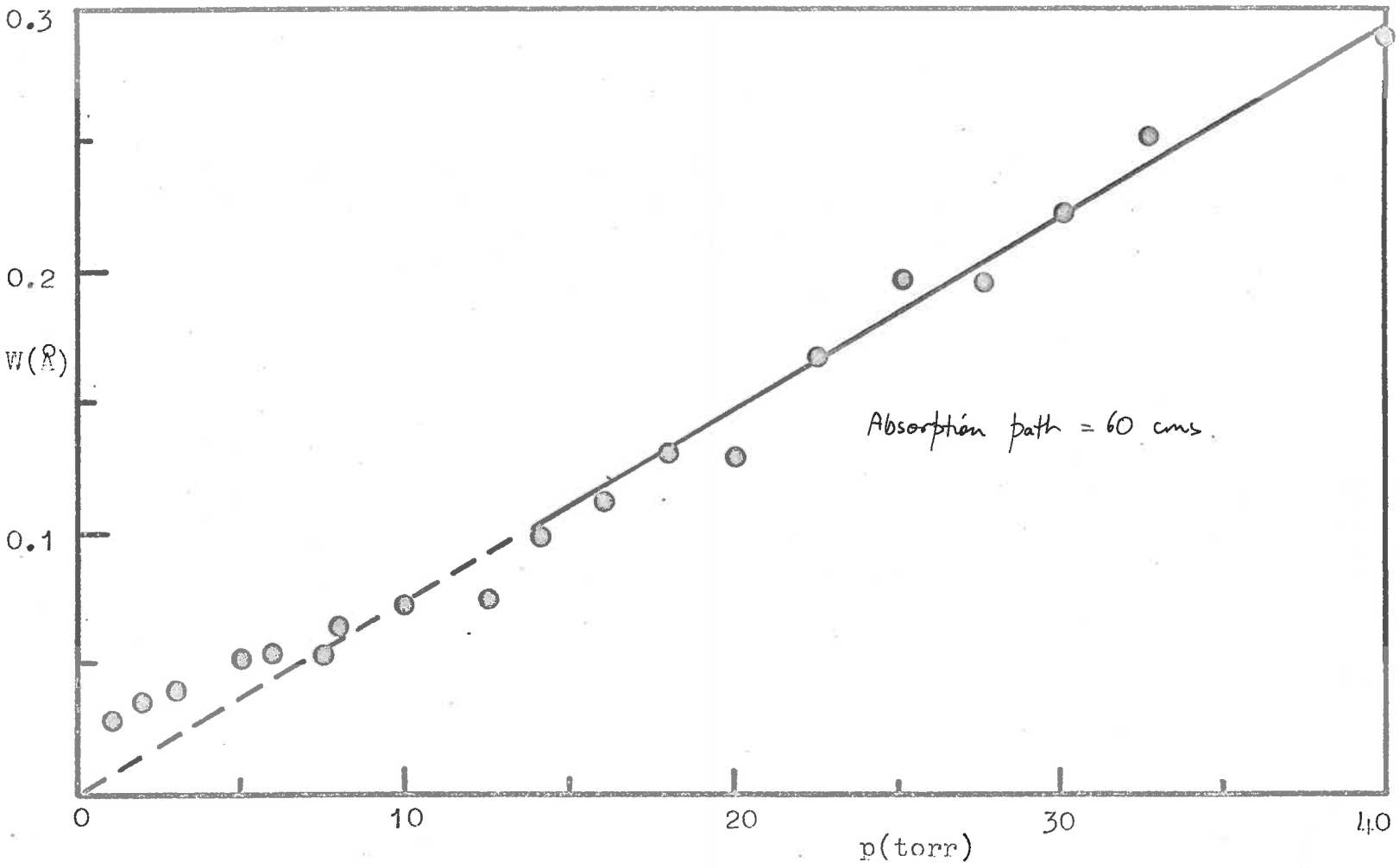

Fig. 2.5 Extension of the curve growth for the $^{1}\Sigma_{4}$ line to high pressures where the line has a mixed Doppler-Lorentz profile.

true k_ν is made up of a line plus some constant level k_o then the observed equivalent width is given by

$$W' = \int 1 - e^{-[k_o+k_\nu]a} \, d\nu$$

$$\approx W - k_o a W + k_o a \nu \text{ (to first order)}$$

where ν is the line width

Thus

$$W = \frac{W' - k_o a \nu}{1-k_o a} .$$

The effect of this continuous absorption is quite significant at high pressures and the results shown in figure 2.6 used the above expression, with an estimate of $k_o a$ from the region between the spectral lines, to give corrected values of W.

It is pointed out below (see section 2.7) that the pressure broadened Lorentz width α_L is directly proportional to the pressure p; that is one may substitute $\alpha_L = \gamma p$ into the asymptotic expansion 2.5.1. At high pressures ξ is large and the expansion reduces to

$$W = \alpha_L \xi e^{-\frac{\xi}{2\pi}} \left[I_o \left(\frac{\xi}{2\pi}\right) + I_1 \left(\frac{\xi}{2\pi}\right) \right]$$

$$\rightarrow 2 \alpha_L (\xi)^{\frac{1}{2}} .$$

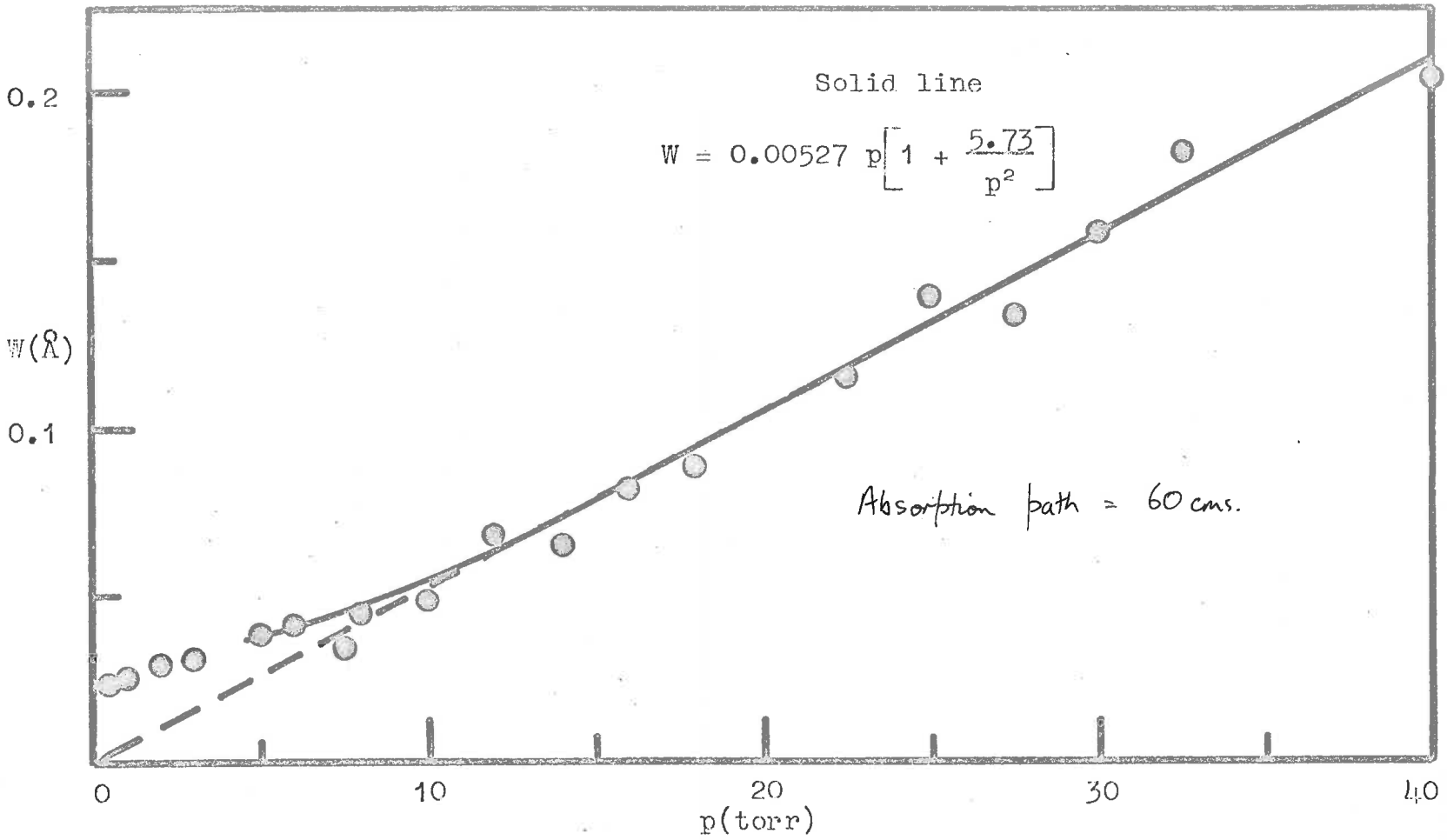

Fig. 2.6 The curve of growth for the mixed profile V_4 line corrected for continuum absorption. Also shown (solid line) is the theoretical curve of growth for the mixed profile.

Introducing

$$\xi = \frac{S\ p\ L\ T_o}{\alpha_L\ 760\ T} \quad \text{and substituting } \alpha_L = \gamma p$$

this becomes

$$W = 2\pi\gamma p \sqrt{\frac{Sa}{\gamma p}} = 2\ \pi p \sqrt{\frac{\gamma SL.T_o}{760\ T}}\ .$$

Figure 2.6 shows the linear dependence of W on p expected when pressure broadening is the dominant feature determining the equivalent width and the slope of the plot gives a value for the pressure broadening coefficient of

$$\gamma = 6.7 \times 10^{-6} \text{Å/torr.}$$

Inserting this value of γ into the asymptotic expansion

$$W = 2(\gamma Spa)^{\frac{1}{2}} \left[1 - \frac{\pi\gamma p}{4Sa} + \frac{3}{8} \frac{\pi}{Sa} \frac{\alpha_o^2}{\gamma p} \right]$$

gives the result for the mixed profile in the intermediate region

$$W = 0.00527\ p \left[1 + \frac{5.73}{p^2} \right] \text{(neglecting the small constant term)}$$

The solid line in figure 2.6 is the curve of this equation and agrees well for as long as the asymptotic expansion holds.

2.7 Pressure broadening

In the case of pressure broadening it is the time between collisions rather than the lifetime of the excited state which determines the width of a spectral line. If it is assumed that a molecule always decays after a collision, kinetic theory gives a lower limit for the width of the spectral line. If α_L is the line width arising from a mean time τ between collisions then (Goody, 1964)

$$\alpha_L = \frac{1}{2\pi\tau} = \Sigma_i \; n_i \; \sigma_i^2 \left\{ \frac{2kT}{m} \left(\frac{1}{m} + \frac{1}{m_i} \right) \right\}^{\frac{1}{2}}$$

where m is the mass of the molecule giving rise to the absorption

n_i is the number density of the ith class of molecule

m_i is its molecular mass

and σ_i is the distance of closest approach of the two molecules.

In a mixture of constant composition, at constant temperature, $n_i \propto p$ where p is the pressure, so that collision line widths are proportional to pressure. This is the assumption made in the previous discussion (see section 2.6).

The kinetic line width can be calculated for molecular hydrogen using a collision frequency of 10^{10}

per sec at 760 torr and 20°C (Hesser and Dressler, 1966). This gives a lifetime of 10^{-10} seconds and a lower limit for the line width of 0.00057Å at 1 atmosphere pressure. The pressure broadening coefficient inferred from the experimental results (section 2.6) implies a line width of 0.006Å at 1 atmosphere and is a factor of 10 greater than the kinetic limit. This indicates that the distance of closest approach of two molecules (σ_i) in their excited state is a factor of ≈3 greater than the ground state collision diameter obtained from measurements of viscosity and conductivity (Uehling, 1934).

Similar estimates of the pressure broadening coefficients have been made for a number of other lines in molecular hydrogen and are all equal within the limits of experimental error (see section 4.6.2).

2.8 Overlapping lines

In the case of lines which overlap the problem of extracting absolute strengths is somewhat complicated.

Let us consider the case of a doublet consisting of two lines of equal intensity which overlap in the sense that they are not resolved with the dispersing instrument being used. If the lines are separated at low pressures then as the pressure is increased the total integrated absorption will grow as that of a line with twice the

strength. As the pressure increases still further the absorption will increase in the frequency region between the two lines until this gap is filled. From this point on the slope of the growth curve will decrease by a factor of ≃2 as the gap between the lines is absorbed out and only the outside wings of the two lines continue to contribute to the absorption. This change to a line of less slope will be very slow, however, as the gap between the lines takes some time to black out completely.

Figure 2.7 shows the growth curve for the P_2R_3 doublet at ≃1096.5Å in the absorption spectrum of molecular hydrogen and it can be seen that the behaviour of the experimental growth curve can be explained in this way. A full treatment of this case has been given by Reiche (1956).

Unfortunately it is difficult to extend this argument in a quantitative way to the case of two lines of unequal strength and thus extract their separate equivalent widths.

2.9 Band Models

Where complete bands of lines are unresolved there are several models which can be used to describe the observed growth curve of the absorption over a band with a variation of pressure.

The Elsasser model (Elsasser, 1942) consists of

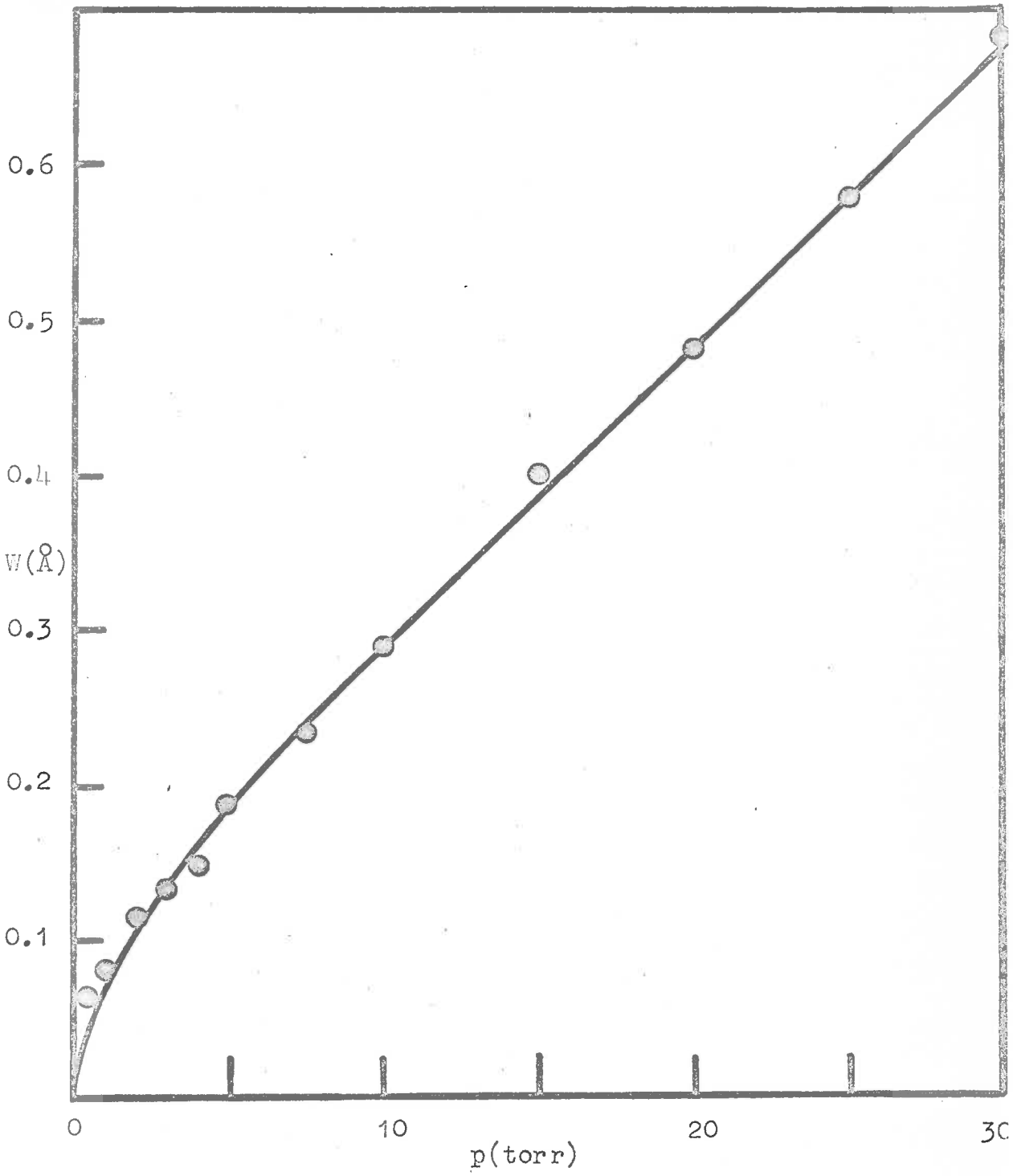

Figure 2.7 Curve of growth for the P_2, R_3 doublet at 10965Å

an infinite array of lines of equal intensity spaced at equal intervals. This model has only been solved for the Lorentz line shape and in the strong line asymptotic limit gives for the average absorption

$$\bar{A} = \text{erf}\ \{\pi y \sqrt{2u}\}$$

where $y = \frac{\alpha_L}{\delta}$ and δ is the average spacing between lines in a band

$$u = \frac{Sa}{2\pi\alpha_L}$$

and erf is the error function.

The behaviour of this "error function growth curve" against a parameter proportional to the pressure is shown in figure 2.8 where $\bar{A}$ is plotted against X, where for this model

$$X = \frac{1}{\delta}\sqrt{\pi S a \alpha_L} = \frac{p}{\delta}\sqrt{\pi S k \gamma}$$

where $a = kp$ and $\alpha_L = \gamma p$.

The Random model (Goody, 1952) takes an array of identical lines randomly distributed over some range of frequencies with an average spacing between the lines of δ. It is assumed that the lines are distributed according to a Poisson distribution and this gives for the average absorption

$$\bar{A} = 1 - \exp\left(-\frac{w}{\delta}\right)$$

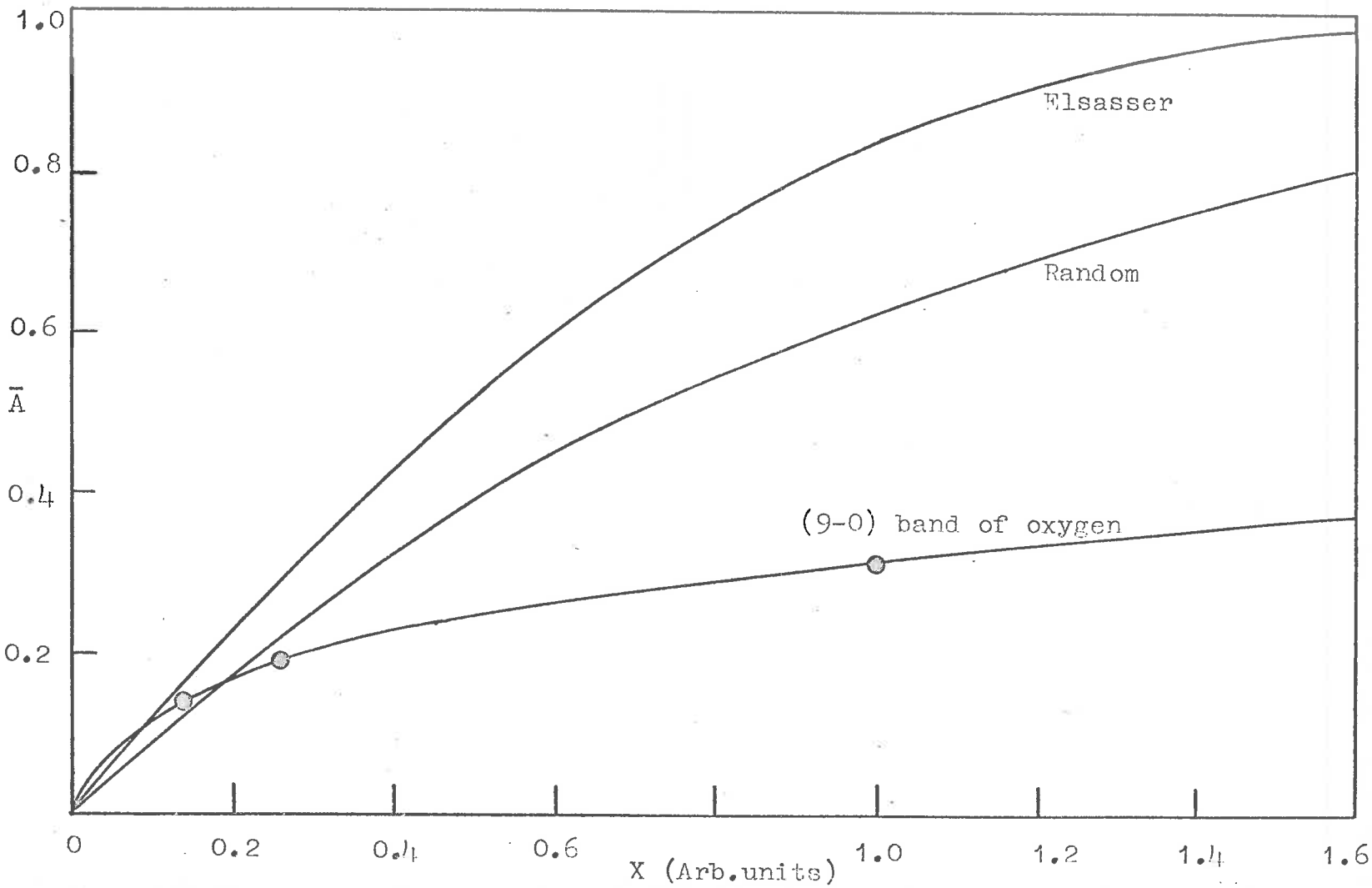

Fig. 2.8 The curve of growth for the (9-0) band in the Schumann-Runge system of molecular oxygen compared with theoretical growth curves using the Random and Elsasser models.

where W is the equivalent width of one line. This result is obtained by allowing the number of lines to tend to infinity. If a Lorentzian line shape is introduced into this equation the growth curve behaves as shown in figure 2.8 where X is now just a parameter proportional to pressure.

An experimentally determined growth curve for the 9-0 band of molecular oxygen at 1830Å is shown in figure 2.8 together with the growth curves for the Elsasser and Random models. It can be seen that the actual absorption grows much more slowly than is predicted by either of these models. This is due to the fact that the actual band has some distribution of strong and weak lines and any gaps in the spectral region where there are no lines, are not taken into account. Both these situations will lead to the growth curve for the observed band following the predicted ones in the low pressure region but breaking away and growing much more slowly thereafter, as the gaps between lines or gaps caused by weak lines are absorbed out more slowly.

CHAPTER 3

Absorption Measurements on Molecular Oxygen

Absorption coefficients for molecular oxygen have been measured using the same technique over the range of wavelengths from 1050Å to 2350Å. The results are shown in figure 3.1. It can be seen that from 1050-1250Å the absorption coefficient varies over a wide range with several valleys of low absorption; this is the so-called "window" region referred to in section 1.4. From 1250-1750Å the absorption coefficient varies relatively slowly over the Schumann-Runge continuum and the region from 1750-2000Å is occupied by the Schumann-Runge bands. The results in this latter region are presented in terms of the effective layer thickness for a range of layer thicknesses corresponding to oxygen densities in the upper atmosphere. Finally, the spectrum from 2000-2350Å is due to absorption in the Herzberg continuum.

The application of these results in measurements of the number density of oxygen in the terrestrial atmosphere is discussed.

3.1 Experimental Arrangement

The experimental arrangement is shown schemati-

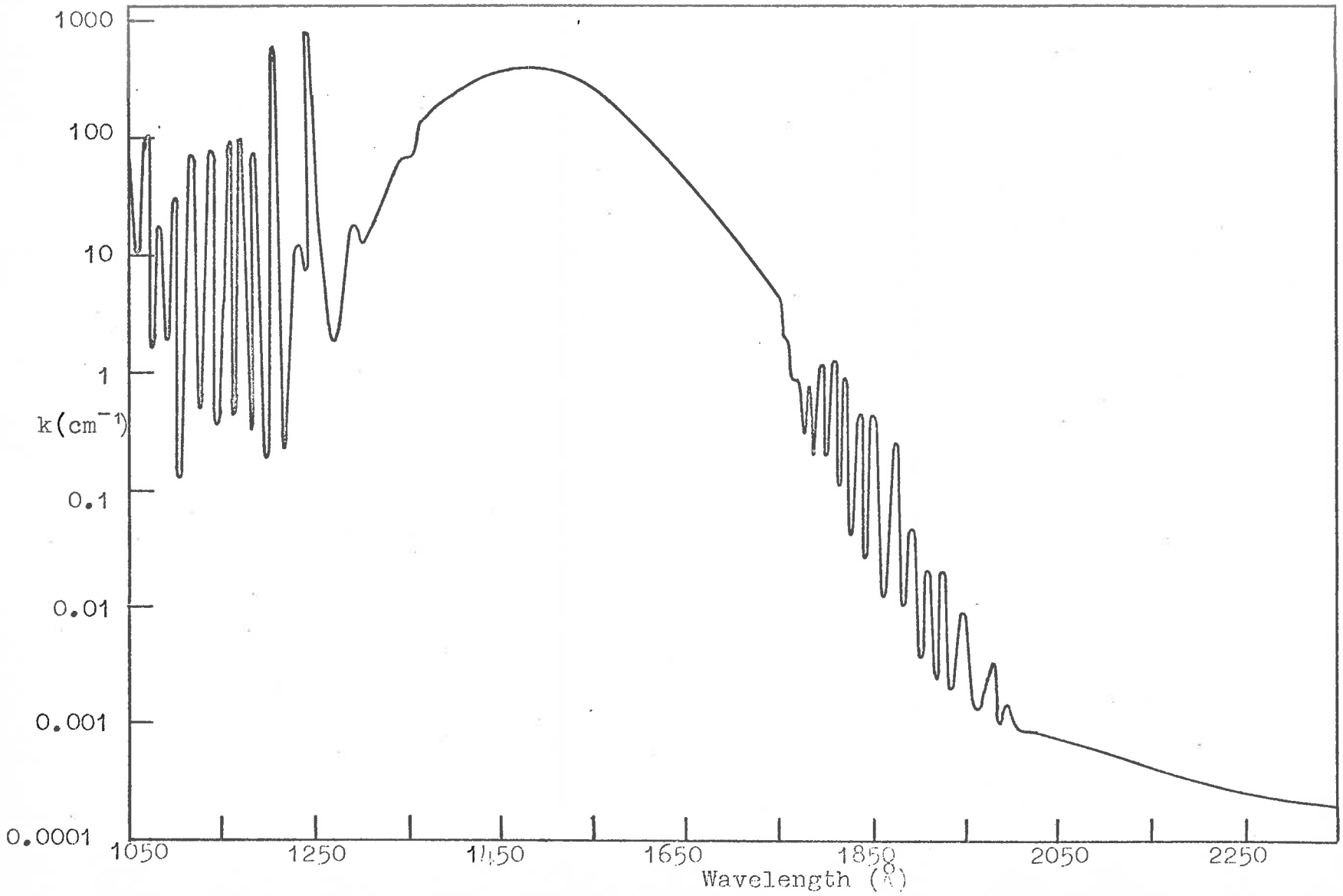

Figure 3.1 Absorption coefficients for molecular oxygen from 1050-2350Å.

cally in figure 3.2. A dispersing instrument fitted with a light source provided a monochromatic beam of ultraviolet radiation which passed into the absorption cell through a lithium fluoride window. This radiation was detected at the remote end of the cell with a phosphor-photomultiplier combination and the flux of the ultraviolet radiation incident on the cell was monitored with a beam splitter arrangement (see section 3.1.5). Pure oxygen was introduced into the cell and the pressure measured with various gauges. The current from the two photomultipliers was recorded continuously as the wavelength of the light incident on the cell was scanned. The absorption coefficient was then calculated using Beer's law except in regions where it was necessary to account for the dependence of the apparent absorption coefficient on the layer thickness (c.f.section 3.4.3).

3.1.1 Light Sources

In general, light sources used in the vacuum ultraviolet region of the spectrum do not approach the ideal of a continuous source of constant intensity for all wavelengths, nor is there an unlimited flux available from any type of lamp.

The most commonly used sources in this region are high current density gas discharges. This method

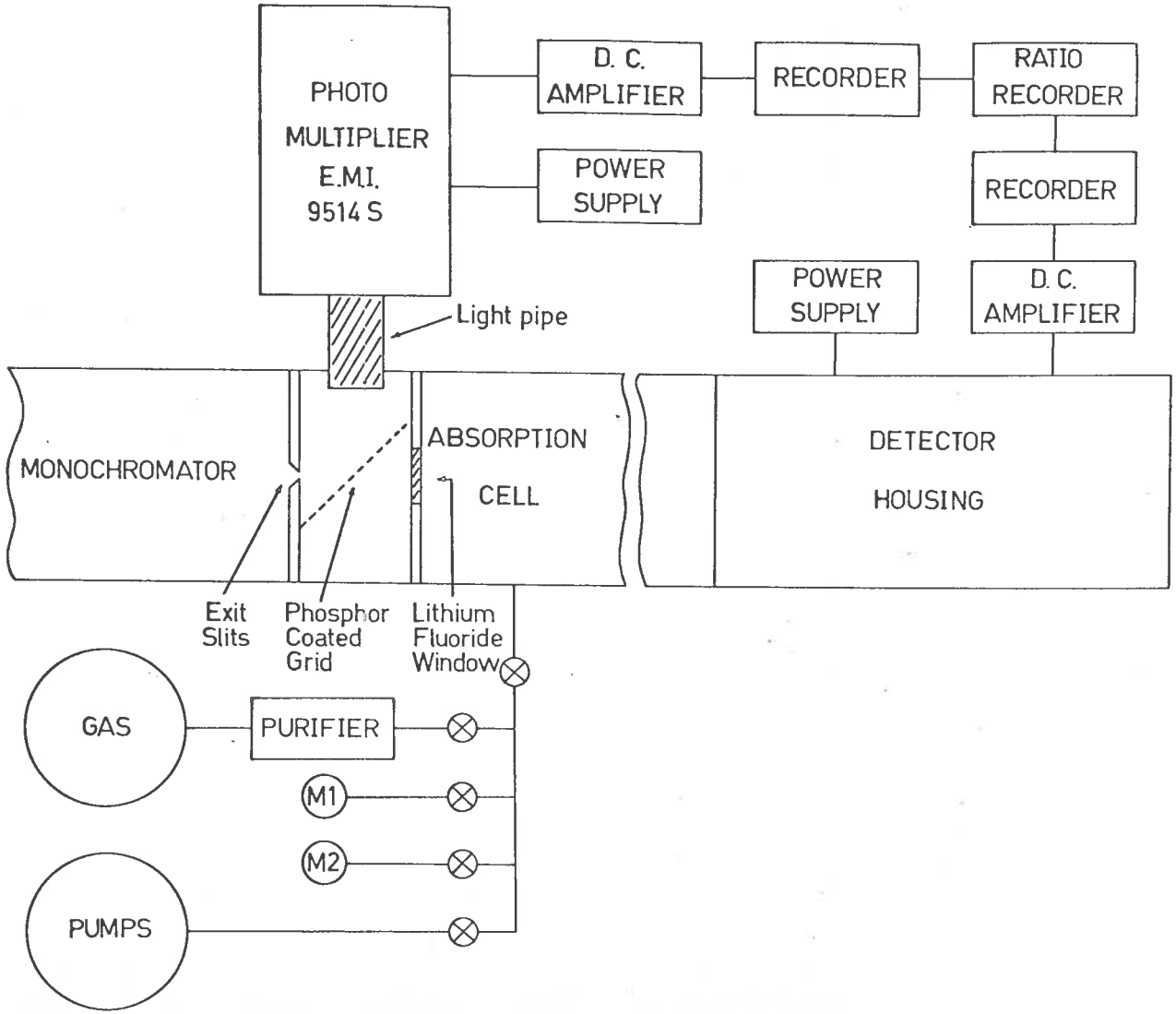

Figure 3.2 Experimental arrangement for absorption measurements on molecular oxygen.

yields a usable intensity over a finite region of the spectrum. The range of wavelengths over which the source emits a continuum is determined by the choice of gas and method of excitation of the discharge. Methods of excitation of the discharge vary from microwave excitation, D.C. high voltage and A.C. High voltage to a mode usually referred to as a condensed spark excitation. (Wilkinson and Byram, 1965; Tanaka et al 1962). The most satisfactory sources available at present, apart from the synchrotron radiation used by Madden and Codling (1965) are those which excite the characteristic continua of the rare gases. These excitation continua have been recorded (Tanaka et al, 1958; Huffman et al, 1965; Tanaka et al, 1962; Wilkinson and Byram, 1965) and the following is a list of the regions of the spectrum which are accessible by the use of these various gases

Argon	1070 - 1400 Å
Neon	740 - 1000 Å
Krypton	1240 - 1700 Å
Xenon	1470 - 1900 Å
Helium	600 - 1000 Å

One of the light sources used in this work

utilized the excitation of the many-lined spectrum of molecular hydrogen by an A.C. high voltage discharge. In this case the high voltage was applied to the lamp through a series resistor to stabilise the discharge (see figure 3.3(a)). As can be seen from figure 3.4 this spectrum, in the region from 1050-1700Å, contains many lines and does not approach the ideal case described previously. This source must be used with some care so that it does not introduce false structure into the absorption spectra due to misalignment of the wavelength scales between consecutive scans.

A much more satisfactory spectral distribution of radiation was obtained using a relatively high power discharge in argon. In order to obtain the continuum radiation from argon, a high current density was necessary in the discharge tube and consequently the mode of operation of the lamp was altered. A bank of capacitors was charged to a high potential and then discharged across the capillary of the lamp in order to achieve the required current density. The voltage on the capacitors built up until a spark gap in series with the lamp broke down discharging the capacitors across the capillary filled with argon. The breakdown conditions of the spark gap were stabilised by illuminating it with

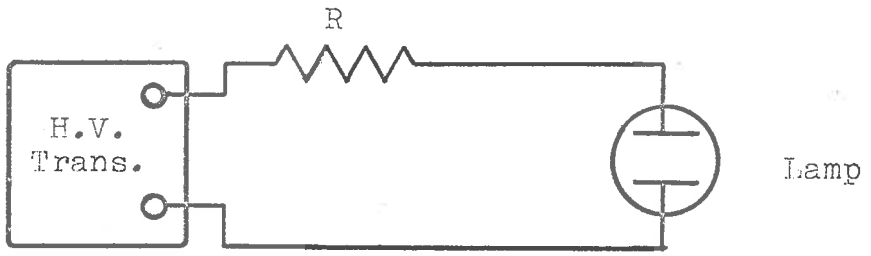

Figure 3.3(a) A.C. excitation of discharge lamp.

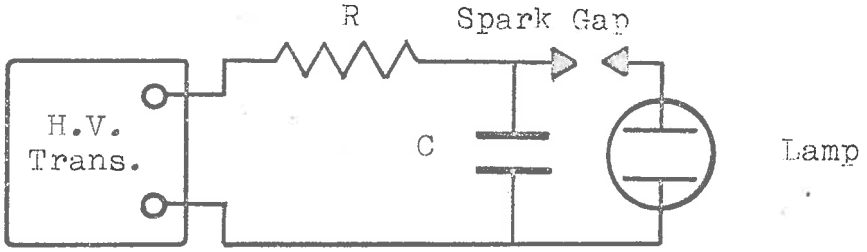

Figure 3.3(b) Condensed spark excitation

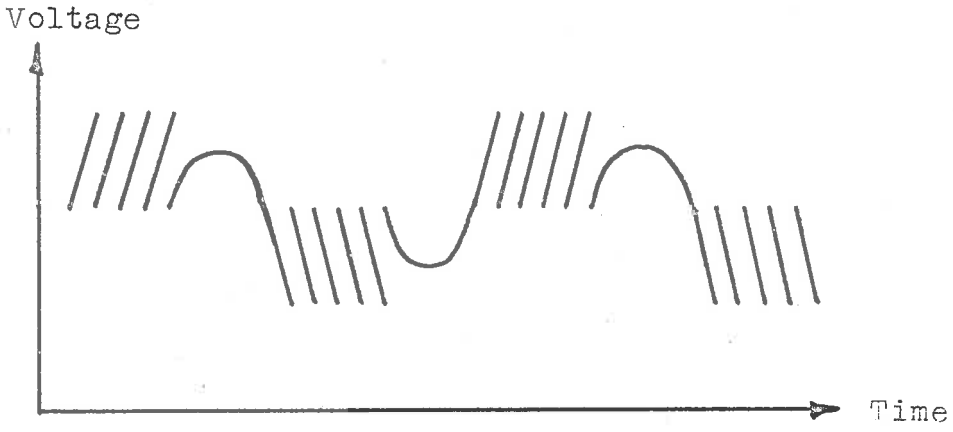

Figure 3.3(c) Waveform appearing across discharge lamp under condensed spark excitation.

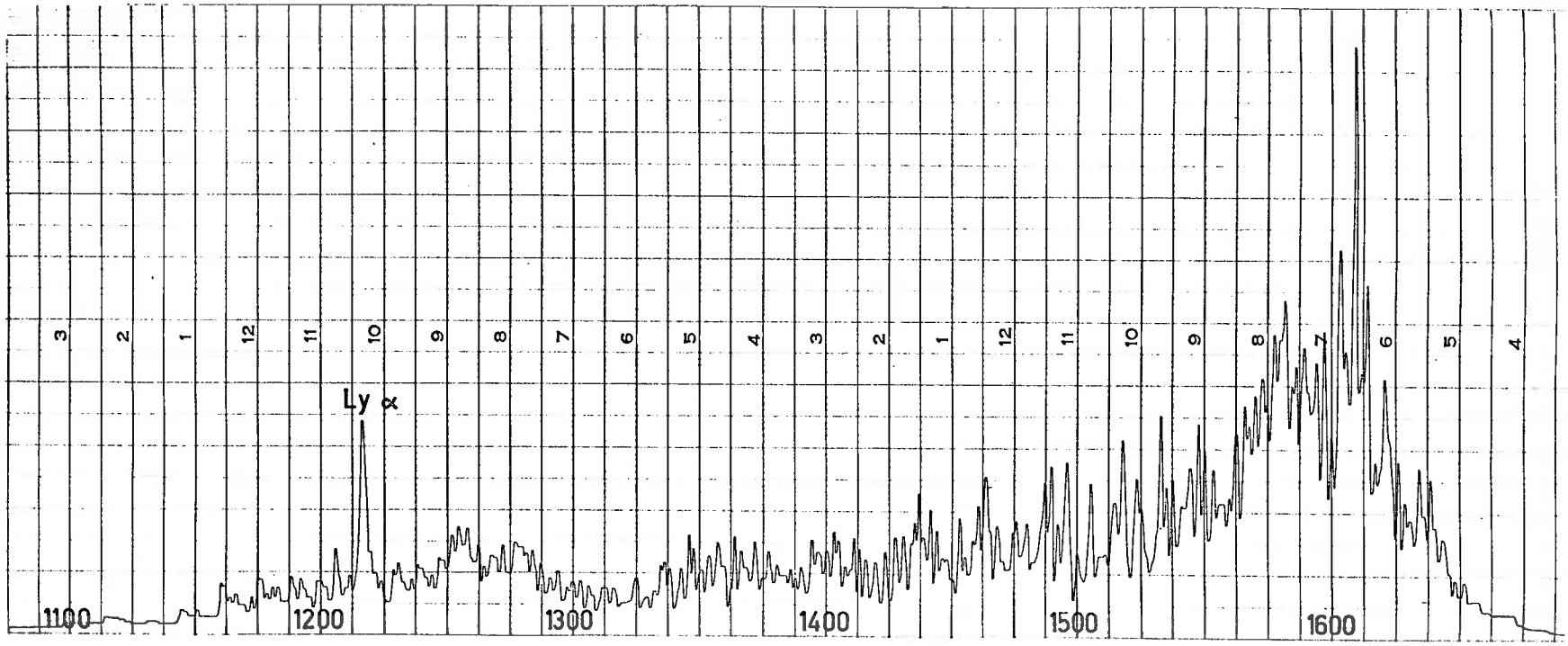

Figure 3.4 Spectrum from the discharge lamp containing molecular hydrogen.

ultraviolet radiation from a small mercury discharge lamp with a quartz envelope and by blowing away the ionised air with a jet of compressed air. If an A.C. high voltage is applied to the capacitors as in figure 3.3(b) the resultant wave form on the lamp appears as in figure 3.3(c) where the capacitors are charged and discharged a number of times during each half cycle of the A.C. voltage. This mode of excitation gives rise to unstable diatomic argon ions which subsequently decay to their ground state giving rise to a continuous spectral distribution from 1070-1400Å as shown in figure 3.5. For this phenomenon to occur it is necessary to have a relatively high pressure (200 torr) of argon in the discharge tube to enhance the formation of the diatomic ions.

Most of the work on molecular oxygen was done using the much more intense many-lined spectrum of molecular hydrogen owing to the fact that in order to maintain a pressure of 200 torr in the lamp, modifications to the monochromator were necessary. (See section 3.1.2.)

3.1.2 Dispersing Instrument

The dispersing instrument used in the absorption measurements on molecular oxygen was a Model 235 McPherson monochromator. This is a ½ metre Seya-Namioka

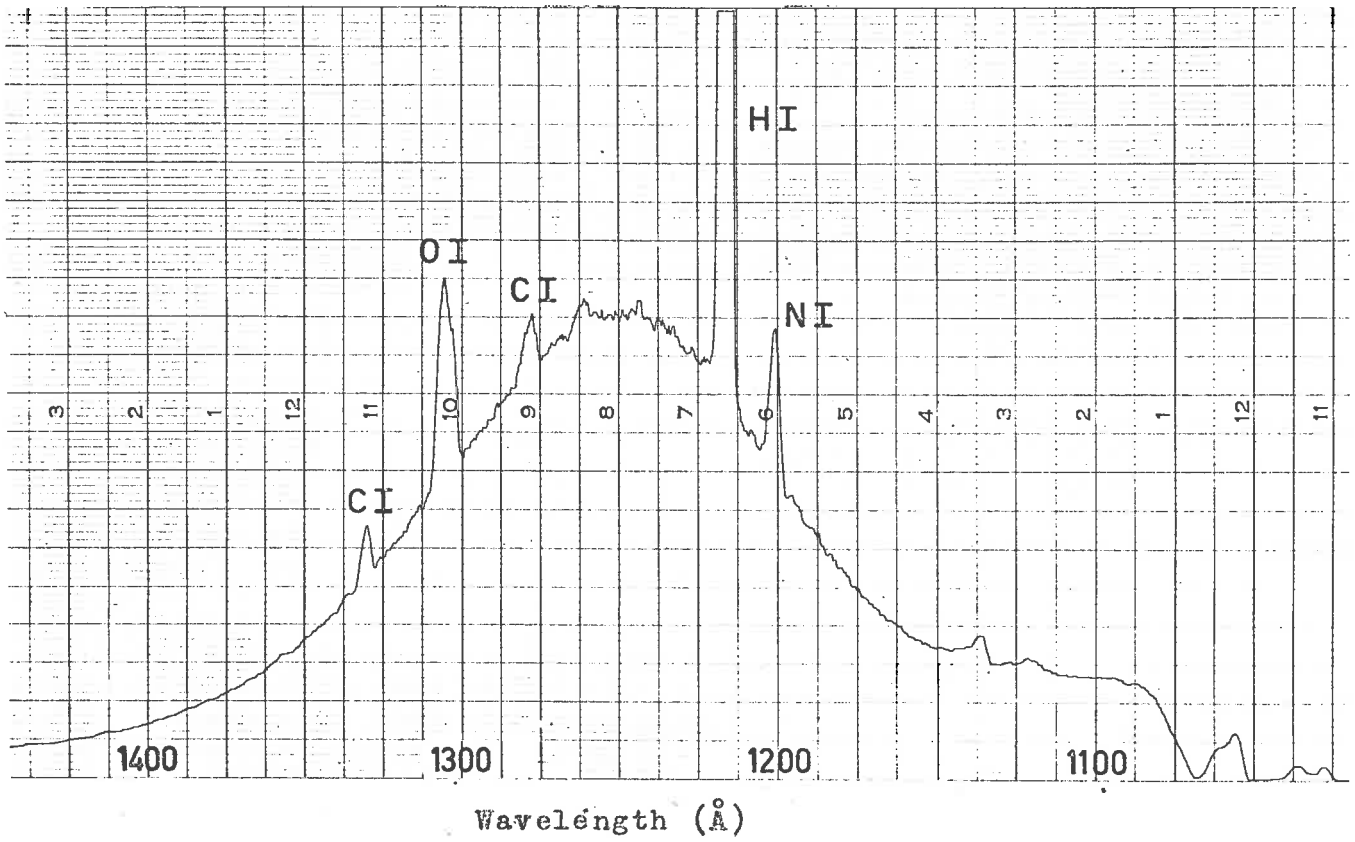

Figure 3.5 Spectrum from the high pressure discharge lamp using argon.

instrument and is fitted with a concave grating of 600 lines/mm blazed for 2000Å.

The first order dispersion of the instrument is approximately 34Å/mm giving a best usable resolution of about 1Å corresponding to slit widths of 30 microns. Variable width bilateral slits are fitted allowing a choice of band pass for the instrument. The monochromator is restricted to first order but suffers a slight disadvantage in that a small correction must be made for the background light (that is light of wavelengths substantially different from that set on the machine) which is scattered into the exit beam (see section 3.2).

The "wavelength" emerging from the exit slits may be set manually or a range of wavelengths can be scanned electrically at various speeds with a synchronous motor. A feature of this particular type of instrument is that focus is maintained at the exit slit while the wavelength is altered merely by a rotation of the grating on its axis.

The main chamber containing the grating is evacuated with a conventional 4" oil diffusion pump surmounted by a water cooled cold trap and backed by an oil filled rotary pump. The chamber may be evacuated to approximately 2×10^{-7} torr and the system is

adequately protected against failure of power or failure of cooling water.

In normal use a Hinteregger type lamp is fitted to the entrance port and the system is operated without a window between the lamp and grating chamber. Gas from the lamp is, however, constrained to flow through only the slit opening into the main chamber. This aperture may typically be 4mm x 30 microns and, with a pressure of about 2 torr of hydrogen in the lamp, the main chamber can be maintained at approximately 10^{-5} torr.

In order to operate the lamp with high pressures of argon the entrance slit assembly was modified to allow a high speed Rootes pump with a suitable backing pump to be connected immediately after the entrance slits. This allowed a large proportion of the gas leaking through from the lamp to be pumped away directly without it entering the main chamber. With this arrangement, and a pressure of about 50 torr in the lamp, the pressure in the main chamber could be maintained at approximately 10^{-4} torr.

3.1.3 Detectors

Detectors for the vacuum ultraviolet region fall into two general classes; those which are used to

measure the absolute flux of the radiation falling on them and those used to measure relative intensities of radiation.

The first class of detectors is far less common since available fluxes in this spectral region are generally low and most "absolute" radiation detectors are relatively insensitive. Thermopiles have been used with some measure of success (Packer and Lock, 1951; Watanabe and Inn, 1953; Knapp and Smith, 1964) but, in general, elaborate precautions must be taken to measure signals which are of the order of the magnitude of the background from these detectors. Also in this class are ionisation chambers, filled with one of the rare gases, which make use of the fact that above the ionisation threshold for the gas the quantum efficiency is 100%. This type of detector is rather clumsy to use and is limited to wavelengths shorter than 1022Å (the ionisation threshold of xenon). Samson (1964) and Metzger and Cook (1965) have used this type of detector to determine relatively low absolute fluxes quite successfully.

The second class of detectors is widely used where measurements of absolute flux are not necessary; most detectors which fall into this category are

relatively simple to use. By far the most useful detector is a photomultiplier tube which has been made sensitive to this region of the spectrum with a phosphor (usually sodium salicylate). Other detectors include gas filled ionisation chambers and platinum cathode photomultipliers.

3.1.3(a) Sodium Salicylate

Vacuum ultraviolet radiation incident on sodium salicylate causes it to fluoresce with a peak in the spectral distribution of the emitted radiation at about 4250Å. The spectral distribution of this radiation is quite well matched with the spectral sensitivity of a photomultiplier with an S-type cathode and these photomultipliers are generally used to view the fluorescent radiation. This particular phosphor has several advantages over most others.

Firstly, it has a high quantum efficiency (94% at about 1200Å) and the relative quantum efficiency as a function of wavelength is reasonably constant from 500-3000Å although there is a slight increase in efficiency from 1000-1600Å (Watanabe and Inn, 1953; Allison et al, 1964; Samson, 1964; Knapp and Smith, 1964). Secondly, although the relative quantum efficiency decreases with the age

of the coating, this effect is not a rapid one (0.06% per hour). This decrease is due to a combination of two effects; a decrease due to prolonged exposure inside the vacuum system, largely caused by exposure to minute traces of oil vapour, and a decrease due to exposure to a large number of energetic photons. (Samson, 1964; Knapp and Smith, 1964). Thirdly, sodium salicylate is stable under vacuum; an important feature, since the fluorescent material is always inside the vacuum system (Allison et al, 1964). Finally, the material is readily available and easy to apply to most surfaces.

In the present work, sodium salicylate was applied, either directly to the face of the photo-multiplier tube or to a glass plate or metal surface, by spraying a solution of the material in ethyl alcohol onto the surface with an atomiser and drying the droplets of solution as they fell, with a jet of warm air. Coatings were kept relatively thin where the fluorescent radiation was being observed in transmission, to avoid absorption by the fluorescent material itself. In cases where large areas of sodium salicylate were to be viewed with the usual 95145 EMI photomultiplier, which has a 2" diameter cathode, a perspex light pipe was optically

coupled between the glass plate coated with sodium salicylate and the photomultiplier. This was necessary when long cell lengths were being used in order to collect all the radiation emerging from the exit slit, as the beam from the monochromator diverges quite rapidly. The light pipe served to increase the collecting efficiency of the detector.

In all cases the photomultipliers were operated with the cathode at negative high voltage and this made it necessary to introduce a shield between the photomultiplier and the earthed case in which it was normally operated. A sheet of aluminised Mylar wrapped around the glass envelope and connected to the cathode potential proved to be an adequate electrostatic shield.

3.1.3(b) Other Detectors

A gas filled ionisation chamber was also used as a detector; this device has the advantage that it is sensitive to only a narrow band of wavelengths, thus overcoming the problem of scattered light of undesirable wavelengths which may enter the exit beam. The ionisation chambers were constructed by Carver and Mitchell (1964) and a number of different bandpass detectors

was available. For the experiment using molecular oxygen as the absorbing gas, the chosen chamber had a sapphire window and was filled with mesitylene giving it a spectral sensitivity limited to the region 1420-1480Å. This detector was used in determining precise absorption coefficients for the peak of the Schumann-Runge continuum.

For the region 2000-2350Å a "solar blind" C.B.S. type CL1064 photomultiplier was used directly in order to minimise corrections for background light. The spectral response of this tube is limited to the region 1700-2600Å.

3.1.4. Absorption Cells

Because of the wide range in the magnitude of the absorption coefficients which were measured a wide range of cell lengths was employed. The absorption coefficient for molecular oxygen varies over about 7 orders of magnitude over the range of wavelengths from 1050-2350Å and in order to keep within a convenient range of gas pressures in the cell it was necessary to alter the length of the cells. An attempt was made to maintain approximately 50% attenuation of the incident flux on passing through the cell at all times.

The absorption cells employed ranged in length

from 0.13cms to 300cms, all were made of copper and all were fitted with a lithium fluoride window at the entrance end of the cell; all cells were fitted with 'O' rings so that the lengths could be altered easily.

The shortest absorption cell was variable in length from about 1mm to 20mm depending on the size of the spacer placed in it. The next range of cells were variable in length from 2cms to 20cms in steps of about 5cms and a large 6" diameter cell was adjustable in length from 50cm to 300cm in 50cm steps.

All the cells were evacuated with a 2 inch oil diffusion pump fitted with a liquid air cold trap and backed by a rotary pump. Pressures of approximately 10^{-6} torr could be maintained in all cells.

3.1.5 Beam Splitter

In order to compute the absorption cross section of a gas it is necessary to measure the intensity of the radiation incident on and transmitted through a gas. Since the light sources are not perfectly stable devices, ideally, the measurement of these two intensities must be made simultaneously. This was achieved by the use of an unusual type of beam splitter due to Ditchburn (1962). Conventional beam

splitters use either mirrors or prisms and these are difficult to use in the vacuum ultraviolet region of the spectrum because of the low reflectivity of mirrors and low transmissivity of prisms. This difficulty is overcome by allowing the radiation emerging from the exit slit of the monochromator to fall on a grid of wires coated with sodium salicylate; some of the radiation passes through the grid and subsequently through the cell and is detected at the other end, whilst the remainder causes the sodium salicylate on the grid to fluoresce and this fluorescent radiation is detected with a photomultiplier. This photomultiplier is placed at right angles to the beam of emergent vacuum ultraviolet radiation and the collecting efficiency of the device is enhanced by the use of a light pipe (see figure 3.6.).

If now, the ratio of the currents from the two photomultipliers is measured with the cell evacuated and then with the cell containing the absorbing gas, the ratio of these two measurements will be the required transmittance.

3.1.6. Recording

The currents from the two photomultipliers

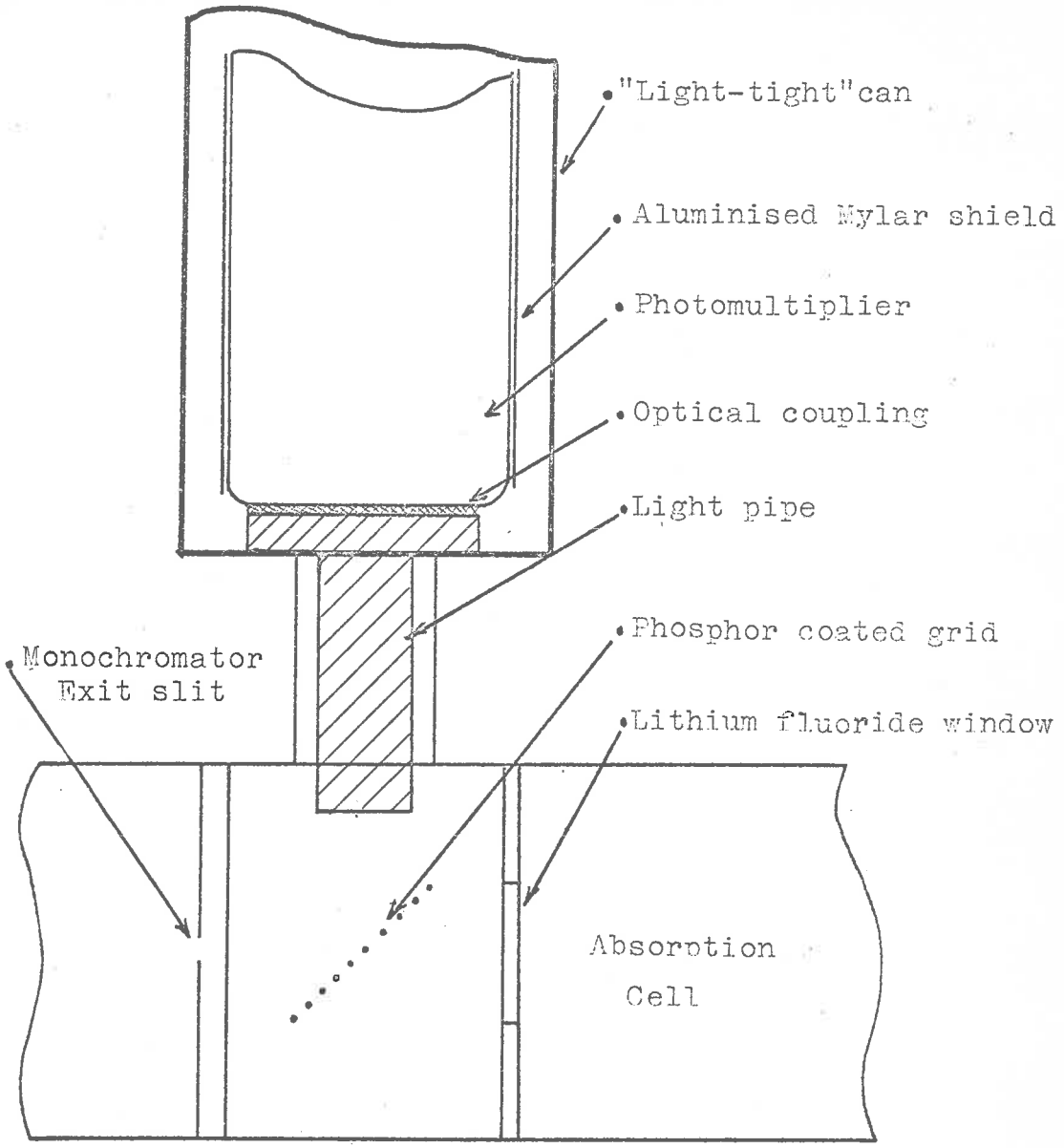

Figure 3.6 The "beam-splitter".

were D.C. amplified (Hewlett-Packard micro-microammeters model 425-A) and recorded using potentiometric chart recorders (Kent). Initially two separate recorders were used (one for each photomultiplier) but subsequently a ratio recorder was developed which allowed direct recording of the ratio of the currents from the two detectors.

3.1.7. Gas and Pressure Monitoring

"Medical" grade oxygen obtained from Commonwealth Industrial Gases was used for this work and purified by passing it into a liquid air trap where it was condensed and boiled off under vacuum for some time before being admitted to the cell through a fine control needle valve. Pressures in the cell were monitored using a Pirani gauge, McLeod gauge, oil manometer or mercury manometer. All gauges, with the exception of the Pirani gauge, were trapped with "cold thimbles" surrounded by a freezing mixture of 50% carbon tetrachloride and 50% chloroform which freezes at approximately -80°C. The oil manometer was filled with Apiezon "C" oil (S.G = 0.875) and was degassed by heating under vacuum for some time before being used. This gauge was used for pressures in the range 1 torr

to 20 torr. Pressures below this were measured with the McLeod gauge and pressures above this with the mercury manometer.

3.2. Scattered Light

When using sodium salicylate detectors as described above, corrections were made for the scattered light, of undesirable wavelengths, in the beam from the monochromator. This involved measuring the intensity and wavelength distribution of this light by placing various windows in the path of the beam. With a window such as lithium fluoride in the path of the beam and with the monochromator set at a wavelength below the transmission limit for this material (<1050Å) only the light of wavelengths above 1050Å is transmitted and measured by the detectors. If now a calcium fluoride window is placed in the beam instead of the lithium fluoride and the monochromator setting left unaltered the intensity of the light incident on the detectors is found to be the same. Barium fluoride, sapphire and spectrosil windows produced a similar result indicating that the scattered light is of a wavelength greater than 1600Å. With a spectrosil window (transmission limit of 1500Å) in the beam the monochromator was scanned from 1050Å to 1500Å and the

intensity of the radiation received by the detectors remained constant indicating that the amount of scattered light is independent of monochromator setting at least in this wavelength region. A correction could then be made for the scattered light by subtracting the appropriate amount of current from the photomultiplier signal. This correction factor was checked throughout the experiment by scanning the monochromator to just below 1050Å and placing a lithium fluoride window in the beam. With this arrangement the detector signals were then offset with the zero control of the current amplifiers.

The mesitylene filled ionisation chamber with a sapphire window was used as a detector at the remote end of the cell to verify the results in the region 1420-1480Å. This detector is insensitive to scattered light and the results showed that the previous corrections for scattered light were quite adequate.

The C.B.S. photomultiplier used as the detector for the region 2000-2350Å also has the advantage of not being sensitive to as much of the scattered light. This photomultiplier used directly (that is without a phosphor) was much more sensitive

to radiation in this wavelength band than was the sodium salicylate sensitised 95145 photomultiplier and this was a decided advantage.

3.3 Procedure

For most of the work on molecular oxygen the many lined spectrum of molecular hydrogen was used as the light source. The power supply for the discharge lamp was operated in the A.C. mode with 60 ma through the lamp. The slits of the monochromator were set at 30 microns giving a resolution of approximately 1Å.

In the region from 1250Å-1750Å a beam splitter monitor and a salicylate sensitised photomultiplier at the end of the cell detected the radiation and the currents from the two photomultipliers were amplified and fed to separate chart recorders. This method involved scanning a wavelength band with the cell evacuated and recording the two currents, filling the cell and scanning and recording again, then evacuating the cell for a third scan to check the stability of the gain of the system. The fact that the grid was coated with phosphor on one side only and the fact that the fluorescent intensity of the radiation from the grid decreased

according to an inverse square law meant that, for the lengths of cells used, the remote detector did not respond to any of the fluorescent radiation from the grid. Pressures in the cell were arranged so that there was approximately 50% absorption over each small wavelength band.

The absorption coefficient of molecular oxygen varies rapidly with wavelength in the region from 1050-1250Å (see section 3.4.5). The molecular hydrogen spectrum in this region contains many lines and in order to avoid errors in the results which might have arisen from the misalignment of successive wavelengths scans the data were taken in a different way. The current I_o from the photomultiplier behind a sodium salicylate coated glass disc at the remote end of the absorption cell was measured with the cell evacuated. Gas was admitted into the cell until the light intensity had fallen to about 50% of its initial value; the pressure and temperature of the gas and the current I from the photomultiplier were noted. The cell was then evacuated and the value of I_o checked for any variation due to charges in lamp intensity. This procedure was repeated several times at each wavelength and then the absorption coefficient calculated from Beer's law. The use of

different cell lengths enabled a relatively small range of pressures to be used.

For the remainder of the wavelength range the ratio recorder was used to record directly the ratio of the two photomultiplier tube currents while the wavelength was scanned both with the cell evacuated and containing a particular pressure of gas. Some raw data of this type are shown in figure 3.7 where the ratio of the two detectors is shown both with the cell evacuated and containing a particular pressure of absorbing gas.

When the monochromator had been modified to allow use of the high pressure argon discharge lamp, measurements in the region 1250-1500Å were repeated with no significant difference in the results.

3.4 Discussion

Previous measurements of the absorption spectrum of molecular oxygen have been made by many workers and the results are presented in a review by Watanabe (1958). Since 1958, absorption coefficients from 1050-1800Å have been measured by Metzger and Cook (1964) the region from 1850Å to 2500Å has been investigated by Ditchburn and Young (1962) and there have been several reinvestigations of the region containing the Schumann-Runge bands (Bethke, 1959; Thompson et al, 1963).

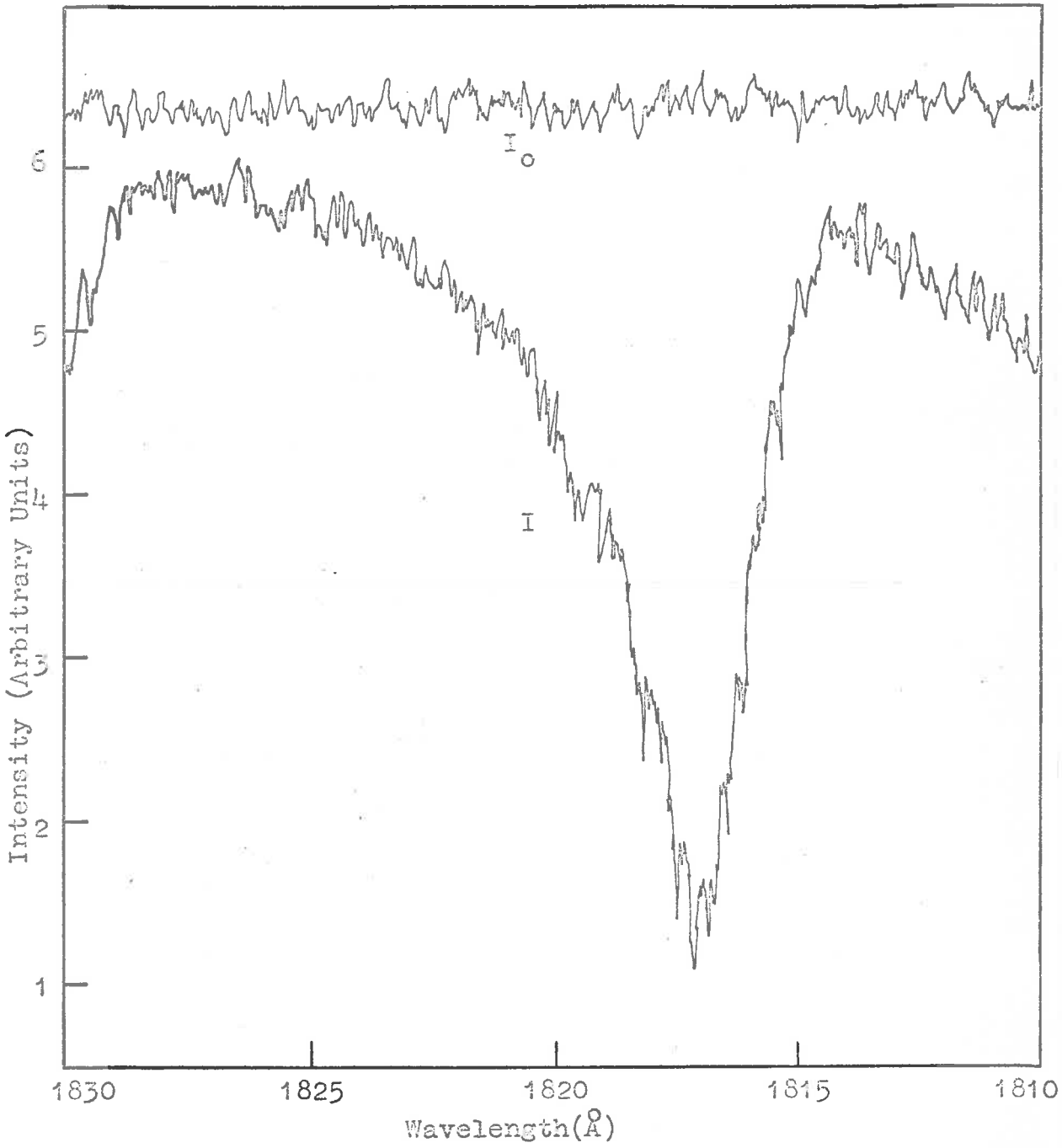

Figure 3.7 Data recorded on the ratio-recorder showing absorption by molecular oxygen.

In this latter region many early workers measured an apparent absorption coefficient which depended on the pressure in the absorption cell, the layer thickness of the gas and the resolution of the dispersing intrument (Watanabe et al, 1953; Ditchburn and Heddle, 1953; 1954). Bethke, 1959, measured the absolute absorption coefficients by pressure broadening the lines and thus smearing out all the structure; these measurements are perhaps the only reliable ones in this region apart from those presented in this thesis.

3.4.1 Potential curves for Molecular Oxygen

The potential energy curves for molecular oxygen are shown in figure 3.8 after Gilmore (1965).

The important band systems leading to ground state absorption in the vacuum ultraviolet region of the spectrum are the Schumann-Runge system $B^3\Sigma_u^- - X^3\Sigma_g^-$ and the Herzberg systems, the strongest of which is $A^3\Sigma_u^+ - X^3\Sigma_g^-$.

The ground state $X^3\Sigma_g^-$ is shown along with many other states, some of them repulsive, leading to the dissociation products $O^3P + O^3P$ at 5.08ev. Included in these states is the upper state of the Herzberg I system, $A^3\Sigma_u^+$.

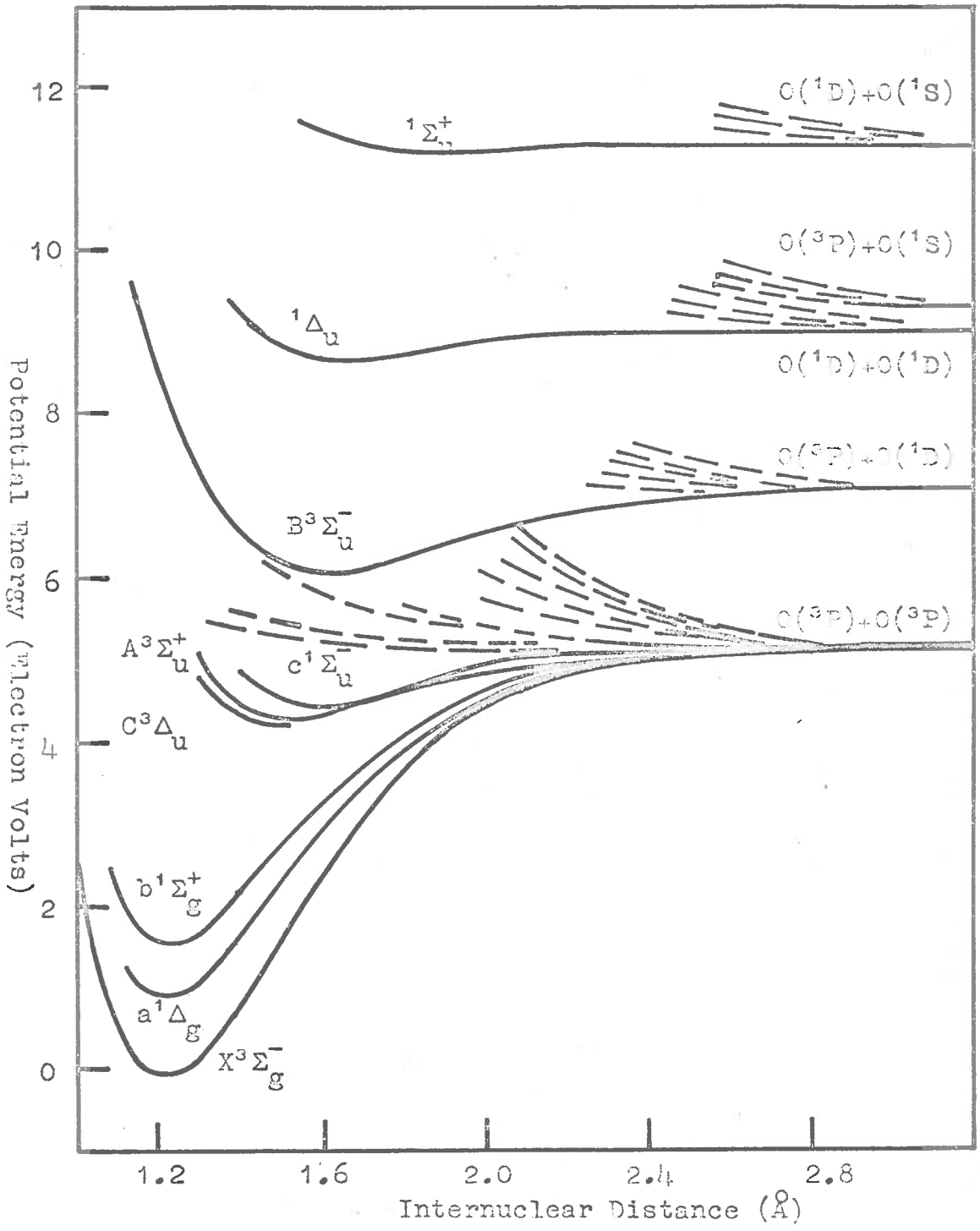

Figure 3.8 Potential energy curves for molecular oxygen (after Gilmore, 1966).

The $B^3\Sigma_u^-$ state which is the upper state of the Schumann-Runge system leads to the dissociation $O^3P + O^1D$ at 1751Å. Some other states are shown leading to the dissociation products $O^3P + O^1S$ at 1333Å and $O^1D + O^1D$ at 1376Å. These states are thought to account for the observed features in the absorption spectrum of oxygen on the short wavelength side of the peak of the Schumann-Runge continuum (Tanaka, 1952).

3.4.2 The Herzberg system

A system of bands and an associated continuum in the absorption spectrum of molecular oxygen between 1850Å and 2600Å was first discovered by Herzberg (1932) who attributed the bands to the forbidden transition $X^3\Sigma_g^- - A^3\Sigma_u^+$ and the continuum to the dissociation $O_2\ X^3\Sigma_g^- \rightarrow O^3P + O^3P$. This is known as the Herzberg I system.

The other Herzberg systems $X^3\Sigma_g^- - C^1\Sigma_u^-$ and $X^3\Sigma_g^- - C^3\Delta_u$ are much weaker and need not be considered in the present discussion.

In the present work absorption coefficients were measured in the continuum region using 0.5 to 3 metre path lengths and pressures from 0.5 to

2 atmospheres in order to measure the relatively low cross-sections. Since there is no structure in the absorption spectrum the analysis is simple and it is not necessary to measure equivalent widths in this region (c.f. section 3.4.3). In agreement with the results of Ditchburn and Young, 1962, the measured cross sections (σ) were not independent of the pressure (p) of absorbing gas and in fact σ was found to increase linearly with p over the pressure range used. This is probably due to the formation of the complex molecule O_4 as suggested by Ditchburn and Young. The concentration of the complex molecule will depend on pressure and may well contribute a term proportional to p to the measured cross-section. The absorption cross-sections measured atvarious pressures and the values extrapolated to zero pressure are shown in figure 3.9. The probable error in these determinations is about 5% and the data were obtained using a monochromator slit width of 60 microns corresponding to a calculated resolution of 2Å. In general, the results compare favourably with those of Ditchburn and Young who used photographic recording techniques and long paths (5, 10 and 30 metres) and high pressures (0.2-5

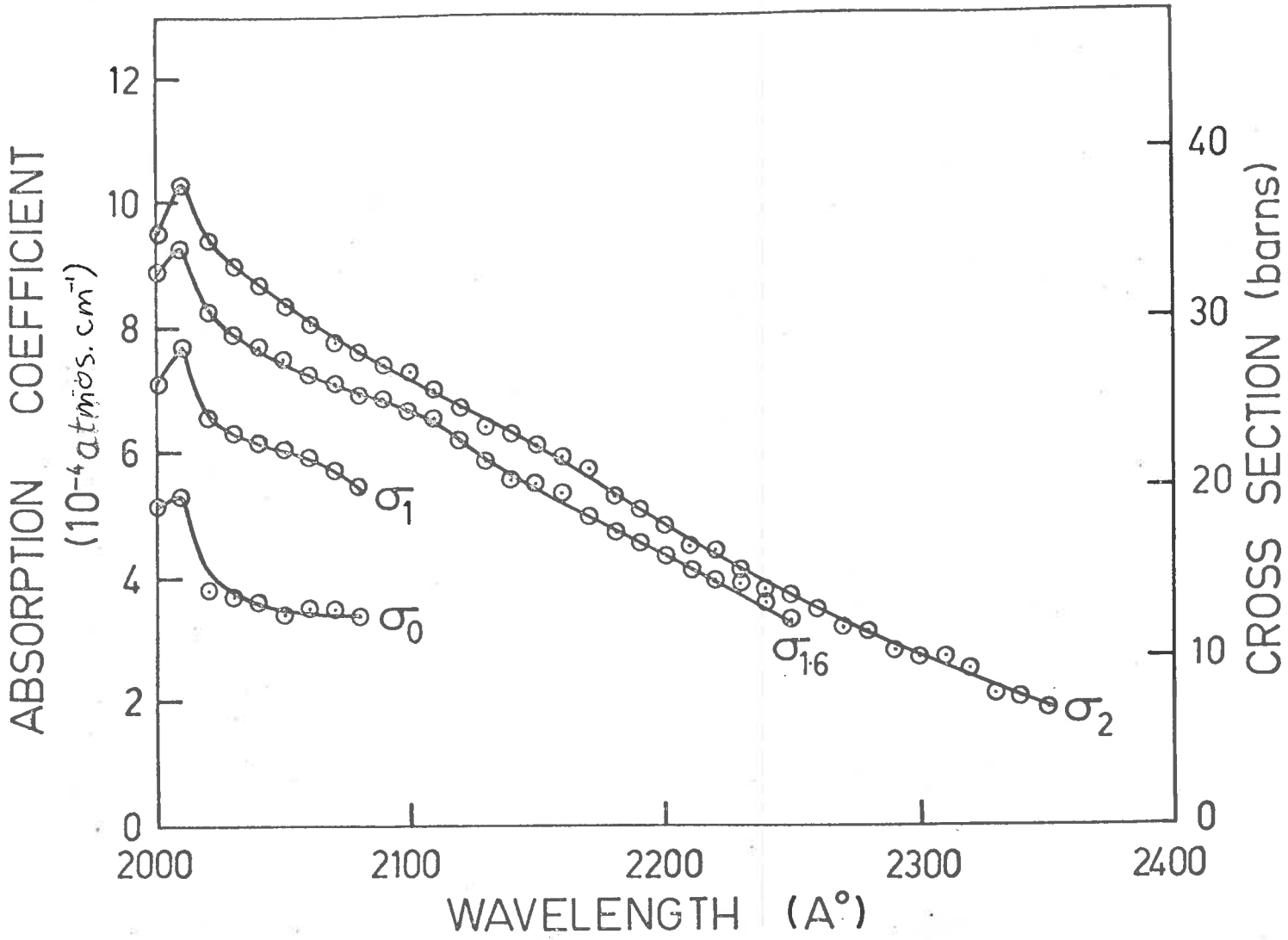

Figure 3.9 Absorption cross sections of molecular oxygen in the region 2000-2350Å. σ_p is the cross section measured at a gas pressure of p atmospheres.

atmospheres to measure the absorption coefficients of oxygen from 1850-2500Å. The cross-sections in this experiment are generally about 10-15% higher than the values reported by these workers.

This continuum is important since it is probably the main source of oxygen atoms below 80km in the atmosphere (Ditchburn and Young, 1962).

3.4.3 Schumann-Runge bands

The region between 1750Å and 2030Å is occupied by the Schumann-Runge bands corresponding to the transition $B^3\Sigma_u^- - X^3\Sigma_g^-$.

A rotational analysis of the Schumann-Runge bands in absorption has been made by Curry and Herzberg (1934) and by Knauss and Ballard (1935). Since then a number of other investigators (e.g. Brix and Herzberg, 1954; Wilkinson and Mulliken, 1957; Watanabe et al, 1953; Ditchburn and Heddle, 1953; 1954; Thompson et al, 1963) have measured absorption coefficients in this region. In early investigations the resolution of the instruments used was insufficient to resolve the rotational structure of the band system. This led to results taken at any given pressure in which the maxima of the vibrational bands were suppressed and the full

depths of the minima between the bands were not resolved. Bethke (1959) has measured the absorption coefficients of molecular oxygen in this region at extremely high pressures (up to 2000 p.s.i.a.) and this had the effect of pressure broadening the rotational lines giving a measure of the true integrated absorption coefficients for the bands.

The estimated width of the rotational lines if they are only Doppler broadened is given by the expression in section 2.4 and if the appropriate values are substituted the result $\alpha_D = 0.001\text{Å}$ at room temperature is obtained.

Using the expression in section 2.7 the collision frequency can be calculated and the pressure broadened width at 1 atmosphere and 20°C is approximately 0.007Å and is proportional to pressure. This agrees well with an estimate which can be obtained from Bethkes results. In his work with an instrument resolution of 0.4Å the lines appear to be pressure broadened to perhaps 0.2Å wide at a pressure of 266 p.s.i.a. This gives a pressure broadened width at 1 atmosphere estimated as $0.2/17 = 0.01\text{Å}$.

In the present experiment a cell length of

143cm and gas pressures varying between approximately 1 torr and 1 atmosphere have been used to measure absorption in the 1-0 to 16-0 vibrational bands with an instrument resolution of 2Å.

The values of W, the equivalent width, for each of the bands were measured at different pressures and the variation of $\bar{A}$ with the pressure p is shown for some of the bands in figure 3.10. As was pointed out in section 2.9 this particular variation of W with p is not amenable to a band analysis treatment due to the gaps in the distribution of the lines and the mixture of strong and weak absorption lines. The measurements of the absorption coefficient are, however, intended for use in measurements of the absorption of solar radiation by the upper atmosphere and thus need only be determined for the range of layer thicknesses likely to be used in such calculations. The expected layer thicknesses might be in the range 0.1 to 10 atmosphere-cms. for an integration over a suitable height range (1-10km).

The values of k, the apparent absorption coefficients, were found to vary empirically as $\frac{1}{\sqrt{p}}$ at least over the range of p from 1 to 50 torr, that is, over a range of n (the layer thickness) from 0.3 to

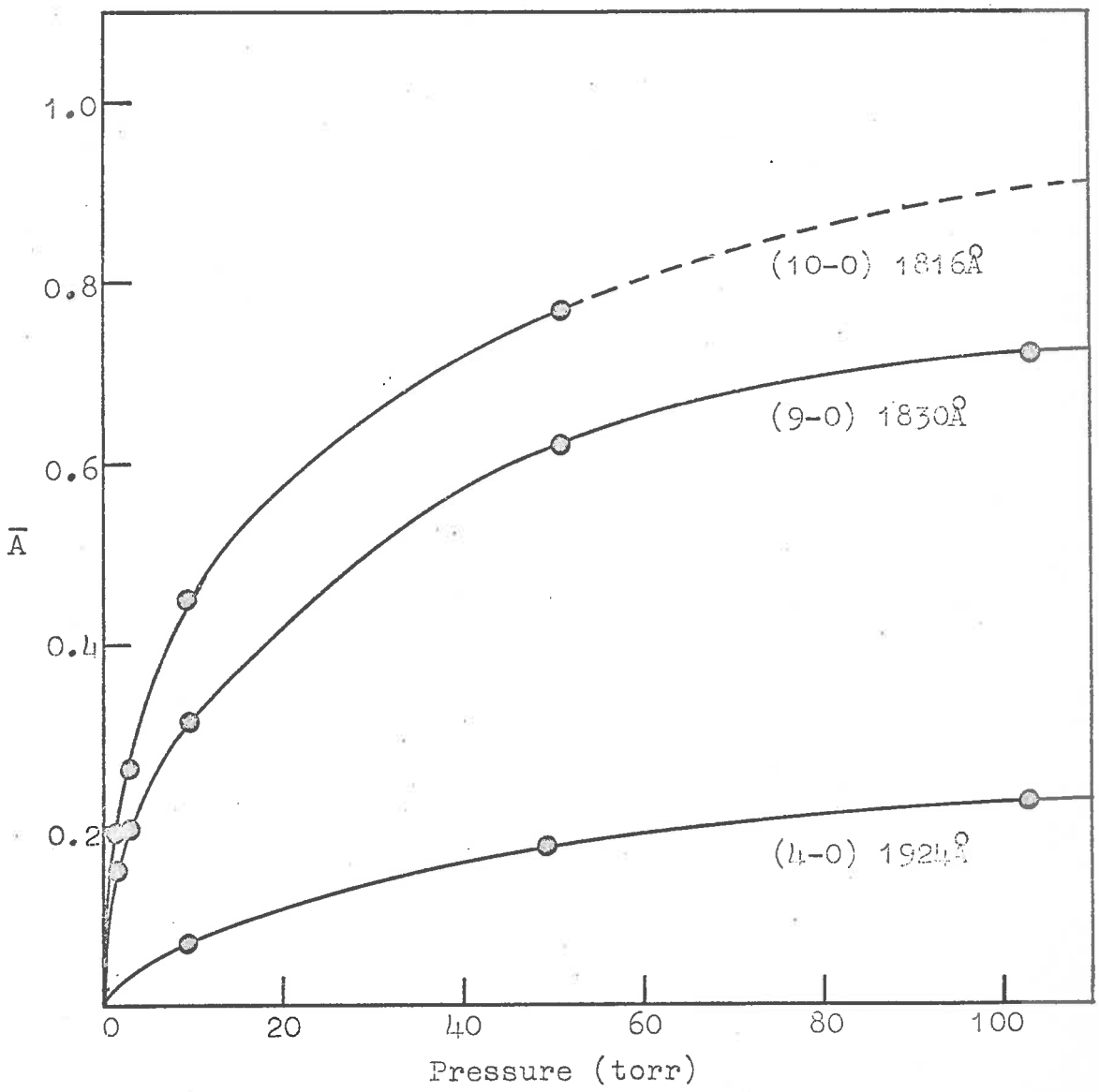

Figure 3.10 Curves of growth for some of the Schumann-Runge bands in molecular oxygen.

10 atmosphere cms. This then provides a reasonable extrapolation procedure for values of n approximately within these limits. For the range 1750-1930Å figure 3.11 shows the cross-sections σ_e evaluated for those values of n for which the transmitted beam was attenuated by a factor $\frac{1}{e}$. The empirical relation $\sigma \propto n^{-\frac{1}{2}}$ which is illustrated for some wavelengths in figure 3.12 indicates that for a variation in n by a factor of order 10 on either side of n_e the appropriate value of σ may be estimated from the relation $\sigma = \left(\frac{\sigma_e}{n}\right)^{\frac{1}{2}}$. Unfortunately the $n^{-\frac{1}{2}}$ relation does not hold at longer wavelengths since the cross-sections in the Herzberg system contain a term which is proportional to pressure. For the intermediate region between about 1900 and 2030Å the observed cross-sections have a complicated dependence on layer thickness; figure 3.13 shows the observed cross-sections in this region taken at a pressure of 1 atmosphere with a 1.5 metre absorption cell.

3.4.4 Schumann-Runge Continuum

The region between 1250Å and 1750Å is occupied by the Schumann-Runge continuum with a maximum absorption cross-section at 1425Å. This

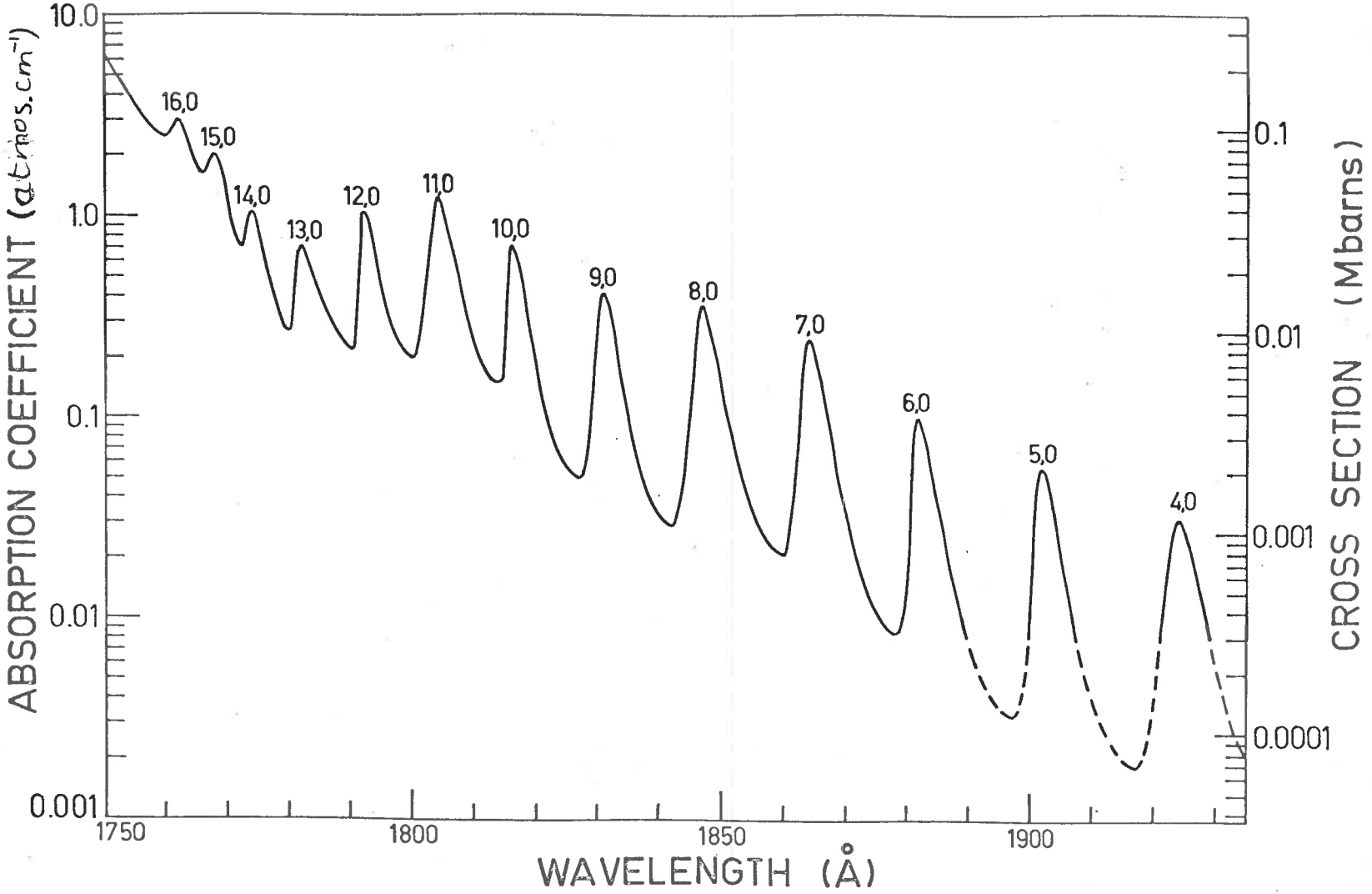

Figure 3.11 "1/e absorption cross sections" of molecular oxygen in the region 1750-1930Å

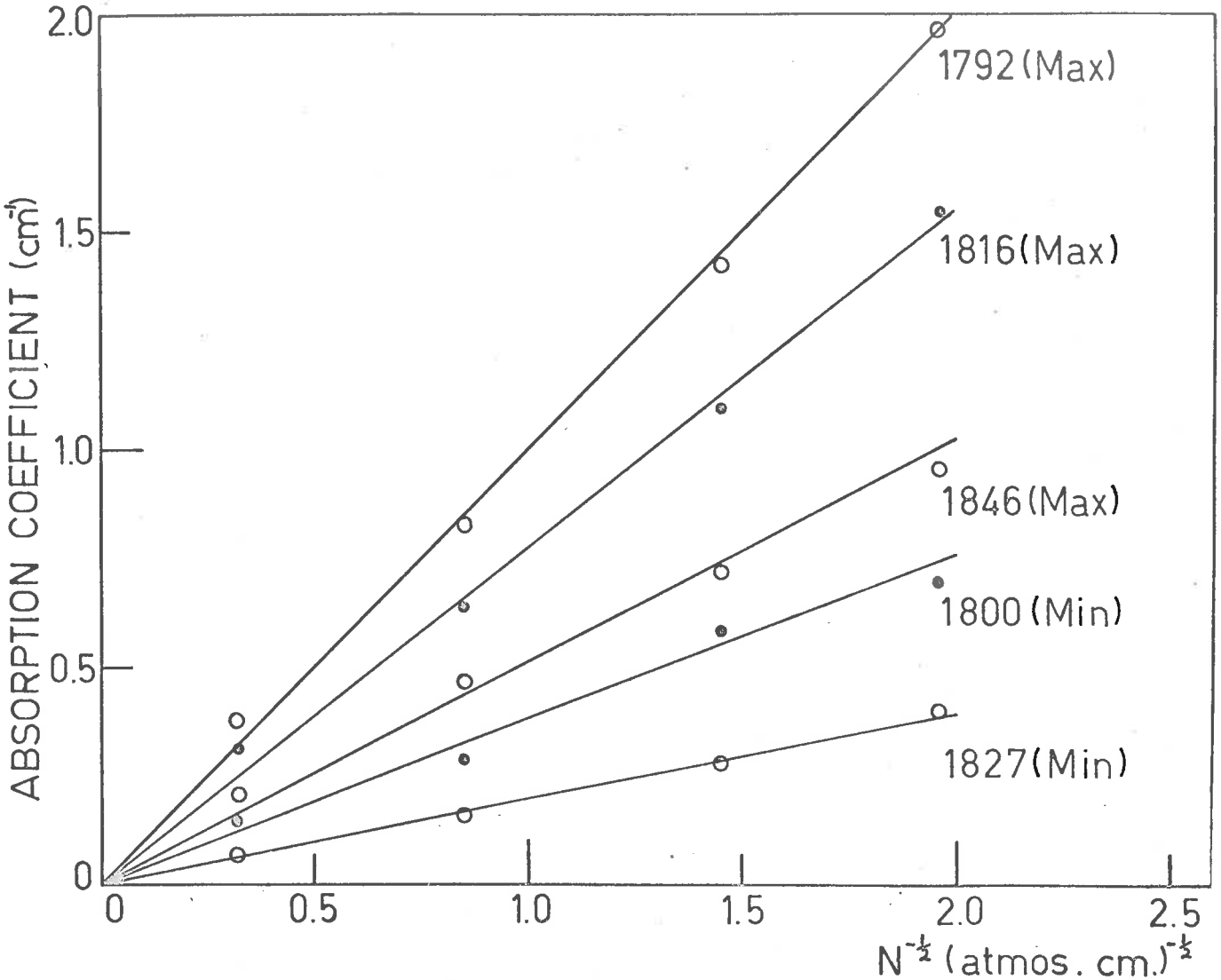

Figure 3.11 Absorption coefficients in the Schumann-Runge bands plotted as a function of the inverse square root of the layer thickness. The results are shown for some typical wavelengths where the absorption coefficient has either a maximum or minimum value.

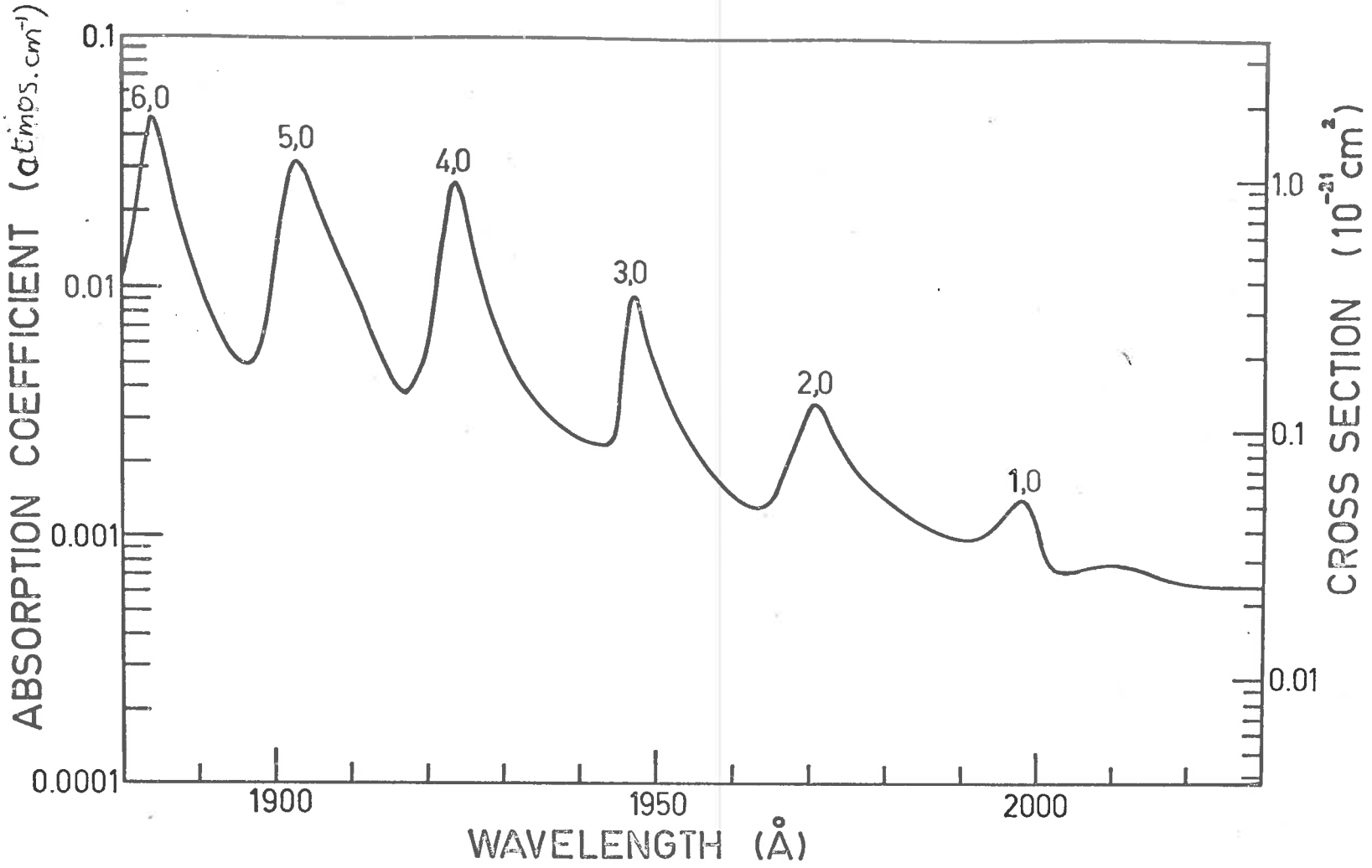

Figure 3.13 Absorption cross sections of molecular oxygen in the region 1900-2030Å measured with a path length of 1.5 metres and a gas pressure of 1 atmosphere.

involves the transition $B^3\Sigma_u^- - X^3\Sigma_g^-$ leading to the dissociation products $O^3P + O^1D$. On the short wavelength side of this continuum there are three different bands or narrow continua with maxima at 1294, 1334 and 1354Å. These have been described previously by Tanaka (1952) and the band or continuum at 1354Å is thought to be associated with the dissociation process leading to $O^1D + O^1D$. Of the other two features at least one and possibly both are thought to result in the dissociation products $O^3P + O^1S$ although this assignment is tentative. Several repulsive states of molecular oxygen certainly exist in this energy region but band assignments are uncertain.

The present data in this region were obtained using 1mm, 5cm and 10cm length absorption cells with gas pressures ranging from 2 torr to 20 torr. A monochromator slit width of 30 microns was used and this corresponds to a resolution of 1Å.

The results are shown in figures 3.14 and 3.15. The main continuum has a rather flat maximum at 1425Å where the absorption cross-section is $(1.48 \pm 0.07) \times 10^{-17} cm^2$ which is in good agreement with the value determined by other workers (e.g. Metzger and Cook, 1965; Watanabe and Marmo, 1956;

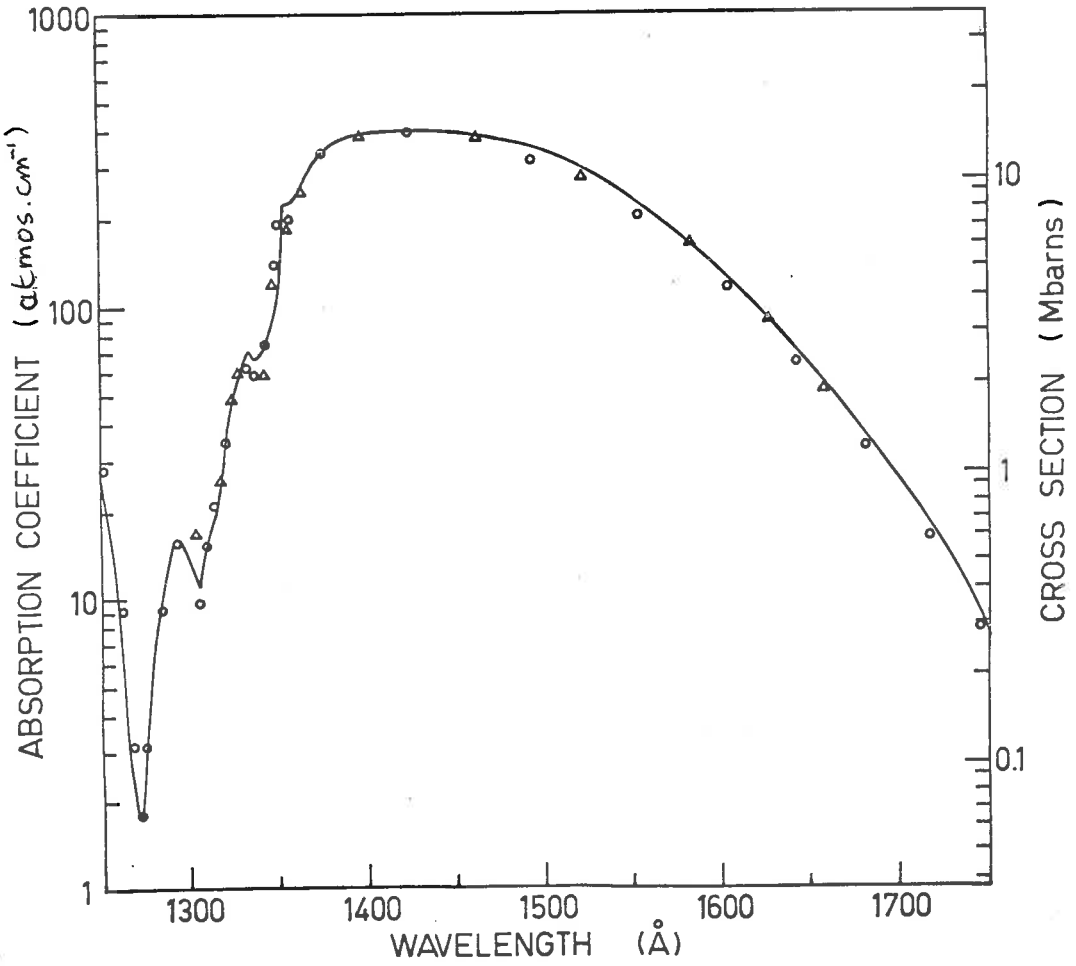

Figure 3.14 Absorption cross sections of molecular oxygen in the region 1250-1750Å. The solid line represents the results obtained in this work, the circles (o) those of Watanabe (1958) and the triangles (Δ) those of Metzger and Cook (1964).

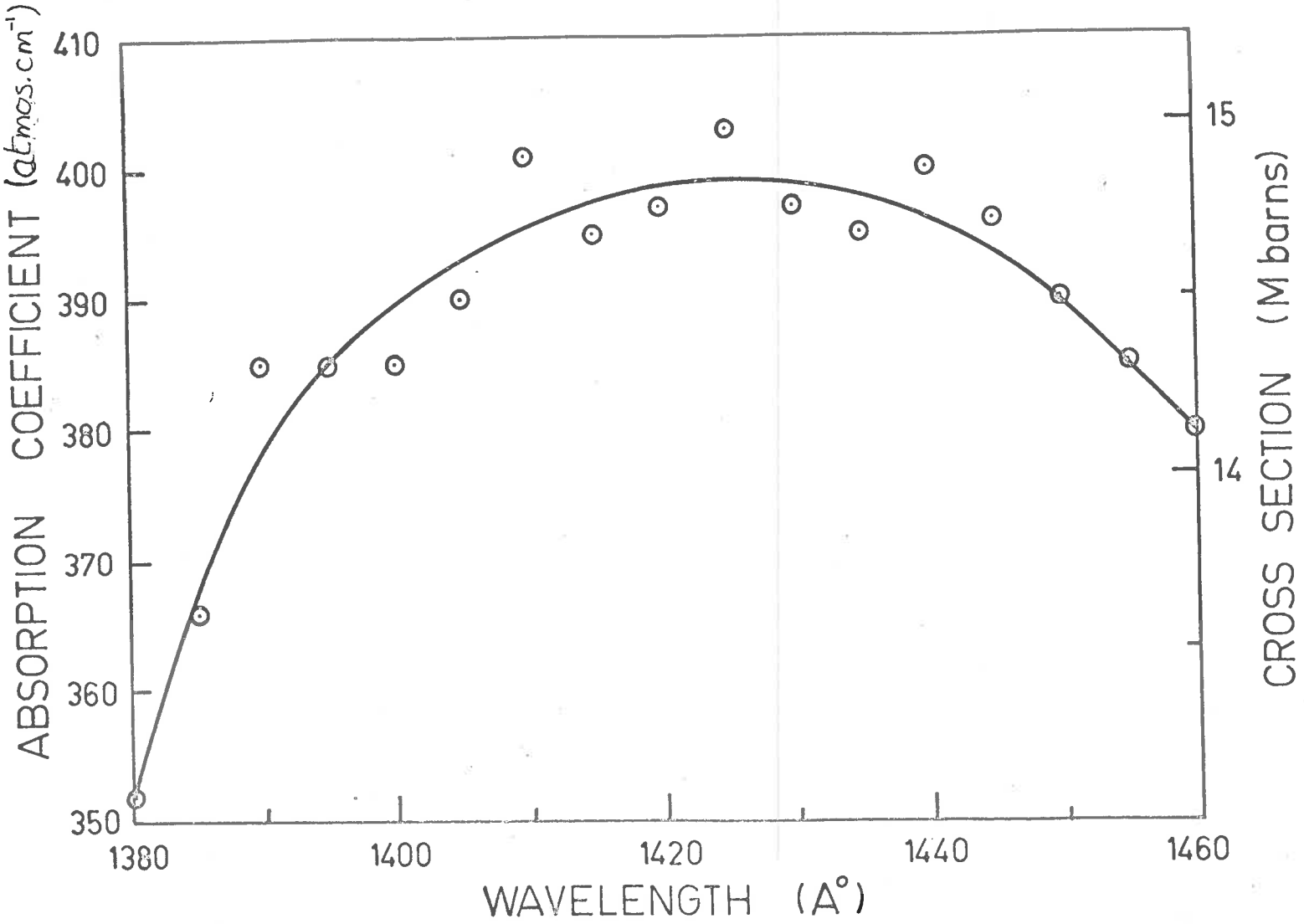

Figure 3.15 Absorption cross sections of molecular oxygen near the maximum of the Schumann-Runge continuum.

Byram et al, 1955; Watanabe et al, 1953). The cross-sections at a number of wavelengths corresponding to strong lines in the ultraviolet spectrum of the sun (Tousey, 1963) are listed in Table I. The estimated error in these cross sections is ±5% except for the OI lines near 1304Å where the error is ±10%.

Table I

Molecular oxygen absorption cross sections at solar lines

Wavelength (Å)	Solar Line	Cross-section (cm^2)
1302, 4, 6	OI	4.6×10^{-19}
1334, 5	CII	2.7×10^{-18}
1394	S_iII	1.4×10^{-17}
1403	S_iIV	1.45×10^{-17}
1548, 51	CIV	8.7×10^{-18}
1656	CI	1.9×10^{-18}
1670	A1 III, F_eII	1.55×10^{-18}

The oscillator strength for the transition $B^3\Sigma_u^- - X^3\Sigma_g^-$ was determined for the principal continuum shown in figure 3.14. The f-value (oscillator strength) is given by

$$f = 4.2 \times 10^{-3} \cdot \int_{\nu_1}^{\nu_2} k_\nu \, d\nu$$ (see section 1.2.1).

For this continuum f = 0.162 where the integration is carried out from 1300Å to 1750Å. This value is in good agreement with previous results (Ladenberg and von Voorhis, 1933; Watanabe et al, 1953).

This continuum is the principal source of oxygen atoms above ≈80km in the atmosphere (Watanabe, 1958).

3.4.5 The window region

At wavelengths between 1050Å and 1250Å molecular oxygen has a complex absorption spectrum and most observed bands have not yet been definitely classified.

The present data in this region were obtained using absorption cells varying in length from 0.1cms to 50cms and gas pressures from 1 torr to 1 atmosphere. The monochromator slits were again set at 30 microns corresponding to a resolution of 1Å.

The results are shown in figures 3.16 and 3.17 and are in agreement with those of Watanabe et al, 1953. Table II shows a comparison between the values for the ~~cross-section~~ absorption coefficient at the various windows and bands obtained in the present work together with those of

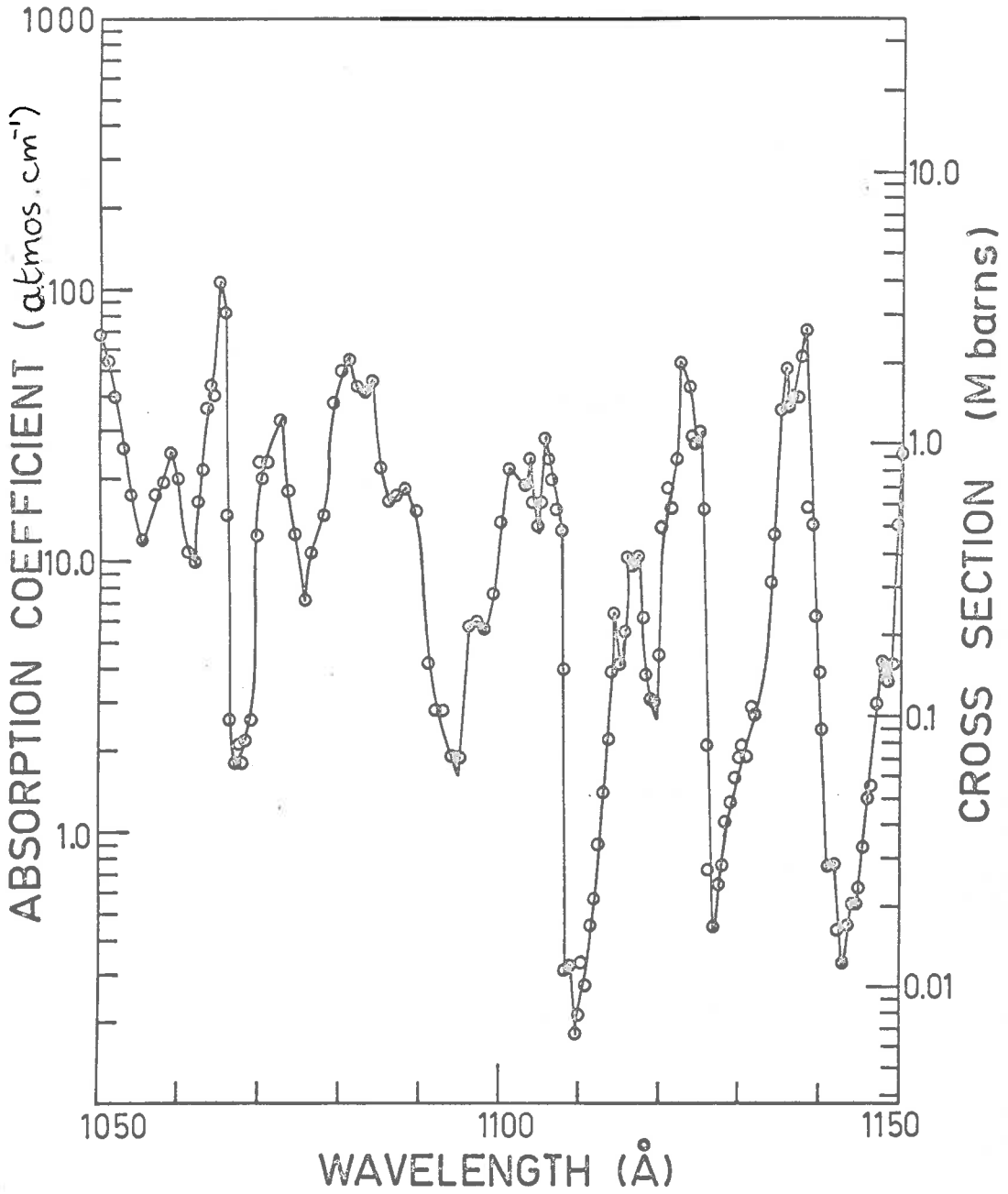

Figure 3.16 Absorption cross sections of molecular oxygen in the region 1050-1150Å.

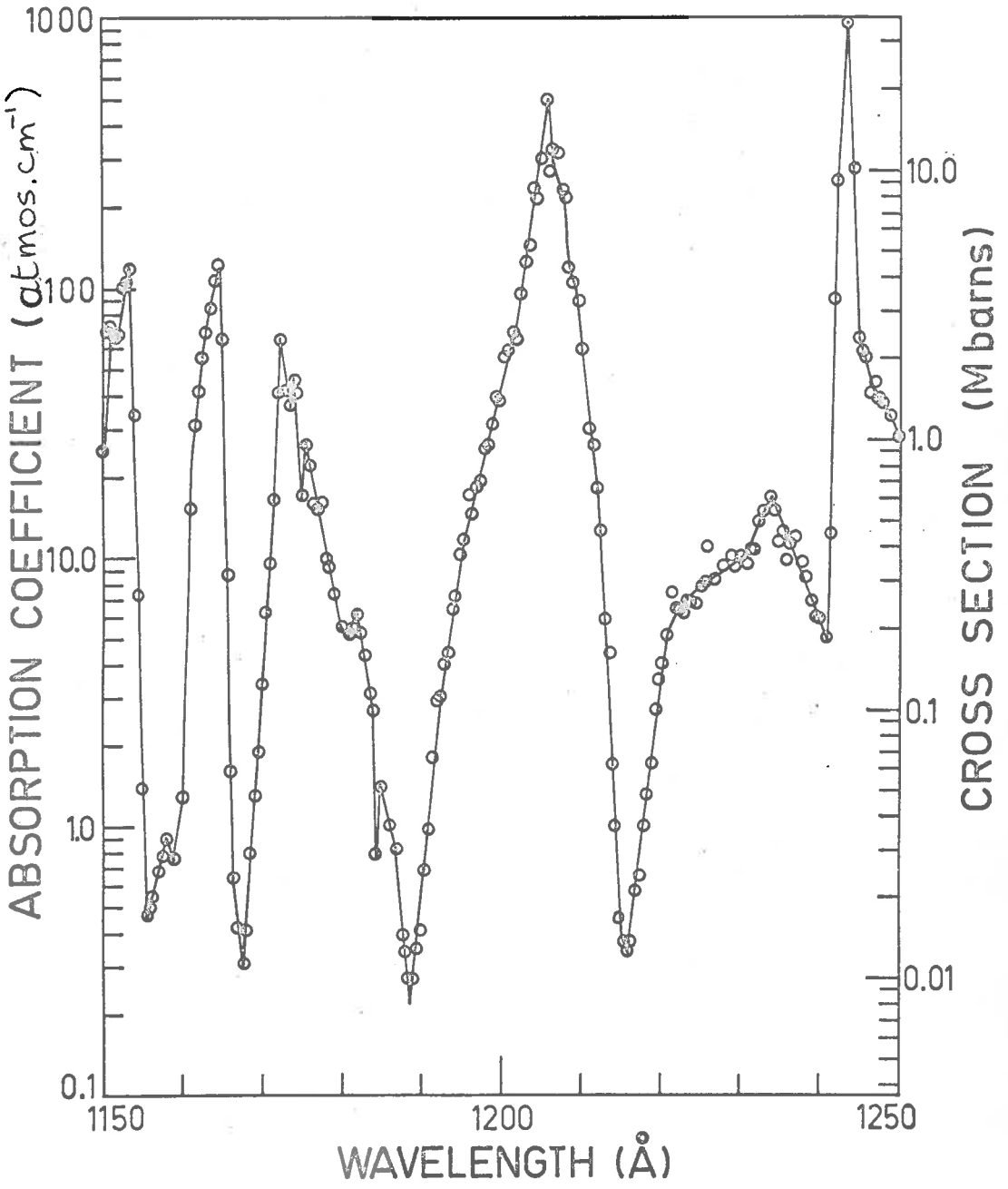

Figure 3.17 Absorption cross sections of molecular oxygen in the region 1150-1250Å.

Watanabe, 1958, and Metzger and Cook, 1964.

Table II

Absorption coefficients for molecular oxygen at various windows and bands. (atmos. cm^{-1})

Feature	Wavelength (Å)	Watanabe et al	Metzger and Cook	Present Work
Window 1	1215.7	0.27	0.28	0.28
2	1187.1	0.18	0.20	0.23
3	1166.8	0.27	0.29	0.27
4	1157.0	0.51	0.44	0.40
5	1142.8	0.26	0.31	0.29
6	1126.9	0.53	0.62	0.49
7	1108.3	0.11	0.20	0.17
Band A	1153	170	200	120
B	1205	510	430	490
C	1244	1450	1200	980

The cross-section determined around the region of the wavelength of the Lyman-α line is shown in figure 3.18.

The cross-section at Lyman-α evaluated at

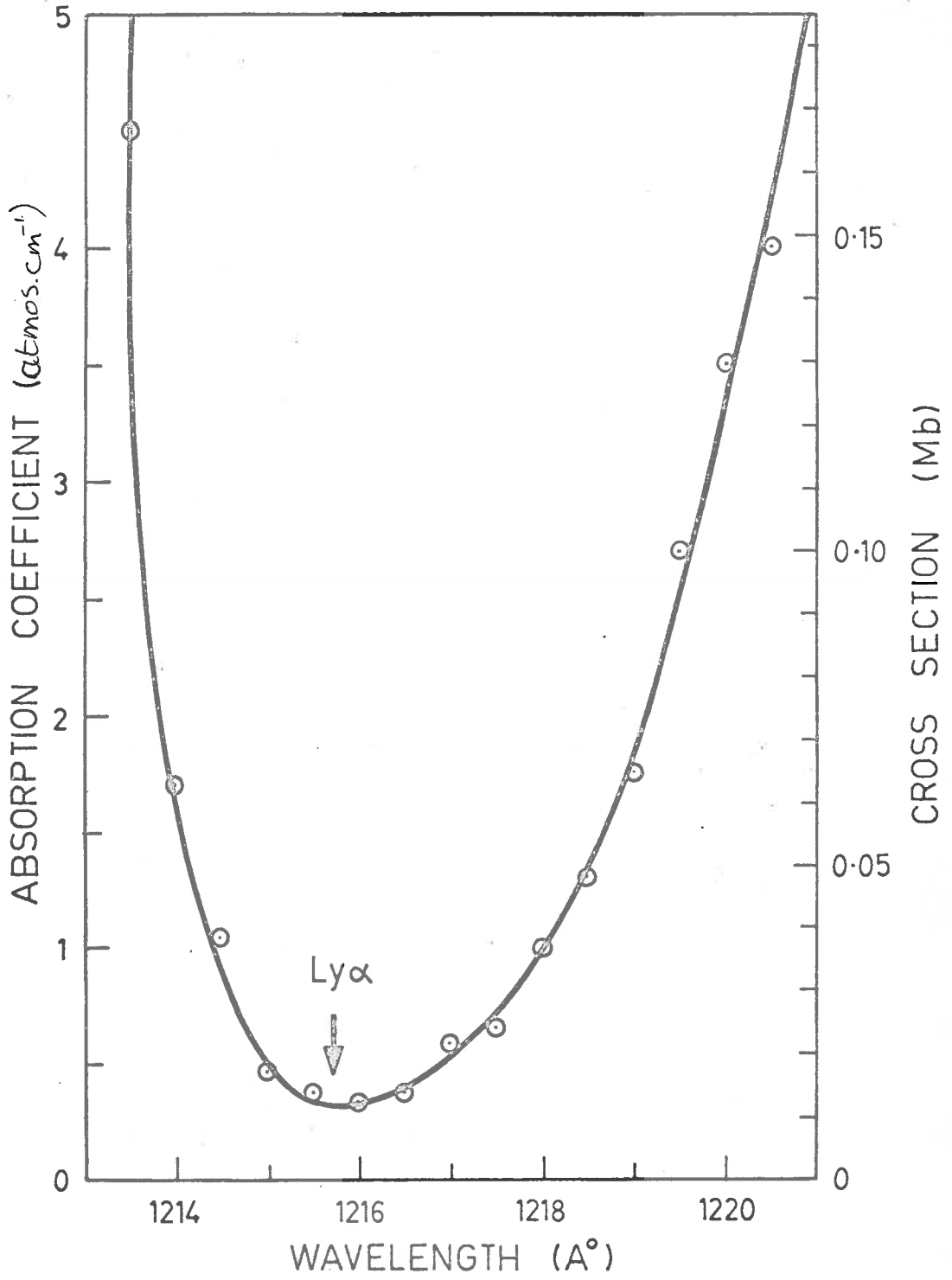

Figure 3.18 Absorption cross sections of molecular oxygen near the wavelength of the solar Lyman-α line.

various path lengths with a fixed pressure was found to be independent of path length but when the pressure was altered the apparent absorption cross-section did not obey Beer's law. This indicated a genuine pressure broadening effect which was presumed to be due to the pressure broadening of the neighbouring bands. This pressure dependence was studied both for pure oxygen and oxygen-argon mixtures and in all cases the cross-section increased linearly with gas pressure as shown in figure 3.19.

The diffuseness of the bands in this region has been ascribed to predissociation by Price and Collins (1935). The bands are expected to be members of Rydberg series but only a few have been identified tentatively by Price and Collins (1935) and by Tanaka (1952) who has reported two progressions one of which might be a member of Rydberg series.

Preston (1940) and Williams (1940) have measured the cross-section at the wavelength of the Lyman-α line (1215.7Å). Watanabe et al (1953), Watanabe and Marmo (1956) and Lee (1955) have measured cross-sections for many wavelengths and their results are in agreement with each other and the present work. Recently Metzger and Cook (1964) have reinvestigated

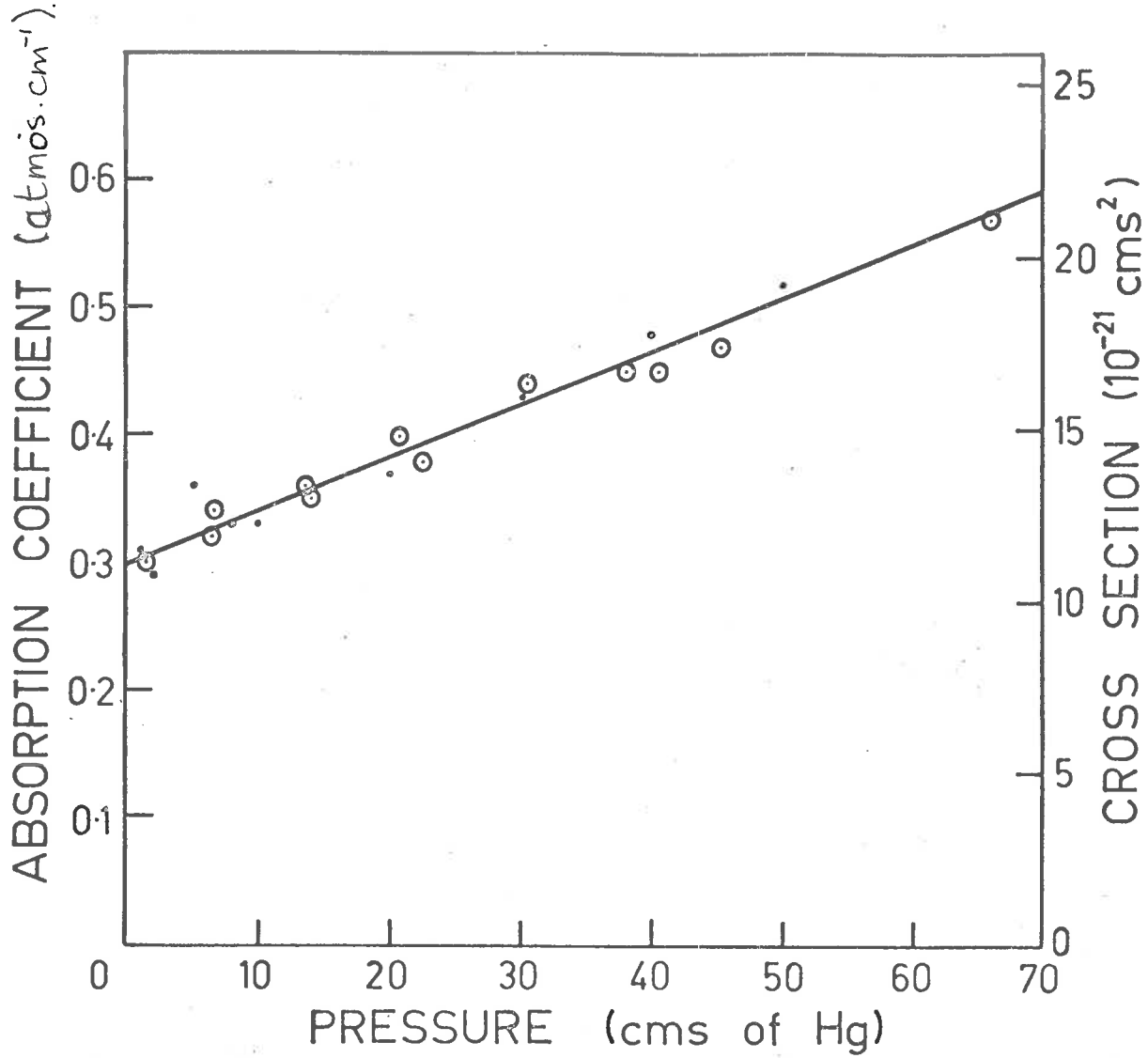

Figure 3.19 Variation of the absorption cross section of molecular oxygen with total gas pressure at Lyman-α (1216Å). The circles shown are oxygen-argon mixtures: the solid points are pure oxygen.

this region and give values for the seven windows of low absorption ($\sigma < 5 \times 10^{-10} cm^2$) and the strong bands in this region (see Table II). The value at Lyman-α and the shape of the absorption curve around it have been investigated by Preston (1940), Watanabe et al (1953), Ditchburn et al (1954) and Lee (1955). The effect of gas pressure on the apparent absorption coefficient at Lyman-α has been reported by Preston (1940) and Watanabe et al (1953). However, using photographic photometry, Ditchburn et al (1954) and Lee (1955) were unable to find any such effect.

This region is important in the study of the ionosphere since solar radiation can penetrate through the seven windows of low absorption down to approximately 70km. The deep window at 1215Å allows the intense solar Lyman-α radiation to penetrate into the D region of the ionosphere. The fact that the spectrum is particularly diffuse in this region suggests that atomic oxygen may be formed in a metastable state by this process in sufficient quantities to be significant in the D region.

3.5 Calculation of atmospheric composition

The ordinary absorption law can be written

$$I = I_0 \exp(-\sigma n x)$$
$$= I_0 \exp(-\sigma N)$$

where n is the number density of gas molecules

σ is the absorption cross section (cm^2)

N is the number of molecules in a column of area 1 cm^2 along the path traversed by the radiation.

A measure of σ can be made in the laboratory so that N can be determined from a measured transmittance.

This method has been used by a number of workers (e.g. Johnson et al, 1951; Byram et al, 1955) to determine number densities in the upper atmosphere by measuring the intensity of the solar ultraviolet radiation at various altitudes. A more detailed treatment of this type of measurement is to be found in Hinteregger (1962) and Mitchell (1966).

3.5.1 Molecular Oxygen Densities

Many workers have used solar radiation in the range 1000-2000Å to determine molecular oxygen concentrations in the atmosphere over a height range from 60km to 180km. Some work with photon counters was done by Friedman et al (1951). Byram et al (1955) used a counter sensitive to the range 1425Å to 1500Å to

determine oxygen densities in the 120km region and repeated the experiment two years later in 1955 and again in 1963. The results are summarized in Friedman et al (1964) and cover the height range from 110km to 180km. Ion chambers were first used for absorption measurements in 1955 by Byram et al (1956), Chubb et al (1958) and later by Kupperian et al (1959). These detectors were essentially only sensitive to Lyman-α radiation except in one case where the chamber responded to radiation in the range 1220-1340Å. Analysis of the data giving the attenuation of the Lyman-α flux as a function of height gave molecular oxygen densities from 70km to 110km.

Similar measurements have been made by Smith et al (1965) and Smith and Weeks (1965) at heights from 70 to 112km and the determinations of molecular oxygen densities by both groups of workers are in excellent agreement.

Jursa et al (1959), (1963), (1965) have used a different technique to measure the attenuation of the solar ultraviolet radiation in the atmosphere: they have flown photographic spectrographs (covering the range from 1000-3000Å) in a rocket pointed directly at the sun. The resolution was sufficient to resolve the

Schumann-Runge bands of oxygen and densities over the height range from 60km to 90km were derived by measuring the attenuation of the solar radiation at these wavelengths. Since the molecular oxygen cross-sections vary by several orders of magnitude over this range of wavelengths, Jursa et al have obtained densities over the complete height range from 60 to 165km.

Hall et al (1963(a)), (1963(b)) have used photoelectric monochromators limited to wavelengths less than 1300Å to obtain densities above 120km. In particular they measured the attenuation of the S_i III solar line at 1207Å.

Molecular oxygen densities from 70km to 130km have recently been measured at Woomera (Carver et al, 1964; 1966) using ion chambers sensitive to Lyman-α radiation. The absorption coefficients measured in the experiment reported in this thesis have been used in the analysis.

The results of the determinations of molecular oxygen densities by various workers are summarized in figure 3.20.

Figure 3.20 **The results of experimental determinations of molecular oxygen densities in the range 60 to 180 km by workers using various methods. The height range within which each method is applicable is shown in the figure.**

LEGEND

	——	U.S. Standard Atmosphere 1962
Photographic spectrograph	+	Jursa et al. (1963,1965)
Photoelectric monochromator	■	Hall et al. (1963b,1965)
1450Å Counter	▽	Friedman et al. (1964)
Lyman-α ion chamber	▲ ●	Carver et al. (1964, 1966)
"	◇ ○ □ △	Smith and Weeks (1965)
"	– – – – – –	Kupperian et al. (1959)
1220 to 1350Å ion chamber	· · · ·	Kupperian et al. (1959)

This figure by kind permission of Dr.P. Mitchell.

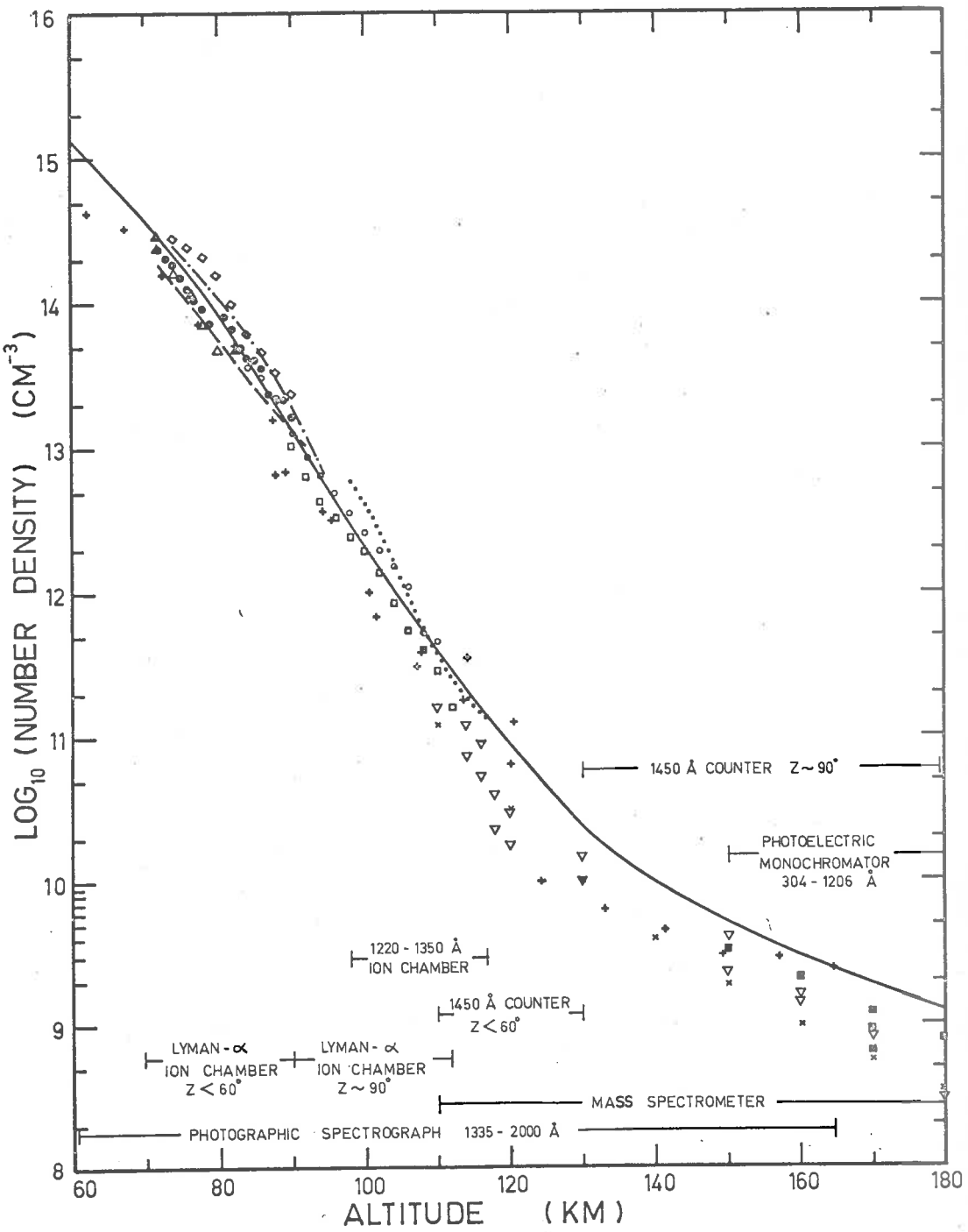
16
15
14
13
12
11
10
9
8
60
80
100
120
140
160
180
LOG10 (NUMBER DENSITY) (CM-3)
ALTITUDE (KM)
1450 Å COUNTER Z~90°
PHOTOELECTRIC MONOCHROMATOR 304 - 1206 Å
1220 - 1350 Å ION CHAMBER
1450 Å COUNTER Z<60°
LYMAN - α ION CHAMBER Z<60°
LYMAN - α ION CHAMBER Z~90°
MASS SPECTROMETER
PHOTOGRAPHIC SPECTROGRAPH 1335 - 2000 Å

CHAPTER 4

Absorption Measurements on Molecular Hydrogen

The experimental arrangement for the determination of the absolute absorption cross-sections for molecular hydrogen in the region 1060-1130Å is described. The measurements were made using a 1-metre near normal incidence monochromator and the absorption spectra were recorded with a digital data handling system, developed for use in conjunction with a 400 channel analyser. This system which led to a marked improvement in accuracy, and a simplification in data reduction, is described in some detail.

The results of these measurements are presented in terms of the absolute line strengths and oscillator strengths for 37 rotational lines in the first four vibrational bands of the Lyman system of molecular hydrogen. The measured values of oscillator strength are compared with the calculated values and found to be in good agreement.

4.1 Introduction

The simplest diatomic system which occurs in nature is the hydrogen molecule. Quantum mechanical calculations have been made for this particular system

(Kolos and Wolniewicz, 1965) and there is reasonable agreement between calculated and measured term values. As mentioned previously, however, (section 1.3.4) the oscillator strengths are much more sensitive to the choice of potential function than are the term values (Peek and Lassettre, 1963).

There have been many high dispersion measurements made on molecular hydrogen in absorption to give the observed term values (e.g. Monfils, 1961(a); 1961(b); Herzberg and Howe, 1959; Namioka, 1964(a); 1964(b); 1965; Dieke, 1958) but there has been little attempt to measure absolute absorption coefficients (or oscillator strengths) directly. Mulliken and Rieke (1941) have estimated the sum of the oscillator strengths from the Lyman bands in molecular hydrogen as 0.65 which can be compared with the calculations of Peek and Lassettre (1963) which gave a value of 0.28. Nicholls (1965) has calculated the Franck-Condon factors for the transitions in the Lyman band system.

This thesis reports measurements of the absolute absorption cross-sections for molecular hydrogen from 1060-1130Å. Oscillator strengths of the rotational lines in the first four vibrational bands of

the Lyman system have been measured. The band strengths for these four bands have been measured and compared with the calculations of Nicholls (1965).

These results are important as they are the first experimental absolute oscillator strengths which may be applied to the problem of investigating the abundance of molecular hydrogen in the galaxy (see chapter 5).

4.2 Previous measurements of the spectrum of molecular hydrogen.

Schumann (1901) recognized that molecular hydrogen was transparent in the wavelength region above the transmission limit of fluorite optics as early as 1901.

Lyman (1928) succeeded in simplifying the spectrum of molecular hydrogen by mixing argon and hydrogen in a discharge tube and later several investigators (Jeppesen, 1933; 1938; Beutler, 1935; 1934; Werner, 1926; Witmer, 1926; Hori, 1927; Dieke and Hopfield, 1920; 1927; Hopfield, 1930; Schaafsma and Dieke, 1929; Hyman, 1930; Beutler et al, 1936) succeeded in photographing the extreme ultraviolet bands of molecular hydrogen and analysing them. Most

of these measurements were made in emission and up to 1936 only Dieke and Hopfield (1927), Hopfield (1930) and Beutler et al (1936) had photographed the absorption spectrum of molecular hydrogen.

In 1943, Tanaka (1944) made a detailed study of the absorption spectrum of molecular hydrogen with a large vacuum spectrograph in order to obtain better information concerning the four electronic states $X^1\Sigma_g^+$, $B^1\Sigma_u^+$, $C^1\Pi_u$ and $D^1\Pi_u$; this work included a vibrational and rotational analysis of the Lyman (B-X) Werner (C-X) and D-X bands but the intensity of the absorption lines was only estimated qualitatively.

Other workers have since made rotational analyses on various sections of these bands (Namioka, 1964(b); 1965; Monfils, 1961(a); 1961(b); 1965; Herzberg and Monfils, 1960; Herzberg and Howe, 1959).

Absolute absorption coefficients, however, were measured for the first time by Lee and Weissler (1952) who measured absorption in the continuum region at about 50 wavelengths. In 1955 Wainfan et al (1955) measured the photoionization cross-section of molecular hydrogen at about 9 wavelengths and later some additional absorption measurements were reported by Bunch et al (1958). Cook and Metzger (1964) have recently

measured photoionization and absorption cross-sections of molecular hydrogen and deuterium in the region from 580Å to 1000Å. A measurement of absorption in molecular hydrogen between about 1070Å and 1100Å has recently been made by Wilkinson and Byram (1965) who have not given details of the strengths of the observed lines.

There is, then, a notable lack of absolute absorption measurements in the Lyman bands and in particular in the region from 950Å - 1130Å which is important to the study of interstellar absorption (see section 5.2).

4.3 General methods

The rotational lines in molecular hydrogen are well separated from each other (≈1Å). Since the resolution of the dispersing instrument was much greater than the natural width of the lines appearing in the absorption spectrum of molecular hydrogen but not as large as the separation between the lines the experiment was designed to measure the equivalent width of each individual line. A comparison of the width of the resolution function of the instrument (≈0.3Å) and the width of the spectral lines (0.0056Å)

meant that the most accurate method of obtaining absolute line strengths was from a measure of equivalent width with the layer thickness of the absorbing gas chosen so that the average absorption lay in the "Doppler region" of the curve of growth for each of the lines. A small layer thickness would mean that the equivalent width was changing linearly with layer thickness but in this case the average absorption would be too low to measure; a larger layer thickness would mean that the equivalent width was changing slowly with layer thickness. It was estimated that the ideal situation would be to record an average absorption over the spectral line of approximately 3%.

In order to measure this relatively low absorption accurately, a new system of recording the data was developed in which the accuracy of the data could be increased simply by increasing the time taken to record it. As a consequence of this requirement a new system for data handling and analysing was developed.

4.4 Experimental Apparatus

4.4.1 Monochromator

A 1 metre near normal incidence monochromator*

---

* McPherson model 225

was used in this work and this increased the available flux/bandpass ratio by approximately a factor of 15 compared with that available from the ½metre Seya-Namioka instrument (see section 3.1.2). This instrument (the 1 metre monochromator) was fitted with a 1200 lines/mm grating blazed at 1200Å giving a first order dispersion of 8.3Å/mm.

4.4.2 Light Sources

In order to avoid false structure in the absorption spectra due to misalignment of the wavelength scale between successive scans it is desirable to use a continuum light source. In this experiment the discharge lamp was operated with a high pressure (200 torr) of argon in the lamp and excited in a condensed spark mode (see section 3.1.1). The lamp was operated without a window between it and the monochromator and this involved the use of the differential pumping equipment described in Appendix A. The entrance slit was set at 100 microns giving a resolution of about 1Å.

When the entrance slit was restricted to 25 microns (≈0.3Å) it was necessary to use a relatively high power input to the lamp (500 watts) in order to obtain sufficient intensity in the exit beam from the

monochromator. This arrangement proved unsatisfactory since particles of aluminium were eroded from the body of the Hinteregger type lamp and these drifted onto the slit faces rapidly clogging the slits.

Since in this experiment, measurements were restricted to wavelengths above the transmission limit of lithium fluoride, this problem was overcome by inserting a lithium fluoride window between the lamp and the entrance slit of the monochromator and modifying the lamp as shown in figure 4.1. In this arrangement argon flowed through the lamp from one end to the other, the flow rate being maintained by a small mechanical pump.

The lithium fluoride window placed in this position, however, was subjected to a considerable amount of staining. This effect has been noted by Huffman et al (1965) who attribute it to the intense undispersed vacuum ultraviolet radiation passing through the window causing photochemical decomposition of the minute amount of oil vapour present in the vacuum of the monochromator. This gives rise to a brownish-yellow stain on the window thereby reducing its transmission. Blowing a jet of helium onto the window on the entrance slit side to flush away traces

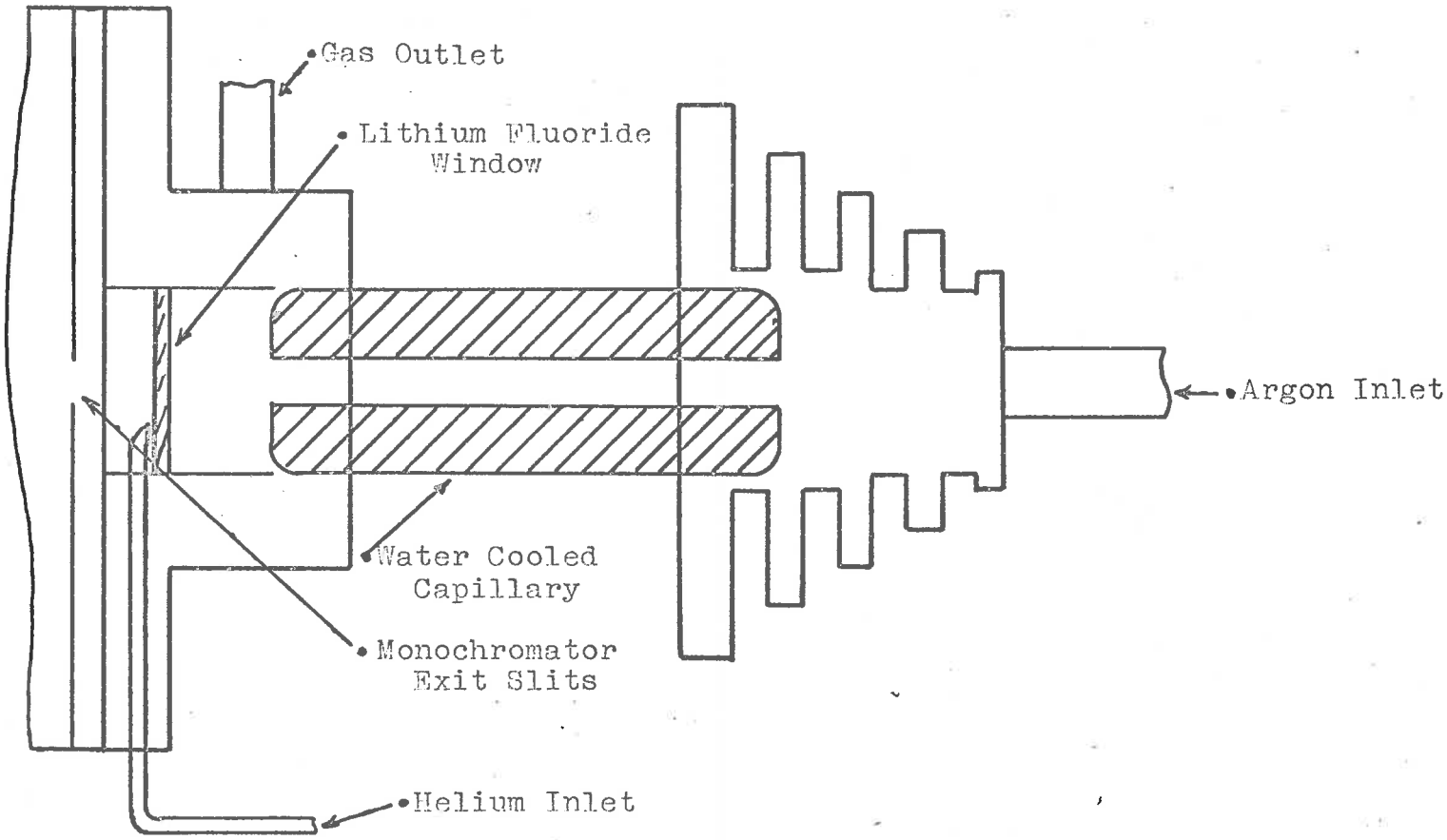

Figure 4.1 Schematic diagram showing the modified Hinteregger lamp.

of oil vapour overcame this problem to some extent. With these refinements the lamp was relatively reliable but a certain amount of staining of the window still occurred necessitating its replacement every 24 hours even when the lamp was operated with only moderate power. If the lamp was operated with the maximum power available the window staining was much more rapid and the window was only usable for 3-4 hours.

4.4.3 Cells and vacuum systems

Cells and pumping systems similar to those described in sections 3.1.4 were used in these experiments. Care was taken to ensure that all cells were clean and leak free to avoid the presence of impurities which might overshadow the absorption due to hydrogen when the pressure of hydrogen in the cell is low.

Standard commercial grade hydrogen was used and purified by passing it through an array of palladium diffusion tubes heated with a tantalum strip heater. The tubes and heater with the vacuum vessel into which they are fitted are shown schematically in figure 4.2. This particular system was very reliable and allowed filling rates of up to 100 litre torr/minute when operated with a pressure differential of 10p.s.i. across the tubes.

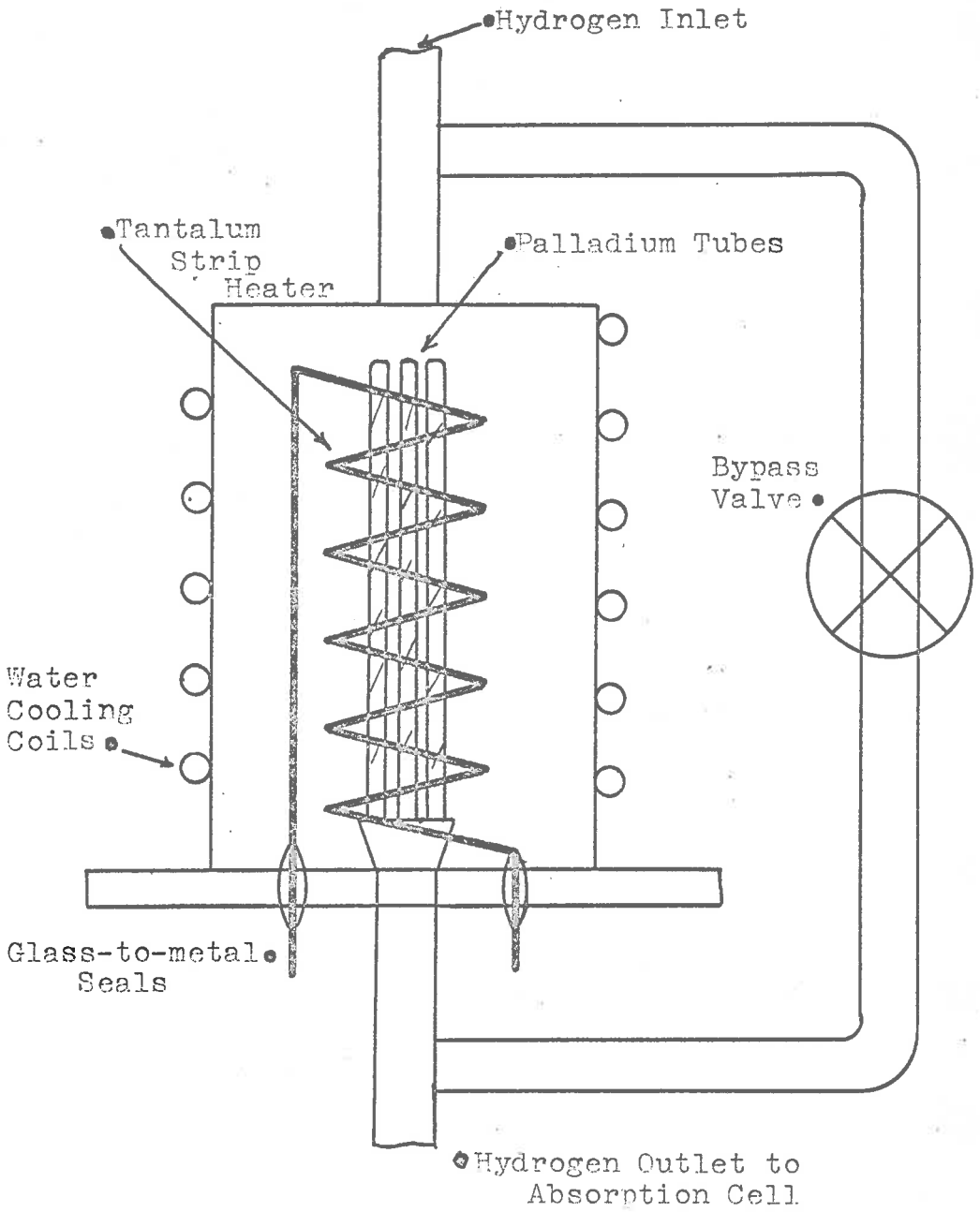

Figure 4.2 Schematic diagram of the palladium diffusion tube purification unit.

4.4.4 Detectors and Beam Optics

The radiation emerging from the exit slit of the monochromator is in the form of a beam which diverges and the distribution of the intensity of the radiation across the beam varies as the wavelength changes (Stewart, 1966). It is therefore necessary to view the complete beam with both the beam splitter and the remote detector rather than just sample a part of the beam.

One of the most sensitive detectors of radiation in the range 2-1500Å is a magnetic electron multiplier (Bendix). This device fitted with a tungsten cathode is essentially a noise free detector since both the cathode and secondary emission surfaces have a high work function.

The collecting area of this particular device is, unfortunately, limited to an area of approximately 18mm × 15mm so that it cannot be used as a detector at the remote end of the cell. For typical cell length (50cms) and with the exit slit set at 4mm × 25 microns the beam diverged to an area of approximately 30mm × 40mm and this meant that a glass plate coated with sodium salicylate was used as the detector; this was viewed with a 2" diameter photomultiplier.

Throughout the experiments on molecular hydrogen the detectors were sodium salicylate coated plates or grids viewed by E.M.I. type 95143 photomultipliers as described previously (see section 3.1.3(a)) and the radiation incident on the absorption cell was monitored with a beam splitter at all times. Both photomultipliers were watercooled to stabilize the gain of the detection systems.

4.4.5 The Digital Recording System

In general, as mentioned in section 4.3, it was necessary to measure very small amounts of absorption in this particular experiment. In order to do this accurately with the low flux available from the argon discharge source it was necessary to improve the signal to noise ratio considerably over that obtained in the work on molecular oxygen. The main sources of noise are the fast statistical fluctuations of the signals from the photomultipliers due to random thermal emission from the cathode and the fluctuations of lamp intensity with a somewhat longer time constant.

The statistical fluctuations can obviously be reduced by integrating the signal from a detector for a long period. If, however, the fluctuations of intensity

have a period of the order of the integrating time they will not be reduced. One method of reducing these long period fluctuations is to sample the integrated signal at time intervals, long compared with the fluctuations, and use the average level recorded.

An ideal system, then, is one which integrates the signal from each detector for a set time (say 1 second) and samples this signal at longer time intervals (say every 2 minutes) and adds the samples together to give an average determination. This type of data handling can only be achieved by converting from an analogue to a digital system and using some type of memory. A 400 channel analyser* if used in time mode provides the equivalent of 400 scalers which may be addressed sequentially. A system was developed in which the analogue signals were converted to digital form and stored in the multi-channel analyser with the facility of a variable integrating time and the ability to recycle the recording as many times as required. An advantage of this method of data handling is, of course, the convenience with which the data can be analysed with the direct use of a computer. A block diagram of the apparatus is shown in figure 4.3.

If the wavelength of the monochromator is scanned

---

* R.I.D.L model 34-12B

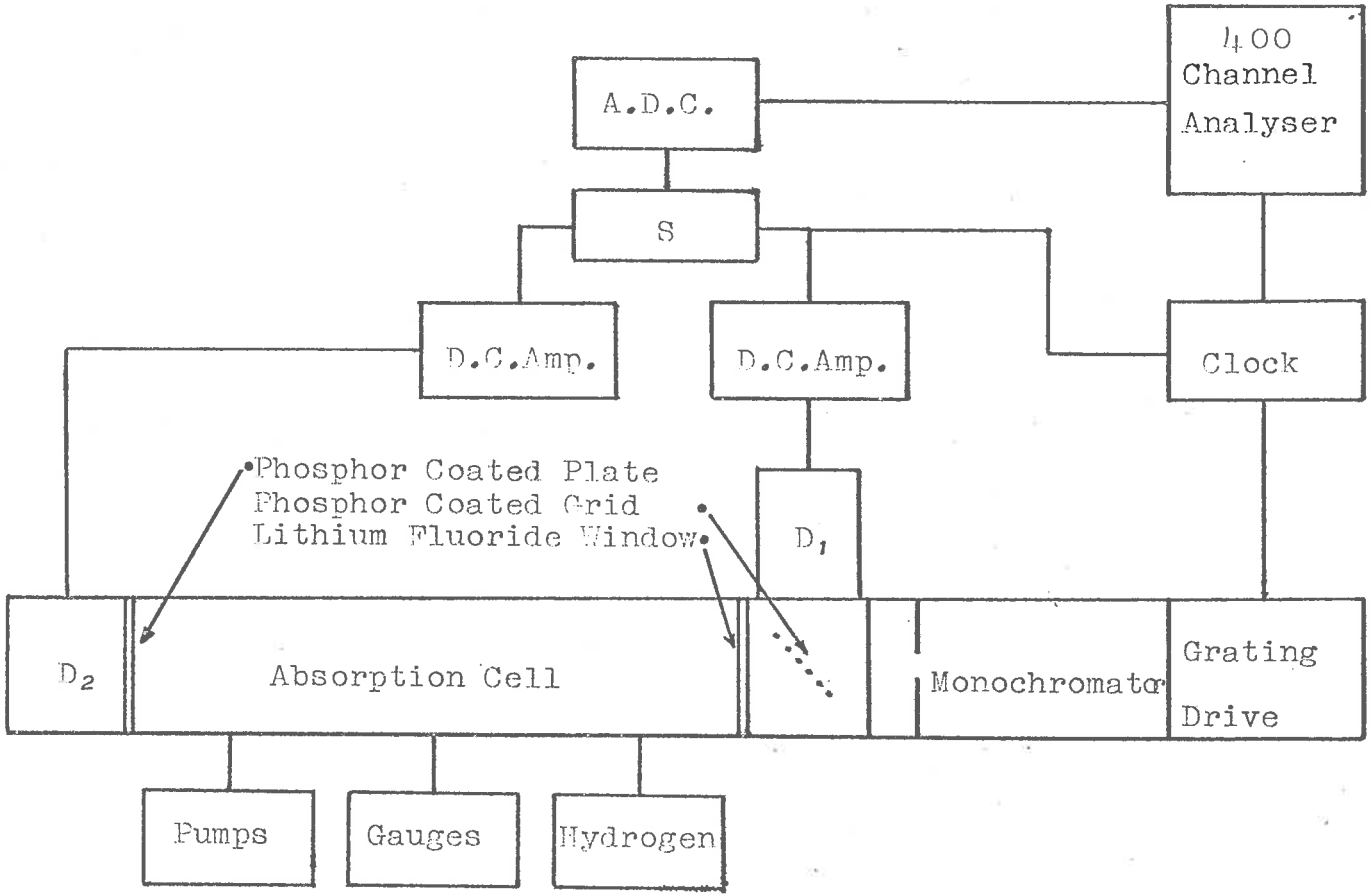

Figure 4.3 Block diagram of the experimental arrangement for the measurements of molecular hydrogen absorption.

and the outputs from both detectors are recorded digitally the sequence of events occurring is as follows; the wavelength scan is started; at the required starting wavelength an inhibit voltage is removed from the multi-channel analyser and the output of the D.C. amplifier on detector 1 is fed via the switch S to the analogue to digital converter (A.D.C.); this provides a train of pulses of a frequency proportional to the input voltage which are fed to channel 0 of the multi-channel analyser. After a preset time in the range from 1/2000 min. to 2 min. a pulse from a "clock" operating from the mains frequency (50c/s) switches S to the alternate position and advances the address of the multichannel analyser by one channel. Now, the output of detector D2 is passed via S to the A.D.C. which feeds a train of pulses to channel 1 of the multichannel analyser; when the same time interval has elapsed S is tripped to the opposite position and the analyser advanced to channel 2 and so on. Thus the multichannel analyser stores a set of two interlaced spectra in alternate channels. The mains clock simply counts down the 50c/s to the required frequency using a number of bistable multi-vibrators and is prevented from addressing the multichannel analyser until the inhibit voltage is removed. A reset

facility ensures that the spectra recorded from D1 and D2 always appear in even and odd channels respectively. Subsequent scans may therefore be added to the existing contents of the analyser memory, and scanning continued until the data is sufficiently smooth.

The details of all subsidiary circuits are given in Appendix B.

4.4.6 The Analogue to Digital Converter (A.D.C.)

The function of the A.D.C. is to convert an analogue voltage derived from a Hewlett Packard D.C. amplifier to a train of pulses with a frequency accurately proportional to the input signal. There is an advantage in designing a converter which operates continuously and makes use of all the analogue information rather than one which merely samples the analogue signal repetitively. An integrating analogue to digital converter was therefore designed consisting, in principle, of a voltage integrator, level detector and a reset circuit which discharged the integrator each time it reached a preset level. The reset pulses constitute the digital output. The circuit for the completed A.D.C. is shown in figure 4.4. The resistors R1 and R2, the condenser C1 and the monolithic

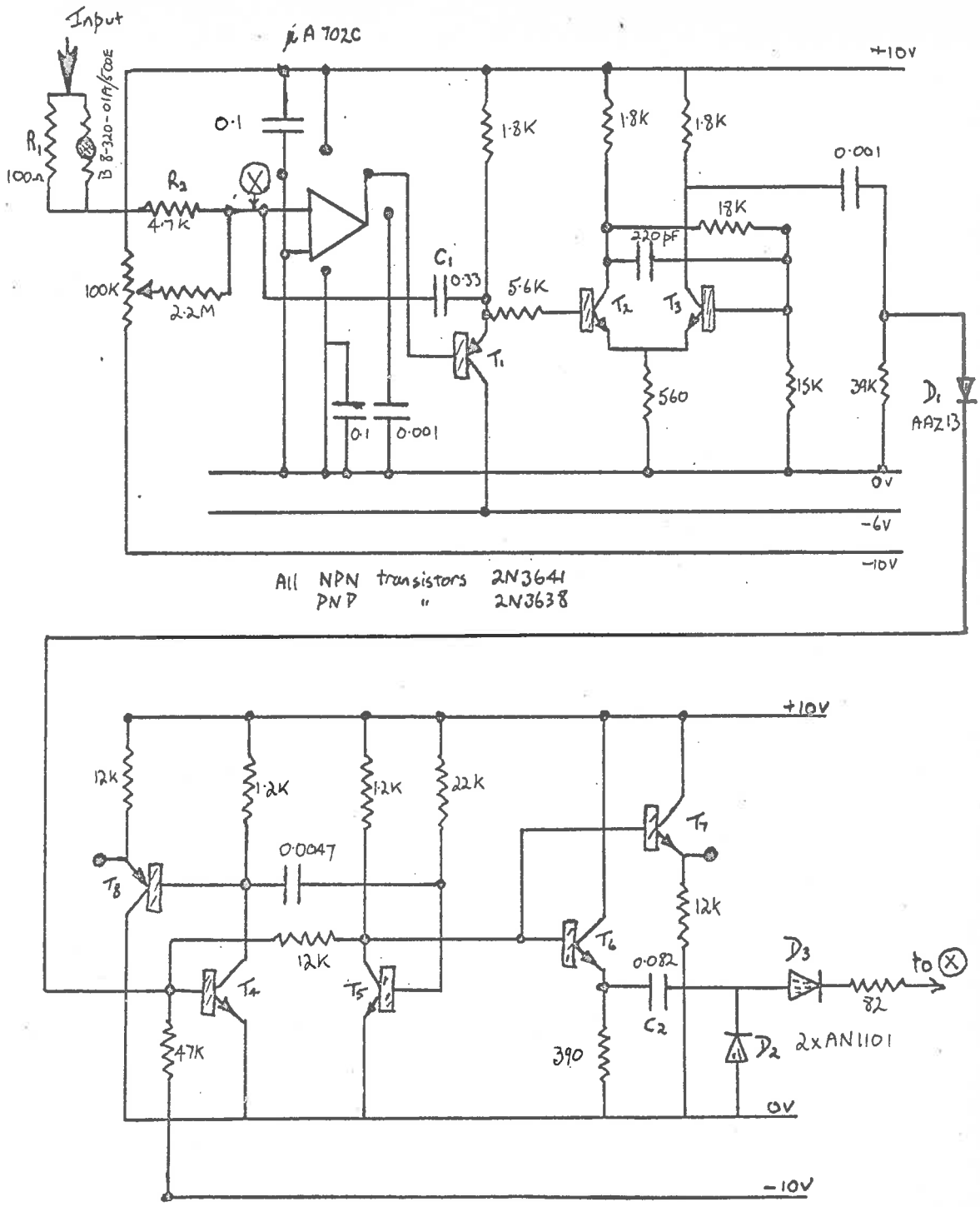

Figure 4.4 Circuit for the analogue to digital converter.

d.c. amplifier* constitute the integrator. When a constant negative voltage is applied to the input the integrator output rises linearly with time until it crosses the threshold of the Schmidt trigger T2, T3. The output of the Schmidt trigger fires a monostable T4, T5 and the positive going output pulse from the monostable provides a quantity of charge via the diode pump C2, D2, D3 to reset the integrator. The discharge time is approximately 5μ secs.

The actual A.D.C. built was found to have a non-linearity of 0.1% which increased to 0.5% at low input voltages (<10mv). After temperature compensation the short term stability was 0.03% and the long term stability (over 8 hours) was 0.1%. Temperature compensation was achieved by placing a negative temperature coefficient thermistor in the input circuit as shown in figure 4.4.

4.4.7 Output and data handling

From the multichannel analyser data were readily available in printed form from a digital printer (Hewlett Packard model H23-562A). This form of output was often used where little reduction of the data was necessary. To facilitate data handling a unit was designed

* Fairchild type μA 702C

and constructed to transfer information from the multichannel analyser directly to an I.B.M. model 026 card punch. By decoding the binary coded decimal information from the analyser with sets of relays and scanning with a uniselector to detect a unique closure (one of 10) for each digit, one of the interposer magnets on the punch was operated and a numeral punched for each binary coded decimal from the multichannel analyser. The information from the analyser was presented in parallel form at the output; that is three binary coded decimals indicating the channel number and five binary coded decimals giving the count in that particular channel were presented simultaneously at the output. The 8 banks of relays decoded this information simultaneously and the uniselector scanned each bank sequentially and operated the punch to give 8 decimal digits before the next channel was read out. The circuits for the decoder are discussed in Appendix C. The format was arranged such that the channel number (0-399) and the count for each of 8 channels were punched onto one card in succession. Thus the original experimental absorption data could be transferred directly to cards in a form suitable for

automatic processing by a computer (C.D.C. 6400).

4.5 Procedures

4.5.1 Methods for large values of average absorption

Transmission measurements for molecular hydrogen were first made with high gas pressures (large average absorption - up to 30%) in order to identify all the lines appearing in the spectrum. A typical transmission curve for one region in the molecular hydrogen absorption spectrum is shown in figure 4.5.

For these particular results the spectrum of the radiation emergent from the monochromator was first recorded, over a 10Å band of wavelength, with the absorption cell evacuated. This used all 400 channels of the multichannel analyser and took 40 minutes to complete; the last 10 channels of information were recorded without radiation falling on the detectors in order to provide a background level. This information in the multichannel analyser was then transferred to punched cards. Next, the same wavelength band was scanned, this time with the cell containing pure molecular hydrogen at the required pressure and the information was again punched out. Finally the same band of wave-

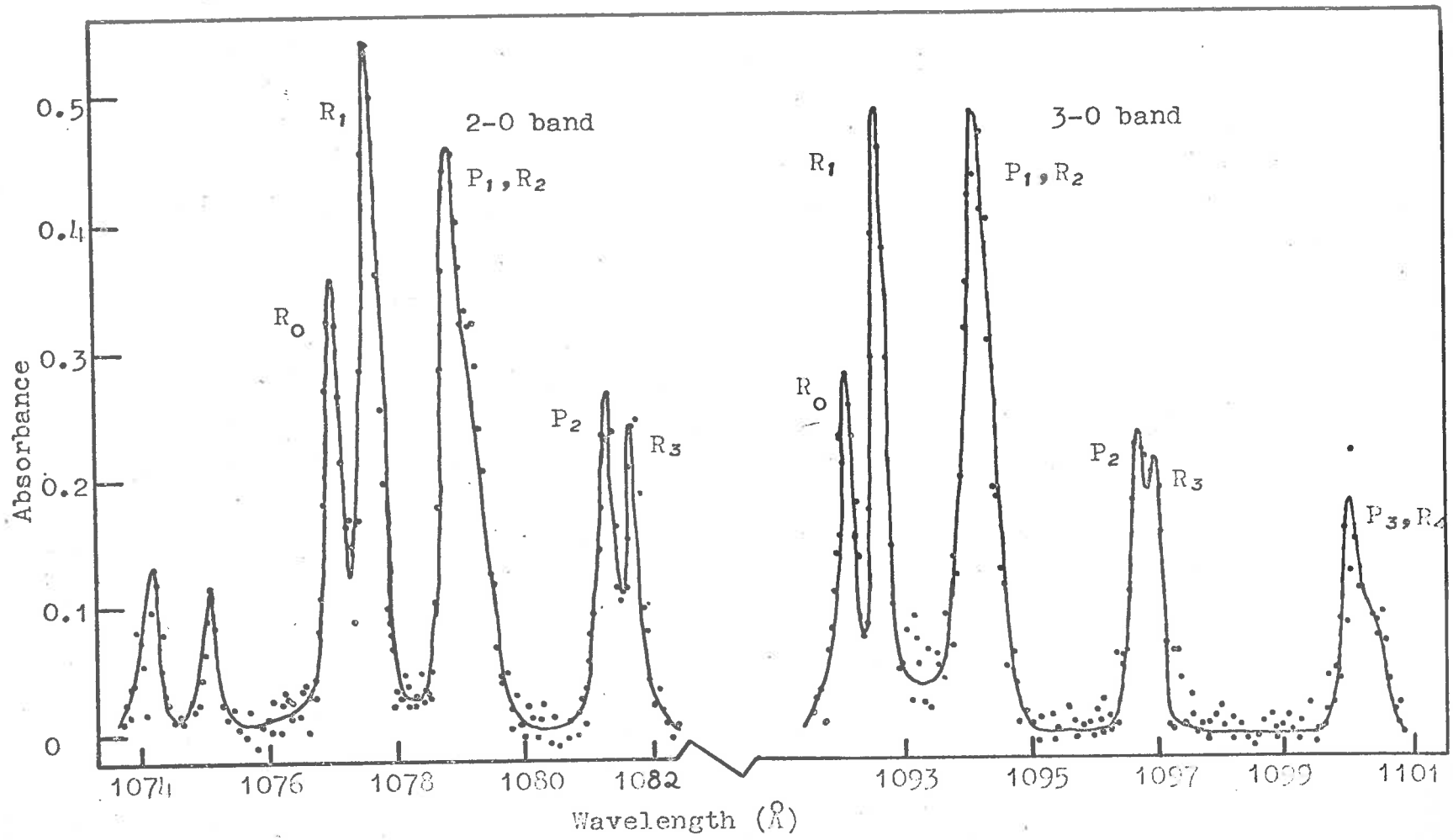

Figure 4.5 A typical transmission curve showing some absorption lines measured at relatively high pressures.

lengths was scanned again with the cell evacuated, and the information punched out. These three sets of punched cards were then fed with a simple computer programme into the C.D.C. 6400 computer to give a transmission curve of which figure 4.5 is typical. The program used the average value of the ratio between the signals from the two detectors in the two scans with the cell evacuated and the ratio of the signals from the two detectors in the scan with the cell full to give a value for the transmission at a particular wavelength. Thebackground levels for each detector as recorded in the last 10 channels of each scan were subtracted from the counts in the appropriate channels. The programme was used, then, to make a linear interpolation between the gain of the system before and after the scan with the cell full and to use this value to calculate the transmission.

4.5.2 Methods for low values of average absorption

In most cases the value of the average absorption to be measured was very small (c.f. section 4.3) and more accurate transmission data were required. In these cases the results were obtained in a slightly different way. The spectrum from the monochromator

over a 5Å band of wavelength was recorded in the first 200 channels of the multichannel analyser with the absorption cell evacuated. The cell was then filled with hydrogen to the appropriate pressure and the absorption spectrum recorded, this time in the second 200 channels of the multichannel analyser. The cell was then evacuated and a further scan added into the first 200 channels; the cell was filled and the absorption spectrum added to the second 200 channels and so on. Each wavelength scan took 2 minutes to complete so that a complete cycle took about 10 minutes, allowing for time to fill and evacuate the cell. The cycling was continued until the fluctuations on the numbers in the multichannel analyser were reduced to a suitable level. The data were then transferred to punched cards and the transmission was calculated with a simple programme. Background levels were recorded in a similar way to that described in section 4.5.1. In this way any long term drift in gain of the two detectors and any long term lamp fluctuations had no effect on the transmission since they were common to both scans made with the cell evacuated and those made with the cell containing the absorbing gas.

4.6 Results

4.6.1 Identification of the spectral lines

In order to identify all the lines appearing in the absorption spectrum of molecular hydrogen, the region from 1060-1125Å was measured with good resolution (≈0.2Å) and a relatively high pressure of absorbing gas (≈2 torr). The spectrum from the monochromator was recorded as described in section 4.5.1. The results are shown in figure 4.6 where the signal from the remote detector is plotted against wavelength. This gives a good estimate of the position of the lines and the data can be plotted in this way since the flux of radiation emerging from the monochromator does not vary significantly as the wavelength is altered except near 1067Å. It can be seen that the rotational lines occur in 4 vibrational bands; the (0-0) (1-0), (2-0) and (3-0) vibrational bands of the $B^1\Sigma_u^+ - X^1\Sigma_g^+$ electronic transition. These bands are the Lyman bands and involve transitions from the ground state $X^1\Sigma_g^+$ to the first excited singlet state $B^1\Sigma_u^+$, and in this case exclusively from the $v'' = 0$ level in the ground state.

Unfortunately there is no light from the argon discharge source in the region from 1066Å to 1069Å making this region inaccessible in the present experiments;

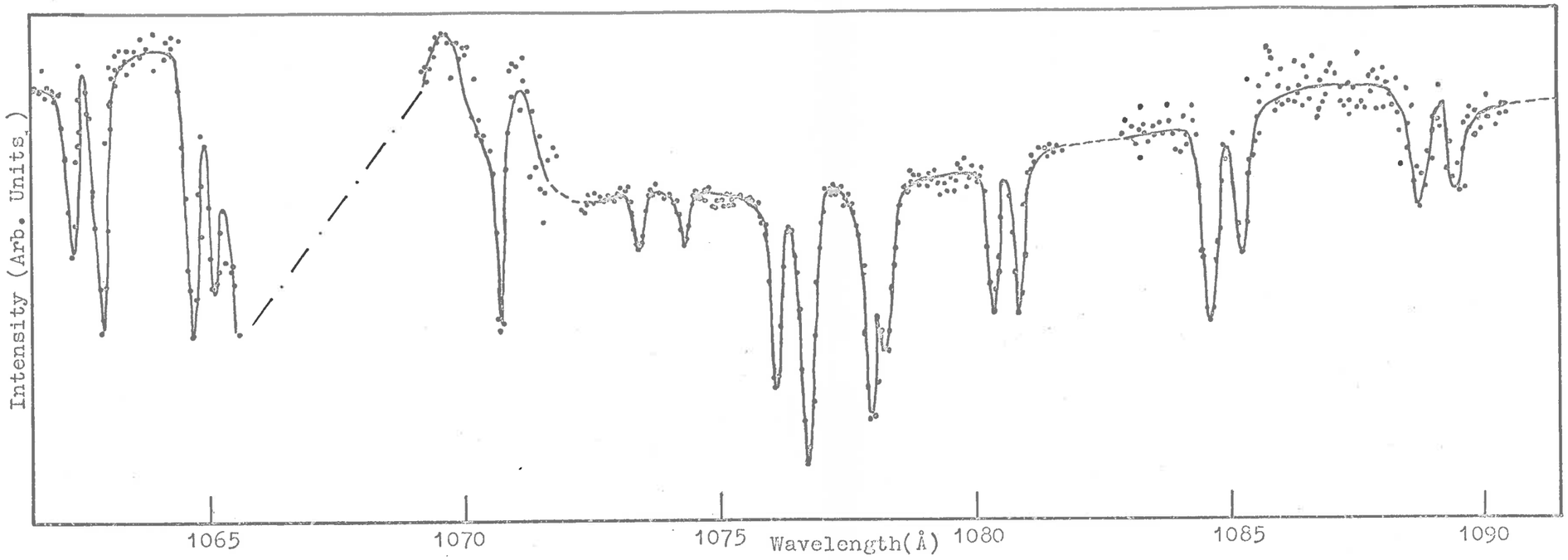

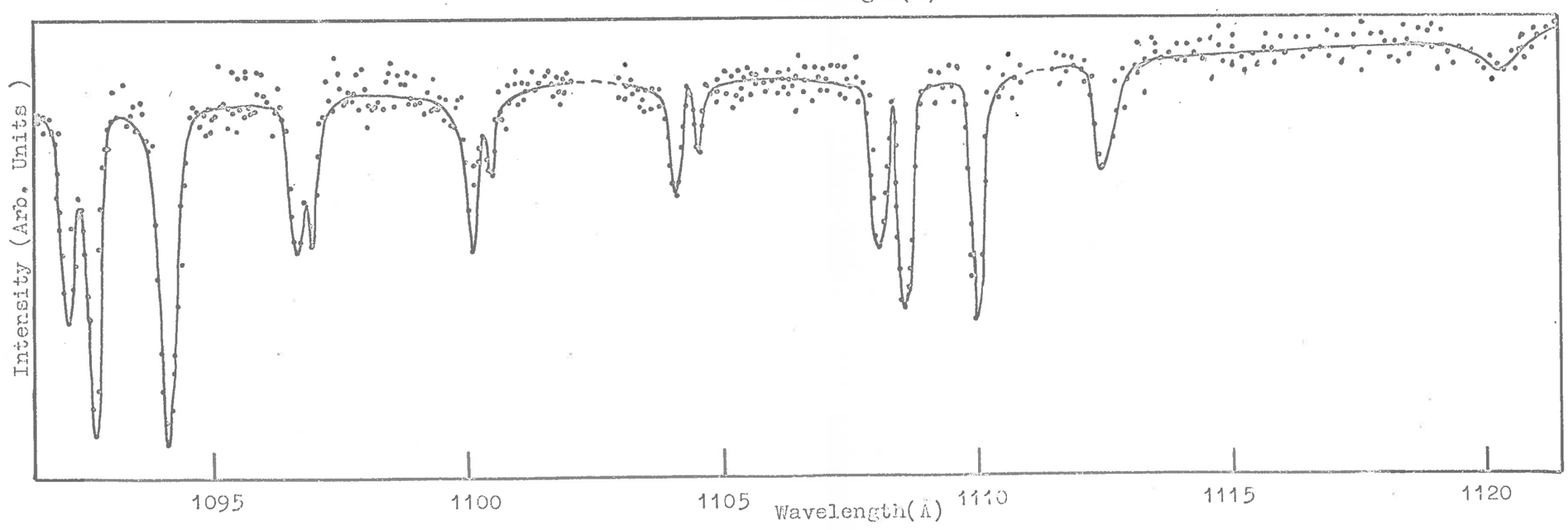

Figure h.6 The absorption features in molecular hydrogen from 1060-1125Å, taken with a high pressure of absorbing gas.

this accounts for the missing data in the middle of the (3-0) band.

The wavelengths of the rotational lines were calculated using the data of Herzberg and Howe (1959) and it is these wavelengths which appear in the diagram.

4.6.2 Absolute line strengths

It is possible that each of the rotational lines may have a different pressure broadening coefficient (γ). If the equivalent widths of the lines are measured with high pressures of absorbing gas where the line has essentially a pure Lorentz shape the absorption grows linearly with pressure (see section 2.6) and a measure of the slope of the growth curve gives an estimate of $(\gamma S)^{\frac{1}{2}}$ (see section 2.6). This means that in order to estimate the strength S of a line some assumption must be made about γ for each line (that is γ must either be assumed to be constant for all the lines or some function of the type of line being investigated - it may for example be a function of the total angular momentum of the molecule in its particular excited state).

To avoid having to make any assumptions, the equivalent width for each line was measured at low pressures (1-300 microns) where the absorption is growing

as that of a pure Doppler line; that is at pressures low enough so that collision broadening is unimportant. (See section 2.5). At these pressures there is the additional advantage that lines close together do not overlap, since the average absorption is low - the equivalent widths of the two lines can be obtained individually.

Once a measure of the equivalent width of a line has been obtained at a particular pressure, cell length and temperature, the general curve of growth (figure 2.1) for a Doppler line can be used to read off a value of ξ for the measured equivalent width. Now $\xi = \frac{Sa}{\alpha_D}$ and the values of both a, the amount of absorbing material, and α_D, the Doppler width, are known so that S can be calculated. Since, having measured the value of W, it was necessary to estimate the value of ξ as accurately as possible it is advantageous to measure values of equivalent width in the region where W is a rapidly varying function of ξ. A value of $\frac{W}{\alpha_D} \approx 3$ was chosen and the pressure in the cell was adjusted until the equivalent width measured was $\approx 3.\alpha_D$. This was a compromise between a value of $\frac{W}{\alpha_D}$ which gave an average absorption too low to measure accurately and a value of $\frac{W}{\alpha_D}$ which was in the region

where a small error in the measured equivalent width would give a large error in the value of ξ. The value of $\frac{W}{\alpha_D} \approx 3$ was nominated, then, and the pressures chosen to minimise the amount of extrapolation along the curve of growth from this point.

In cases where two lines were not resolved the strengths of the two lines were assumed to be of the same order and the equivalent width of the combination was measured and divided accordingly. This was done in the cases of the unresolved pairs of lines in Table III listed together with the wavelengths of the two lines. The assumption that the strengths of the two lines are of the same order can be justified by noting that when the equivalent width of the combination of two lines was measured with the smallest layer thickness available in this experiment, the value of $\frac{W}{\alpha}$ was far in excess of 3. This means that either one line is extremely strong (approximately 20 times stronger than any other line in any of these bands) and therefore the second line is making little contribution to the equivalent width or that both lines are contributing to the measured equivalent width which makes them approximately the same strength.

Table III

Unresolved doublets in the experiment on molecular hydrogen absorption

Band	Lines	Wavelength ($\mathring{A}$)
1-0	P_1	1094.05
	R_2	1094.24
0-0	P_1	1110.07
	R_2	1110.13
0-0	P_2	1112.50
	R_3	1112.60
0-0	P_3	1115.91
	R_4	1116.05

The raw data used to determine absolute line strengths are presented in figure 4.7 where the absorption is shown for each line together with the pressure of gas used in the absorption cell for the measurement of equivalent width. These data were obtained

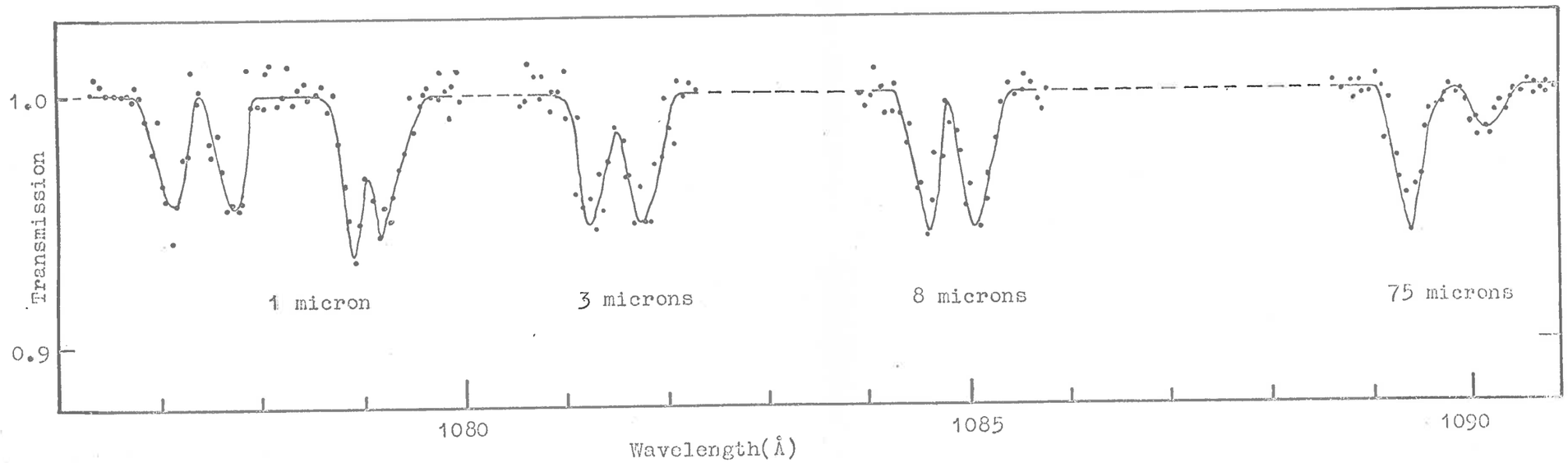

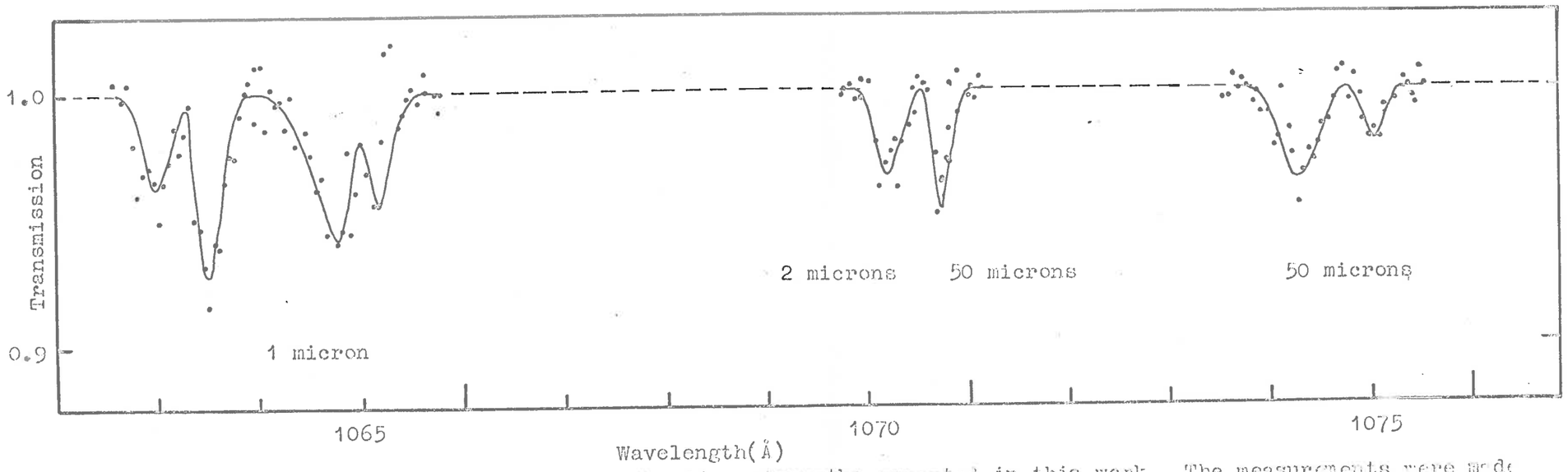

Figure 4.7(a) The raw data used to measure the line strengths reported in this work. The measurements were made with maximum absorption generally ≤ 0.

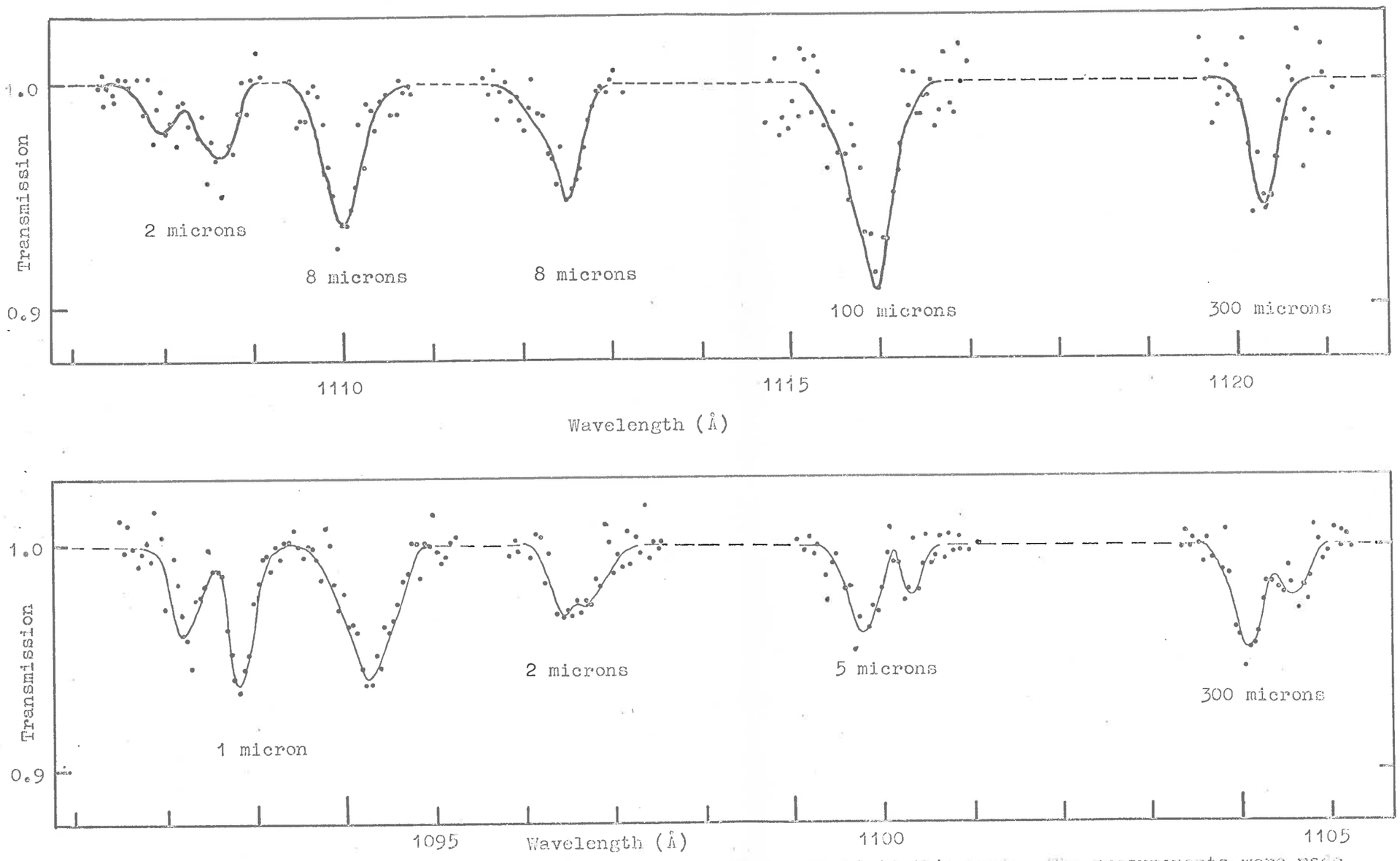

Figure 4.7(b) The raw data used to measure the line strengths reported in this work. The measurements were made with maximum absorption generally $\leq 6\%$.

in the manner described in section 4.5.2 since this involved measuring average absorptions which were generally <6% for most lines.

The absolute line strengths obtained from these measurements are shown in figure 4.8 and are estimated to be correct to within a factor of 2.

In some cases even with the lowest pressure (1 micron) of gas which could be used in the cell (that is the smallest layer thickness available) the value of $\frac{W}{\alpha}$ which was measured for a single line was much greater than 3. The two cases in question are the R_1 lines for both the (3-0) and (2-0) bands. The value of S for the R_1(3-0) line was estimated by observing that the measured value of W at 1 micron pressure was 0.025 and that the single isolated line of strength S=12 which was measured in detail had a value for W of 0.025 at 500 microns. Thus a good guess for the strength of the R_1(3-0) line might be S= 500×12 = 6000 (atmos.cm^{-1}.A°)

Some data taken in the region 1074Å to 1101Å at relatively high pressures (2 torr to 30 torr) allowed a comparison of the strengths of the R_1 lines for the (2-0) and (1-0) bands (see figure 4.5). It was assumed that the pressure broadening coefficients for these two lines were the same (a valid assumption since they both

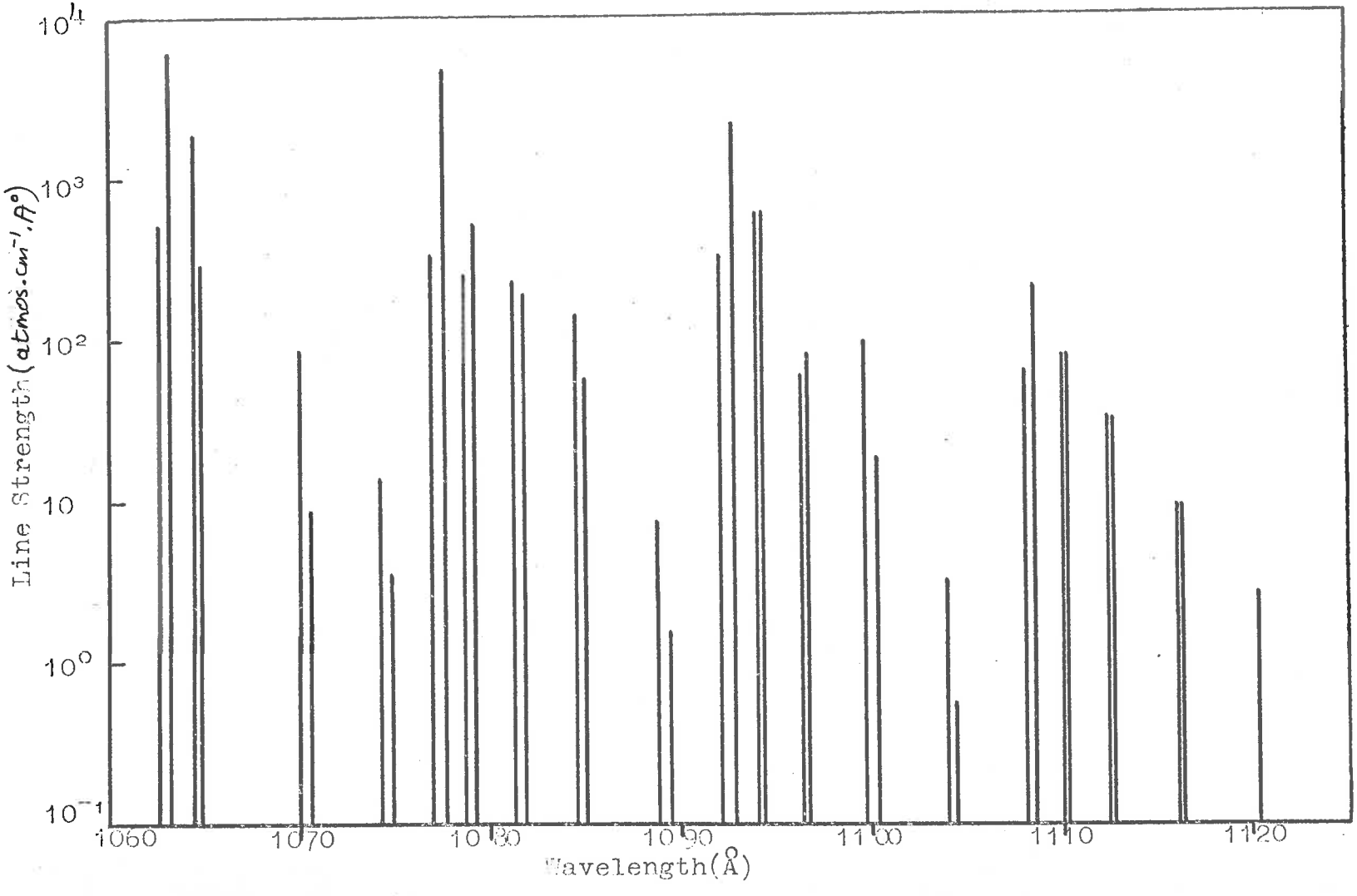

Figure 4.8 Line strengths for some rotational lines in molecular hydrogen.

involve $J'' = 1 \rightarrow J' = 2$ transitions) and the relative strengths of the two lines measured. Assuming that the value of the strength of the $R_1(1-0)$ line was correct, as measured previously, the strength for the $R_1(2-0)$ line was calculated as 4940. (atmos.cm^{-1}.A°). This data also allowed a calculation of the pressure broadening coefficients for various lines in this region since the absolute strengths of all the lines were known. The values of γ are shown in Table IV.

Table IV

Pressure broadening coefficients of various lines

Band	Line	Wavelength(Å)	γ(Å/torr)
2-0	P_2	1081.27	7.8×10^{-6}
2-0	R_3	1081.67	9.3×10^{-6}
1-0	R_0	1092.20	6.7×10^{-6}
1-0	P_2	1096.44	11.7×10^{-6}
1-0	R_3	1096.73	9.7×10^{-6}

It can be seen that the pressure broadening coefficients calculated in this way are of the same order for all the lines.

4.6.3 Oscillator Strengths

The quantity called the line strength S which has been measured is given by

$$S = \int k_\lambda \, d_\lambda \quad .$$

Therefore

$$\int k_\nu \, d_\nu = \frac{10^8 S}{\lambda^2}$$ where λ is the wavelength of the line in Angstrom units.

If now the substitution

$$N_m = \alpha . n_o$$ (where n_o is Loschmidt's number)

is made in the expression for the oscillator strength in terms of the integrated absorption coefficient (see section 1.2.1) the relationship between the oscillator strength, and S, the line strength, becomes

$$f = 4.197 \frac{S}{\alpha \lambda^2}$$

where α is the fraction of molecules in a particular initial state.

The rotational levels of the ground vibrational-electronic level were assumed to be populated according to a Boltzmann distribution with a modification due to the statistical weights of particular levels.

The gas was assumed to be at 25°C and the statistical weight factors g_J were obtained using (Herzberg, 1950)

$$g_J = \begin{cases} 3(2J+1) & \text{for odd } J \\ 2J+1 & \text{for even } J \end{cases}$$

Table V shows the values of α calculated in this way for the first 6 rotational levels of the ground state. The smaller values of α (those on the tail of the Boltzmann distribution) are relatively sensitive to a change of temperature but the accuracy of the results is not sufficient to warrant a correction for the variations in temperature of the absorbing gas of about 2 degrees.

Table V

Ground state populations

J	g_J	α
0	1	0.132
1	9	0.662
2	5	0.115
3	21	0.086
4	9	0.004
5	33	0.001

Using these values of α, the oscillator strengths for all the lines were calculated from the measured strengths. Table VI shows the line, the wavelength, the measured line strength S, the oscillator strength f, and for comparison a set of calculated oscillator strengths F.

Table VI

Oscillator strengths for some rotational lines in the absorption spectrum of molecular hydrogen

Band	Line	Wavelength(Å)	Strength	$f \times 10^3$	$F \times 10^3$
0-0	R_0	1108.130	67.7	1.75	1.87
	R_1	1108.636	228.0	1.18	1.24
	R_2	1110.126	90.9	2.69	1.19
	R_3	1112.598	34.8	1.37	1.07
	R_4	1116.048	10.2	8.62	1.04
	P_1	1110.066	90.9	0.62	0.47
	P_2	1112.502	34.8	0.75	1.03
	P_3	1115.911	10.2	0.80	0.40
	P_4	1120.238	2.8	0.83	2.38
1-0	R_0	1092.196	361	9.63	8.23
	R_1	1092.732	2167	11.51	5.49
	R_2	1094.294	735	22.43	4.94
	R_3	1096.729	91	3.69	4.70
	R_4	1100.182	20	17.36	4.56
	R_5	1104.596	0.58	2.00	4.49
	P_1	1094.054	735	3.90	2.74
	P_2	1096.443	76	2.31	3.29
	P_3	1099.798	101	4.08	3.53
	P_4	1104.111	3.4	2.93	3.66

Band	Line	Wavelength(Å)	Strength	$f \times 10^3$	$F \times 10^3$
2-0	R_0	1077.136	348	9.55	19.2
	R_1	1077.687	4943	1.86	12.8
	R_2	1079.200	526	16.5	11.5
	R_3	1081.672	197	8.22	11.0
	R_4	1085.094	61.4	54.8	10.7
	R_5	1089.458	1.6	5.67	10.5
	P_1	1078.928	270	1.47	6.39
	P_2	1081.267	235	7.34	7.67
	P_3	1084.559	157	6.51	8.22
	P_4	1088.797	8.4	7.44	8.52
3-0	R_0	1062.871	437	12.3	31.4
	R_1	1063.422	7000	39.3	20.9
	R_2	1064.917	310	9.98	18.8
	R_3	1067.350	-	-	17.9
	R_4	1070.712	9	8.24	17.4
	R_5	1074.989	3.48	12.65	17.1
	P_1	1064.607	1192	6.67	10.5
	P_2	1066.892	-	-	12.5
	P_3	1070.113	91	3.88	13.4
	P_4	1074.261	14	12.74	13.9

If the wave function for the hydrogen molecule is separated into functions representing the electronic motion, nuclear vibration, and rotation of the molecule about its centre of gravity the oscillator strength for a particular transition can be written

$$F = F_e \cdot F_v \cdot F_r \qquad \text{(see section 1.3.3)}$$

where F_e is the oscillator strength for the electronic transition and F_v and F_r are the vibrational and rotational line strength factors depending on the vibrational and rotational quantum numbers involved in the transition.

The theoretical oscillator strengths F in Table VI were calculated using a value for F_e of 0.028 as obtained by Peek and Lassettre (1963), a set of vibrational factors, F_v, (the Franck-Condon factors) determined by the overlap integrals of the vibrational wave functions of the upper and lower levels, by Nicholls (1965) and a set of rotational factors, F_r, given by (Herzberg, 1950)

$$F_r = \frac{J'' + J' + 1}{2(2J'' + 1)} = \begin{cases} \dfrac{J''+1}{2J''+1} & \text{- R branch} \\ \dfrac{J'}{2J''+1} & \text{- P branch} \end{cases}$$

4.6.4 Continuum

Measurements of the transmission of molecular hydrogen were made in the region of 1125Å (where no lines were observed) at relatively high pressures (≈30 torr) in order to determine a maximum value for any continuous absorption in this region.

The results yield an average absorption

$$\bar{A} = 0.002 \pm 0.005$$

which gives a value of the upper limit for the absorption coefficient in this region of $k = 0.008 cm^{-1}$

4.7 Band Strengths

The Franck-Condon factors for the first four vibrational bands of the Lyman system of molecular hydrogen were calculated in this work, using the measured values of the oscillator strength for each of the rotational lines.

The oscillator strengths measured, are the total oscillator strengths for each line and these may be written (see section 1.3.3) as

$$f = f_e \cdot f_v \cdot f_r \quad .$$

In this work the values of f have been measured, the value of f_e was taken as 0.28 (Beek and Lassettre, 1963)

and the values of f_r were calculated from (see section 4.6.3)

$$f_r = \begin{cases} \dfrac{J''+1}{2J''+1} & \text{-R branch} \\ \dfrac{J''}{2J''+1} & \text{-P branch} \end{cases}$$

This meant that f_v was the only unknown in the expression above. In general, then, each of the lines measured in each band ($\simeq$9) gave independent estimates of the Franck-Condon factor for that particular band. These individual estimates were then averaged for all the lines in each band to give the results shown in table VII. The standard deviations quoted are the standard deviations for the mean, calculated directly from the observed variations in the individual determinations of f_v.

Table VII

Franck-Condon factors for molecular hydrogen

Band	Present Work	Nicholls	Ratio
0-0	0.0144 ± 0.005	0.00666	2.2
1-0	0.0538 ± 0.014	0.0294	1.8
2-0	0.0971 ± 0.031	0.0685	1.4
3-0	0.0821 ± 0.020	0.112	0.7

Nicholls (1965) has calculated the Franck-Condon factors for the molecular hydrogen Lyman band system using the vibrational and rotational constants established by Herzberg and Howe (1959). He has used a Morse representation for both the ground state ($X^1\Sigma_g^+$) and the upper state($B^1\Sigma_u^+$) but suggests that this is probably not realistic for the upper state; the results of these calculations are also shown in Table VII and are in good agreement with the experimental values. It can be seen, however, that the ratio of the values of the Franck-Condon factors measured in this work to those calculated by Nicholls, decreases as the transitions go to higher vibrational states in the upper electronic state. As the present results are the average of ≈9 individual determinations of the Franck-Condon factors this is a significant discrepancy and supports the suggestion of Nicholls that the upper state is not well represented by a Morse potential. Indeed, this type of measurement provides a sensitive test of the potential used in calculations of the type made by Nicholls.

CHAPTER 5

Astrophysical Significance of Molecular Hydrogen

The possibility that molecular hydrogen is present in large quantities in our galaxy is suggested, following the work of several people (Hulst, 1948; Spitzer, 1949). Current estimates of the molecular hydrogen concentration are reviewed. The present data are used to estimate the equivalent widths of the lines in molecular hydrogen as a function of interstellar molecular hydrogen concentration and interstellar gas temperature.

5.1 Theoretical estimates of molecular hydrogen abundance

It has been suggested (Hulst, 1948; Spitzer 1949; McCrea and McNally, 1960) that molecular hydrogen forms a significant portion of the mass of our galaxy. There is, as yet, no direct observational evidence for the existence of molecular hydrogen in interstellar space and there exist widely different theoretical estimates of the expected abundance (Varsavsky, 1966).

Oort, 1965, has made estimates of the mass density in the general vicinity of the sun by investigating the dynamics of the observable stars. He concludes that, of the total mass density near the galactic plane

which has been derived in this way, about 20% can be ascribed to interstellar gas and 40% to stars of known types. Thus 40% of the mass of the galaxy remains undetected. To explain this discrepancy one must postulate either the existence of a large number of stars of very low intrinsic luminosity or that a large fraction of the unseen mass is gas, distributed near the plane of the galaxy (Oort, 1965). The first postulate is the one favoured by Oort, but it is possible that the invisible mass is molecular hydrogen. Dorschner et al, 1965, have calculated six models for the distribution of matter near the sun and assuming that all the unseen mass is molecular hydrogen, conclude that this species comprises 75 to 83% of all the interstellar gas. They give arguments to support the idea that the unseen mass is very strongly concentrated near the galactic plane and hence would be unlikely to be composed of stars. This work gives an upper limit to the ratio of molecular to atomic hydrogen of $n_{H_2}/n_H \approx 5$. With an abundance of molecular hydrogen up to this level all the observations of the motions of the stars can still be satisfied. Gould and Salpeter, 1963, and Gould et al, 1963, have examined the problem of the abundance of molecular hydrogen in some detail

and have estimated n_{H_2}/n_H as "likely to be in or near the range 0.1 to 40" and then give arguments to reduce their upper limit to 10. Varsavsky, 1966, in a review paper, takes the estimate of Dorschner et al, 1965, as the upper limit to the ratio n_{H_2}/n_H. He has reviewed the calculations of several workers on the formation of molecular hydrogen in interstellar space by means of dust grains and catalytic agents and the results of some work on the destruction of hydrogen by photodissociation and photoionization (e.g. Hulst, 1948; Spitzer, 1949; Gould and Salpeter, 1963; Knapp et al, 1965) and concludes that n_{H_2}/n_H is between 10^{-4} and 3 to 5.

If the abundance of molecular hydrogen were as high as a few times that of atomic hydrogen some ideas of interstellar space would need to be reexamined (Varsavsky, 1966). Firstly, the total amount of gas in the galaxy would be increased considerably and this would alter current theories of star formation. Secondly, it is easy to excite molecular hydrogen into higher rotational states of the lowest vibrational state by collisions; that is, molecular hydrogen is an efficient cooling agent since these levels when excited can depopulate by radiation allowing energy to escape from the interstellar cloud. This would mean a lower temperature for interstellar matter (Varsavsky, 1966).

5.2 Detection of interstellar molecular hydrogen

Although molecular hydrogen is expected to be present in interstellar space in substantial quantities it has not yet been detected. The reasons for this can be seen by looking at the energy level diagram for molecular hydrogen (Figure 5.1). Because of the low temperature (see section 5.3) of interstellar matter all the molecular hydrogen can be assumed to be in the lowest vibrational level of the ground state. The transitions to be expected then fall into three general classes.

Firstly there may be transitions involving only a change of rotational state of the molecule. The hydrogen molecules in the J=0 and J=1 levels of the ground vibrational-electronic state can reach more excited rotational levels through collisions. De-excitation may then occur through either collisions or quantum emission. Zwicky, 1959, has suggested searching for the line at 84.4μ arising from the transition J=1-> J=0 Osterbrock, 1962, has suggested looking for the line at 42.4μ arising from the transition J=2-> J=1 and Gould, 1964, has suggested that the line at 28.2μ arising from the J=2-> J=0 transition may be detectable in some regions of the galaxy. All these observations would, of course, have to be made from balloons to avoid absorption

Figure 5.1 Energy level diagram for molecular hydrogen.

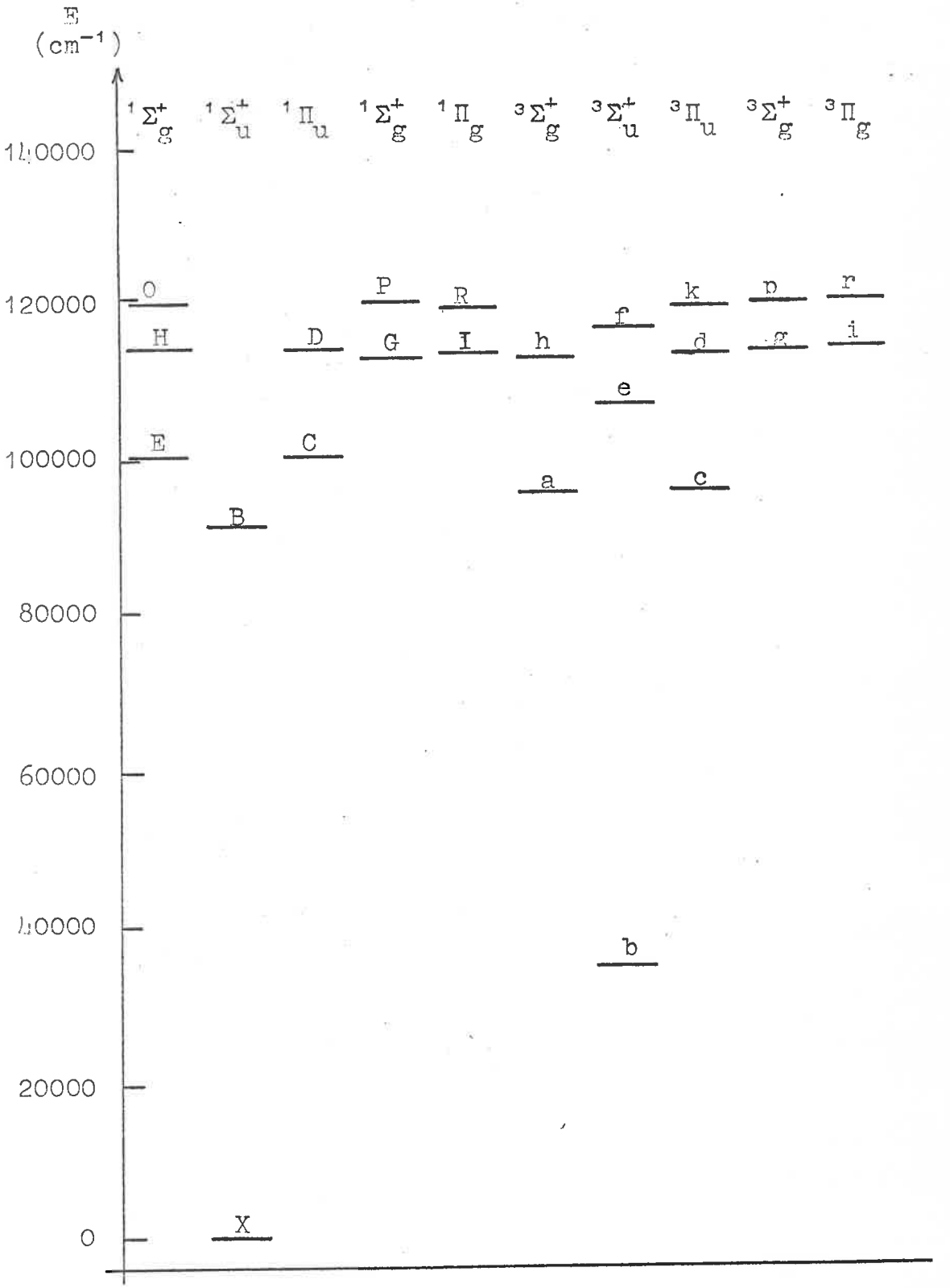

by water vapour in the terrestrial atmosphere. Raich and Good (1964) have made calculations of the transition probabilities of the two ortho-para transitions (J=1->J=0 and J=2->J=1) and arrive at values of one transition in 5×10^{12} years for the line at 84.4μ and one transition every 5×10^{10} years for the line at 42.4μ. These transition probabilities put the expected fluxes below the level of detectability. The transition J=2-> J=0 is an ortho-ortho, quadrupole transition and has a higher transition probability of about one transition in 10^{4} years. It is unlikely however, that this radiation could reach a detectable level anywhere in interstellar space except for regions with extreme concentrations of molecular hydrogen (Gould, 1964).

Secondly, there are vibrational transitions from v=0 to v=1, both in the ground electronic state. In particular the lines v=0, J=0-> v=1, J=2; v=0, J=1-> v=1, J=1 and v=0, J=1-> v=1, J=3 can be expected and all have wavelengths between 2 and 2.5 microns. Some of these lines are not absorbed in the terrestrial atmosphere and Gould and Harwit, 1963, have suggested searching for two particular lines with wavelengths of 2.22μ and 2.12μ. This search could be conducted from

the surface of the earth and is about to be performed with a spectrometer of great light-gathering capacity and good resolution ($10^{-3}\mu$). The other vibrational lines cannot be observed because of the background radiation arising both from local and galactic sources at the wavelengths of these lines.

Finally, there are the electronic transitions, some of which have been studied in this thesis, between v=0 in the ground state and any of the vibrational levels of the excited singlet states. These are allowed electric dipole transitions with a high transition probability which form a series of vibrational-rotational bands lying in the vacuum ultraviolet region of the spectrum with wavelengths shorter than $\approx$1130Å.

Of these three types the vacuum ultraviolet transitions are best suited to a quantitative study of the distribution, abundance and physical condition of molecular hydrogen in interstellar space. Unfortunately the atmosphere of the earth is not transparent to radiation of these wavelengths until heights of 200km are reached. In principle, the observations are simple; a hot star (O or B) is used as a source of continuum radiation and the interstellar absorption lines are registered on this background. The observations must, of course, wait

until they can be performed from rockets or satellites outside the earth's atmosphere. There are two ultraviolet experiments being planned: a medium resolution spectrograph is to be flown on a rocket by Friedman (Varsarsky, 1966) and a high resolution instrument is to be placed in the Orbiting Astronomical Observatory by Rogerson, 1963.

Spitzer et al, 1964, have made theoretical estimates of the equivalent widths of the R(0) lines for the first 13 bands in the Lyman series using various values of n_{H_2}/cm^2, the number of hydrogen molecules/cm^2 in the line of sight. Similar estimates for lines in the first four bands of this series, based on the experimental absorption data reported in this thesis are presented in the following section.

5.3 Calculated Equivalent Widths

The equivalent widths for the lines which may be observed in experiments of the type described above, have been computed using the measured values of the oscillator strength for each line. This has been done as a function of the concentration of hydrogen molecules between the source and the observer and as a function of the temperature of the interstellar gas.

In these calculations interstellar gas temperatures of 75°K, 100°K and 125°K have been assumed since 100°K is perhaps the best estimate of the kinetic temperature of the interstellar gas (Spitzer et al,1964). As has been noted in section 5.1 the number of hydrogen molecules in the line of sight to a hot star (O or B), which is to be used as the source of radiation, is somewhat uncertain. A typical star might be at a distance of 100 to 1000 parsecs and the mean density of atomic hydrogen (n_H) is expected to be approximately 0.7 particles/cm^3 (Spitzer et al, 1964). The abundance of molecular hydrogen is in the range 10^{-4} n_H to $5n_H$ and hence the number of hydrogen molecules in the line of sight probably lies within the range 10^{16}/cm^2 to 10^{21}/cm^2. The calculations presented in this thesis were made for values of n_{H_2}, the number of hydrogen molecules in the line of sight, of 10^{15}, 10^{16}, 10^{17} and 10^{18}/cm^2.

The population of the rotational levels of the ground state of molecular hydrogen was assumed to follow a Boltzmann distribution as before (see section 4.6.3) and the line strengths at interstellar temperatures were then calculated using

$$S_T = S_{298} \frac{\alpha_T}{\alpha_{298}}$$

where S_T is the line strength at temperature T°K

S_{298} " " " " " 298°K

α_{298} is the fraction of molecules in the appropriate ground state at 298°K

α_T is the fraction of molecules in the same ground state at T°K.

The values of the Doppler width (α_D) at temperatures of 75°K, 100°K and 125°K were calculated from the relation 2.4.1. The experimental results of Nesser and Dressler, 1966, provide a value for the Lorentz width α_L. These workers have measured the radiative lifetime for some transitions in the Lyman bands of molecular hydrogen as $\tau = 0.8 \pm 0.2 \times 10^{-9}$ sec. This gives a value for the natural width of the lines (α_L) of 0.00008 Å. Using these values of α_L and α_D the general curve of growth for the mixed Doppler-Lorentz profile was computed using the asymptotic expression (2.5.1). This is shown in figure 5.2. This curve was then used to give the curves of growth for particular lines in the Lyman series as illustrated in figure 5.3 and shown in tabular form in Table VIII. The results are limited to n_{H_2}/cm^2 values of less than $10^{18}/cm^2$ since above these concentrations the equivalent widths of the lines are large and the lines overlap giving rise to

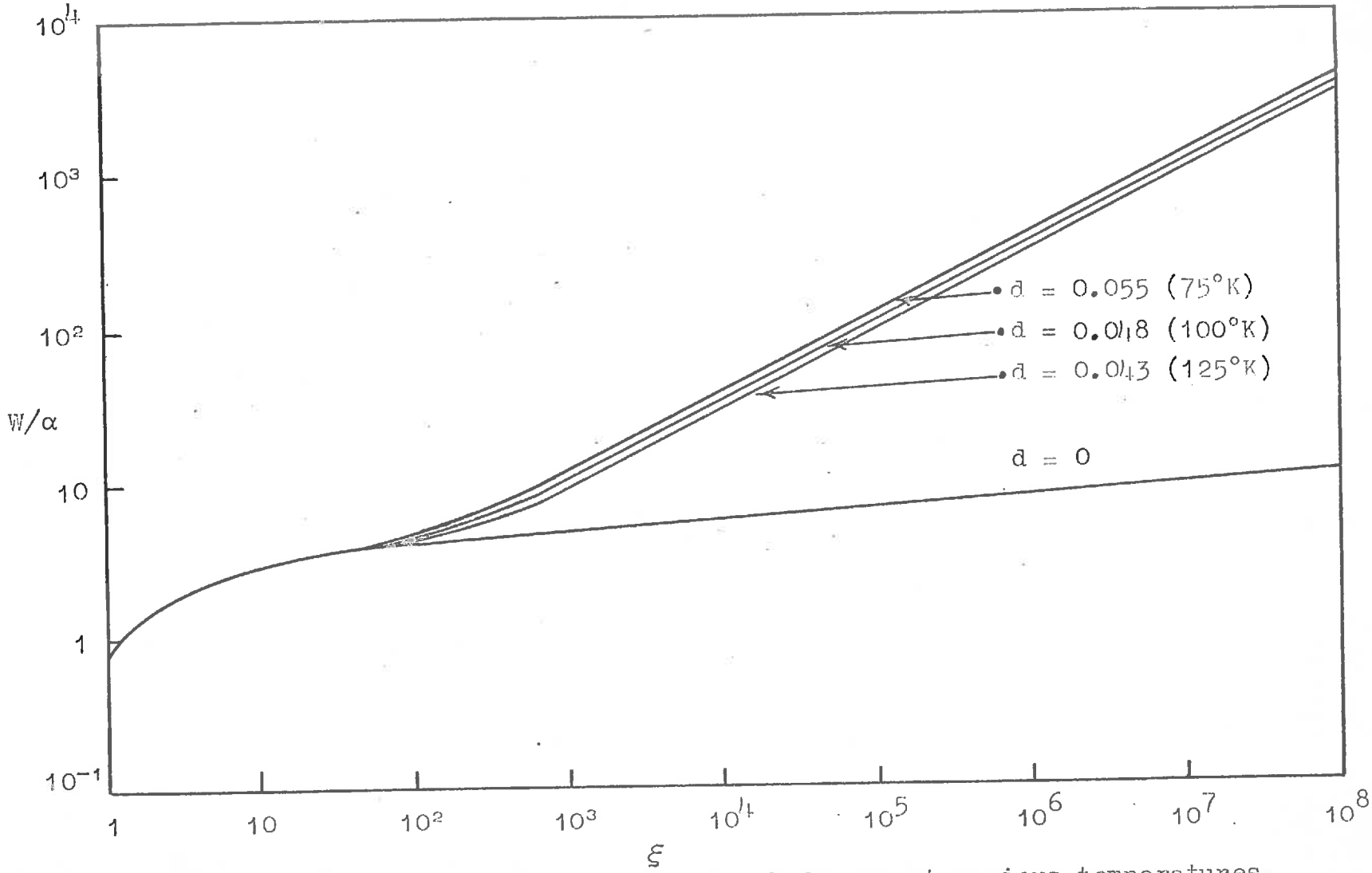

Figure 5.2 Curve of growth for molecular hydrogen at various temperatures.

2-0	R_0	10.2	15.4	35.7	106.9
	R_1	14.7	25.4	73.5	238.0
	R_2	1.5	8.4	13.7	26.7
	R_3	0.03	0.25	2.1	9.2
	R_4	-	-	0.02	0.17
	P_1	5.8	12.1	19.4	53.4
	P_2	0.8	5.4	10.3	19.7
	P_3	0.02	0.2	1.7	8.6
	P_4	-	-	-	0.02
3-0	R_0	10.6	16.4	39.1	116.9
	R_1	14.0	30.1	88.5	273.9
	R_2	1.0	6.4	12.4	21.4
	R_3	-	-	-	-
	R_4	-	-	-	-
	P_1	10.4	16.0	37.7	110.2
	P_2	-	-	-	6.5
	P_3	0.01	0.12	1.1	0.04
	P_4	-	-	-	-

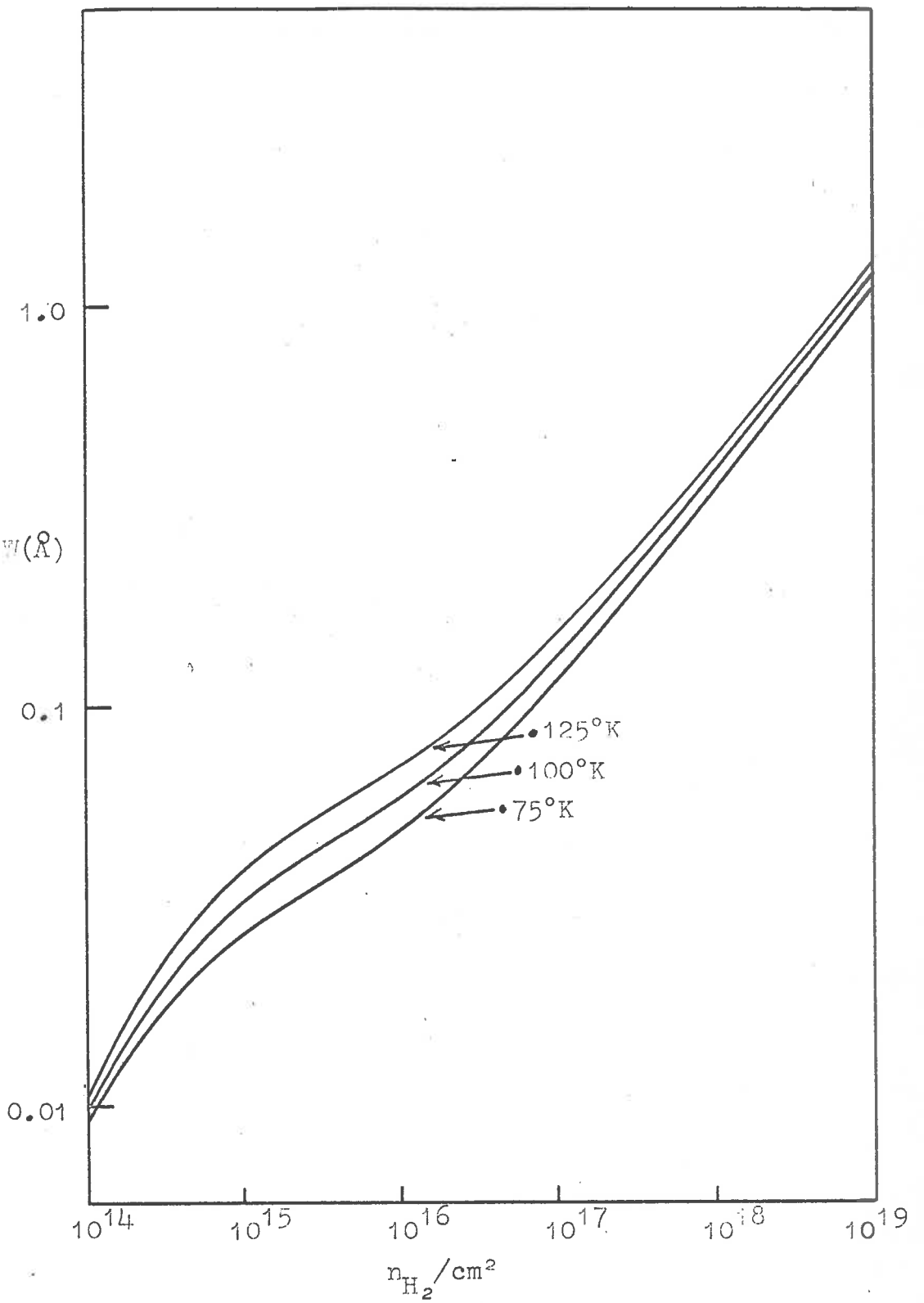

Figure 5.3 Curve of growth for the (1-0) band of molecular hydrogen at estimated interstellar gas temperatures.

Table VIII

Calculated equivalent widths for interstellar absorption lines

(a) Assumed interstellar gas temperature of 75°K

Band	Line	$W \times 10^3$ (Å) calculated for n_{H_2}/cm^2 values of 10^{15}	10^{16}	10^{17}	10^{18}
0-0	R_0	5.6	10.8	19.1	52.2
	R_1	4.2	10.1	16.8	43.5
	R_2	0.08	0.78	5.1	10.5
	R_3	-	-	0.01	0.15
	R_4	-	-	-	-
	P_1	2.06	8.2	12.47	29.6
	P_2	0.03	0.32	2.58	8.8
	P_3	-	-	-	0.04
	P_4	-	-	-	-
1-0	R_0	9.8	16.0	40.6	12.5
	R_1	10.0	16.5	42.1	13.1
	R_2	0.67	4.8	10.1	17.3
	R_3	-	-	0.04	0.41
	R_4	-	-	-	-
	P_1	7.7	12.2	26.7	74.5
	P_2	0.07	0.61	4.6	10.3
	P_3	-	-	0.04	0.44
	P_4	-	-	-	-

2-0	R_0	10.2	15.4	35.7	106.9
	R_1	14.7	25.4	73.5	238.0
	R_2	1.5	8.4	13.7	26.7
	R_3	0.03	0.25	2.1	9.2
	R_4	-	-	0.02	0.17
	P_1	5.8	12.1	19.4	53.4
	P_2	0.8	5.4	10.3	19.7
	P_3	0.02	0.2	1.7	8.6
	P_4	-	-	-	0.02
3-0	R_0	10.6	16.4	39.1	116.9
	R_1	14.0	30.1	88.5	273.9
	R_2	1.0	6.4	12.4	21.4
	R_3	-	-	-	-
	R_4	-	-	-	-
	P_1	10.4	16.0	37.7	110.2
	P_2	-	-	-	6.5
	P_3	0.01	0.12	1.1	0.04
	P_4	-	-	-	-

(b) Assumed interstellar gas temperature of 100°K

Band	Line	$W \times 10^3$(Å) calculated for n_{H_2}/cm^2 values of 10^{15}	10^{16}	10^{17}	10^{18}
0-0	R_0	4.9	11.7	18.7	47.4
	R_1	5.2	12.0	19.4	49.8
	R_2	0.32	2.7	9.9	15.4
	R_3	-	0.05	0.45	3.5
	R_4	-	-	-	0.03
	P_1	2.6	9.8	15.0	33.4
	P_2	0.12	1.1	6.8	12.6
	P_3	-	0.01	0.13	1.2
	P_4	-	-	-	0.01
1-0	R_0	10.2	15.7	36.4	106.9
	R_1	11.7	19.0	48.4	152.0
	R_2	2.2	9.2	14.7	30.7
	R_3	0.01	0.12	1.1	6.5
	R_4	-	-	-	0.06
	P_1	9.2	14.0	30.4	86.8
	P_2	0.27	2.3	9.4	14.7
	P_3	0.01	0.13	1.2	6.9
	P_4	-	-	-	0.01

(c) Assumed interstellar gas temperature of 125°K

Band	Line	$W \times 10^3$ (Å) calculated for n_{H_2}/cm^2 values of 10^{15}	10^{16}	10^{17}	10^{18}
0-0	R_0	4.2	12.2	18.7	43.0
	R_1	5.9	13.2	19.1	43.8
	R_2	0.75	5.1	12.8	19.8
	R_3	-	0.30	2.4	10.3
	R_4	-	-	0.04	0.38
	P_1	2.9	10.9	16.5	3.52
	P_2	0.28	2.3	10.2	15.7
	P_3	-	0.08	0.79	5.6
	P_4	-	-	-	0.1
1-0	R_0	10.4	15.9	32.9	97.2
	R_1	13.1	20.2	50.5	157.1
	R_2	4.4	12.3	19.5	44.5
	R_3	0.07	0.75	5.2	12.9
	R_4	-	-	0.07	0.75
	P_1	10.2	15.7	31.8	93.5
	P_2	0.67	4.9	12.6	19.5
	P_3	0.08	0.8	5.6	13.1
	P_4	-	-	-	0.13

2-0	R_0	10.3	15.7	32.9	95.4
	R_1	15.0	27.3	76.7	24.9
	R_2	3.4	11.4	17.8	38.2
	R_3	0.16	1.4	8.2	14.5
	R_4	-	-	0.23	2.1
	P_1	6.4	13.5	21.7	56.9
	P_2	1.7	9.0	15.0	27.7
	P_3	0.13	1.2	7.3	14.0
	P_4	-	-	-	0.31
3-0	R_0	11.0	16.8	35.9	106.6
	R_1	15.7	31.4	90.5	295.5
	R_2	2.2	9.9	15.7	30.7
	R_3	-	-	-	-
	R_4	-	-	-	0.33
	P_1	11.6	17.6	39.3	119.7
	P_2	-	-	-	-
	P_3	0.07	0.75	5.2	12.9
	P_4	-	-	0.05	0.52

errors in the calculations.

5.4 Conclusions

Morton, 1965, has made theoretical calculations of the spectrum of a B2 star and from this work it can be seen that the lines in the (1-0) band of molecular hydrogen fall in a relatively unobscured region of the spectrum. (See figure 5.4). Most of the other lines lie in regions where atomic lines reduce the flux emerging from the B star considerably. The best wavelength region to search for interstellar absorption by molecular hydrogen using a B star as the source of radiation, will then, be in the range 1090-1105Å.

The calculations of equivalent width presented in section 5.3 show that in order to avoid too much overlapping of individual lines and yet still observe an attenuation due to absorption by molecular hydrogen, the instrument used for the initial search could have a resolution up to about 1.5Å. A resolution of this order would not be sufficient to resolve individual lines in the bands and yet it is fine enough to resolve the R_0R_1 and P_1,R_2 combinations separately. If for example the number of hydrogen molecules in the line of sight is $10^{18}/cm^2$ and the interstellar temperature is 100°K then looking at

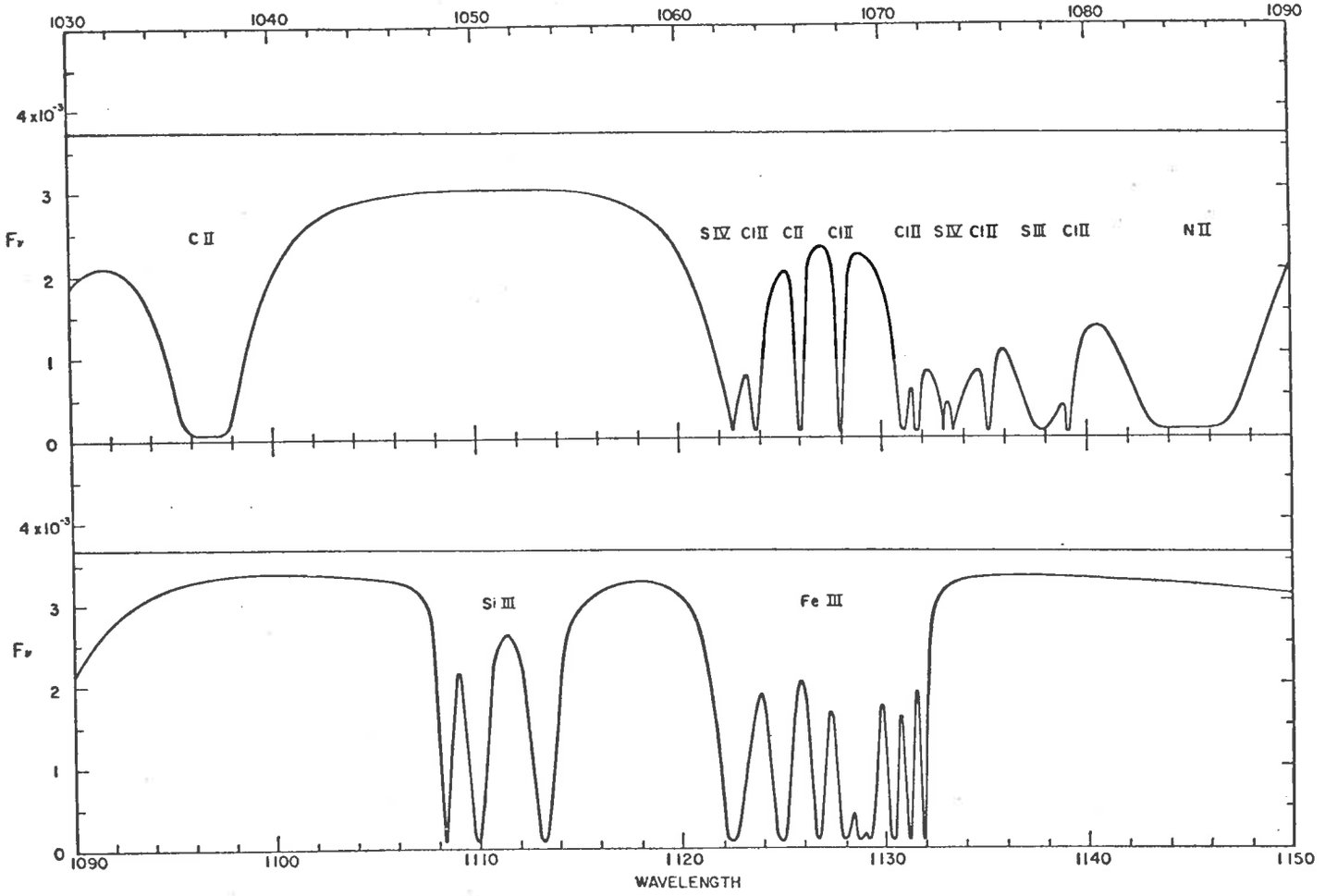

Figure 5.4 Theoretical emission spectrum of a B2 star (after Morton, 1965)

the R_0, R_1 combination of the (1-0) band would give an equivalent width of 0.26Å which would mean an average absorption which is quite detectable. Similarly the P_1, R_2 combination would be separately resolved and give an equivalent width of 0.12Å, again within the limits of detection with an instrument resolution of ≈1.5Å. Measuring the equivalent widths of these two combinations should each give a good estimate of the amount of molecular hydrogen present in interstellar space.

If a high resolution instrument can be flown successfully, this will allow a measure of the equivalent width for each individual line. These measurements of equivalent width can be used to estimate the temperature of the interstellar gas. Let us suppose that the number of hydrogen molecules in the line of sight is quite high (say $10^{21}/cm^2$). A calculation of the equivalent width of the P_3, R_4 combination of the (1-0) band has been made for these concentrations in this work, since these are two relatively weak lines with equivalent widths which do not overlap even at these high concentrations. The calculation of the equivalent width of the total (1-0) band which has been made at these concentrations is in error but not by a significant amount. The parameter

$\frac{W_{P_3} + W_{R_4}}{W_{(1-0)}}$ which represents the equivalent width of the P_3 and R_4 lines divided by the equivalent width of the complete (1-0) band has been calculated for a value of n_{H_2}/cm^2 of 10^{21} and interstellar gas temperatures of 75°K, 100°K and 125°K. The variation in temperature alters the ground state populations according to a Boltzmann distribution (see section 4.6.3) and the results of the calculation are shown in table IX.

Table IX

Variation of equivalent width with interstellar temperature

T°K	75	100	125
$\frac{W_{P_3}+W_{R_4}}{W_{(1-0)}}$	0.25%	0.56%	1.26%

It can be seen from the table that the ratio varies by a factor of ≈5 over the chosen temperature range due to the changing population distribution in the ground state. This means that if this ratio can be measured with a high resolution spectrometer ($\lesssim$0.1Å) then it will be possible to estimate the interstellar gas temperature.

Appendix A

Differential Pumping Systems

A set of subsidiary pumping equipment was installed with the monochromator so that a high pressure discharge lamp could be fitted to the entrance slit of the instrument and a pressure of about 10^{-4} torr maintained in the grating chamber without using a window to isolate the lamp. This feature was also available at the exit slit of the monochromator to allow isolation of the gas-filled absorption cell in the same way - thus the monochromator could be operated in a completely windowless mode and the system was designed to allow a differential pressure of up to 600 torr over either the entrance or exit slits of the instrument.

The differential pumping assemblies* each consist of two chambers isolated from each other and the monochromator by slits kept as small as possible. The optical slits of the monochromator are incorporated in the assemblies and the other slits are restricted to a size just sufficient to allow all the light from the lamp to enter or leave the instrument.

---

* McPherson Instrument Corporation

If a sufficiently high pumping speed is maintained in each of these two chambers and in the monochromator the required differential pressure can be maintained. The required pumping speeds were calculated and suitable pumping equipment obtained.**

Consider the entrance slit differential pumping assembly as an example; gas flows from the lamp where it is at a pressure of 600 torr, through the optical slits of the monochromator into the first differential pumping chamber. It was calculated that with this aperture (typically 4mm by 50 microns) a Rootes mechanical pump could maintain the first differential pumping chamber at about 0.3 torr. The aperture between the first and second differential pumping chambers is about $\frac{1}{2}$mm by 6mm and the pumping speed necessary to maintain the second chamber at about 10 microns is provided by an oil booster pump (21,000 l/min) and a suitable backing pump.

Although the aperture between the second differential pumping chamber and the monochromator is larger again (1mm by 10mm) the 6" diffusion pump and backing pump fitted to the monochromator itself have

---

** Rud Browne and Co. Ltd.

adequate speed to keep the pressure in the grating chamber below 10^{-3} torr under the conditions stated above. A schematic diagram of the system is shown in figure A.1 with the equipment type numbers listed.

The monochromator itself was installed on the edge of a pit of dimensions 12' × 8' × 4' deep which was covered with steel decking. The differential pumping equipment was installed in the pit in such a way that the pumping lines from each set of pumps to the monochromator were kept as short as possible. This design allowed maximum working area around the monochromator and yet relatively easy access to the differential pumping equipment. Butterfly valves were fitted between each set of pumps and the monochromator to allow isolation of any set of pumps from the instrument. A pressure sensing device was installed in the monochromator to close the main chamber valve* if the pressure rose above 0.1 torr. This device uses the current through a Pirani gauge to operate a moving coil relay to trip the release for the valve.

---

* This is a sliding gate-valve which is operated pneumatically.

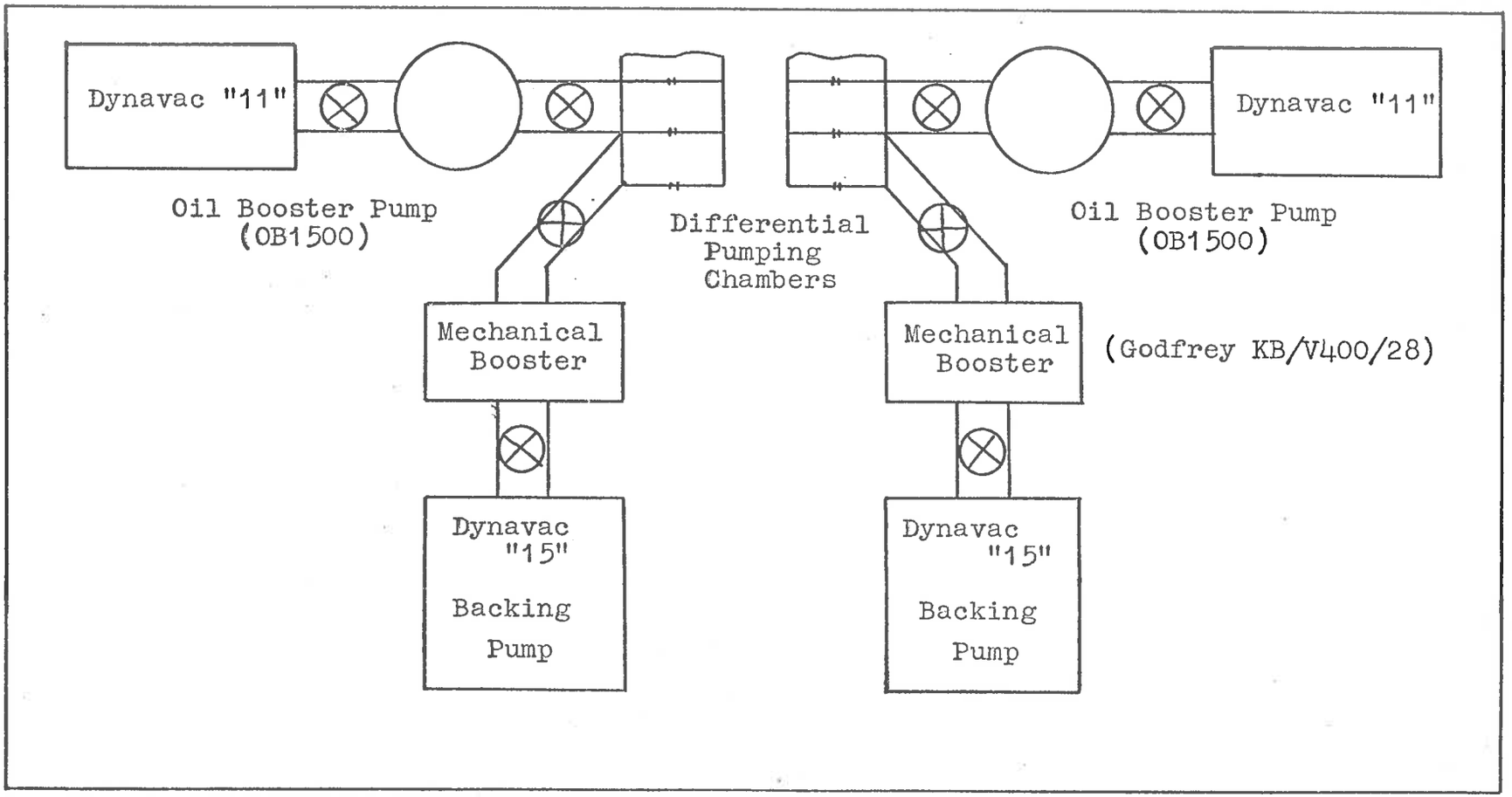

Figure A.1 Schematic diagram of the differential pumping equipment.

Appendix B

Subsidiary circuits for digital data handling

The "clock" used to advance the channel address in the multichannel analyser and to operate the switch S (see figure 4.3) consists of a full or half wave rectifier circuit to provide 100c/s or 50c/s respectively followed by a Schmitt trigger, a monostable multivibrator and a series of binary dividing stages. The 6000c/min or 3000c/min from the monostable is initially divided by 3 and then divided in turn by either 2, 10, 20, 100, 200, 1000 or 2000 to give the required pulse repetition rate. These dividing facilities are controlled by series gates on the outputs of the divide by 2 units and divide by 5 units. The circuits are shown in figures B.1 (a), (b), (c), (d) and (e). These "clock" pulses are fed directly to the address advance input of the multichannel analyser and via a bistable to two reed relays with gold plated contacts which constitute the switch S. The switching circuit is shown in figure B.2.

A set of relays is used to provide start, stop and reset facilities for the system. The "start" control initiates the operation of the address scalar and removes

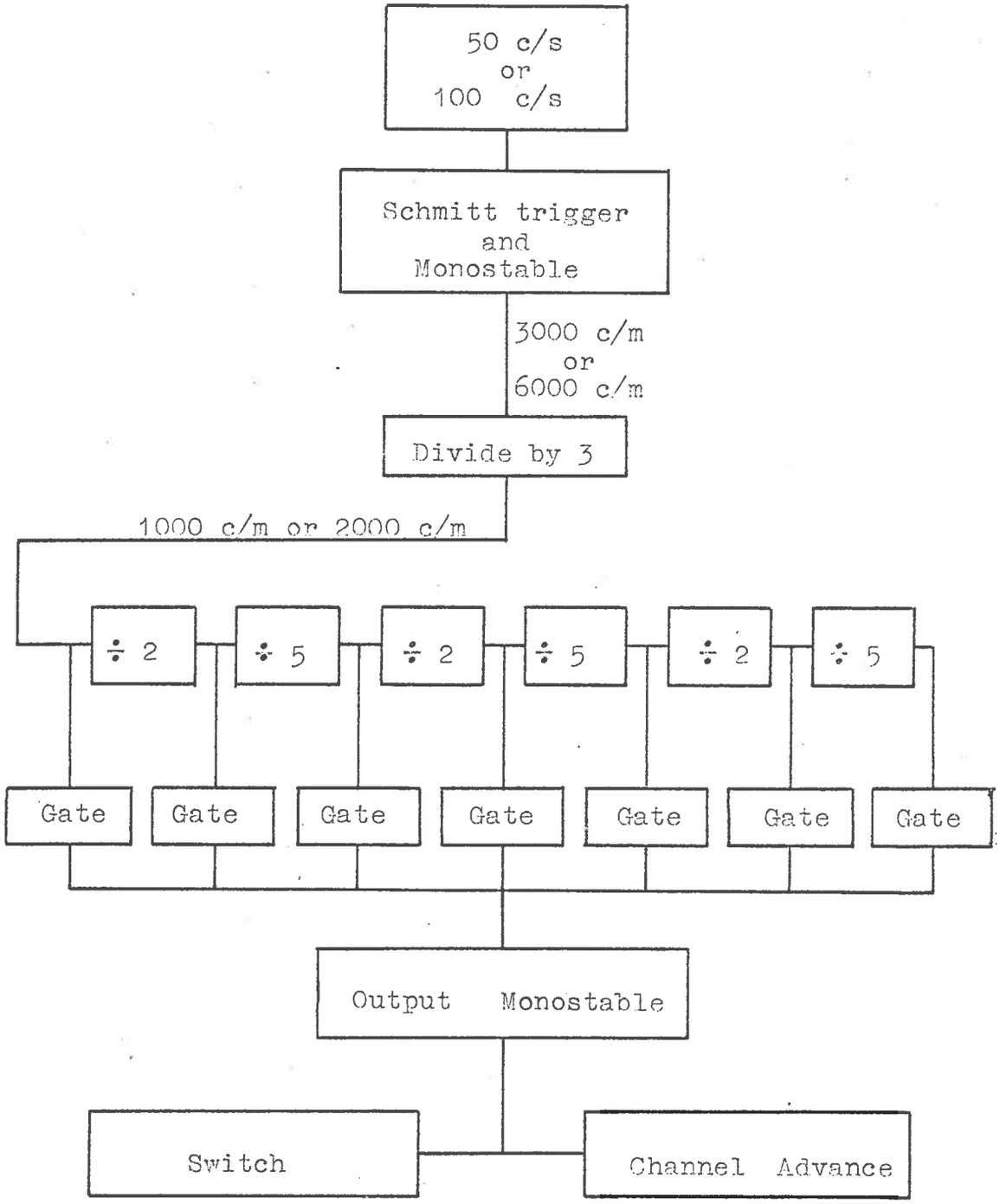

Figure B.1(a) Schematic diagram of the subsidiary circuits.

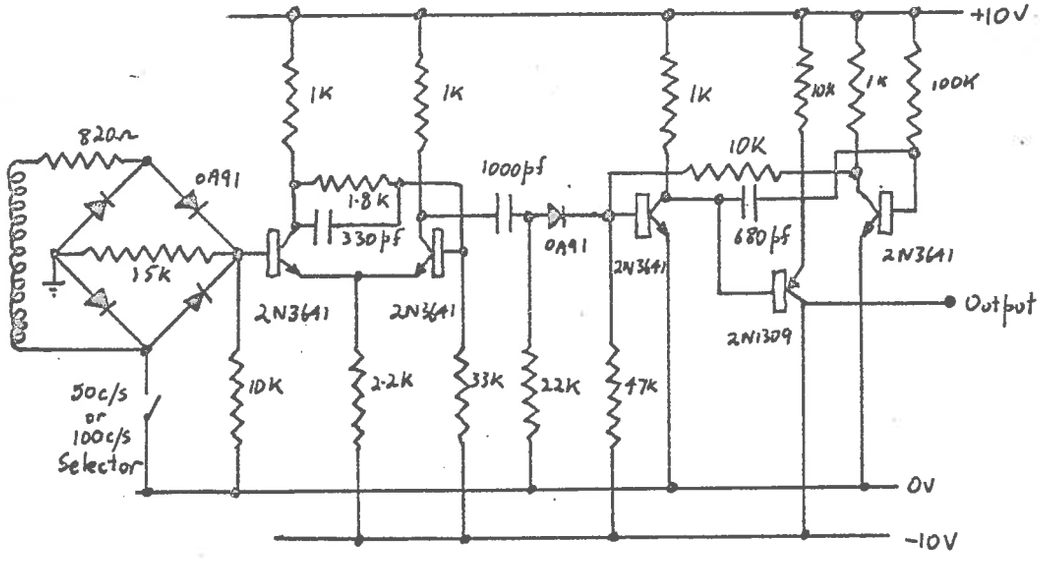

Figure B.1(b) The input circuit for the clock including the Schmitt trigger and monostable circuits.

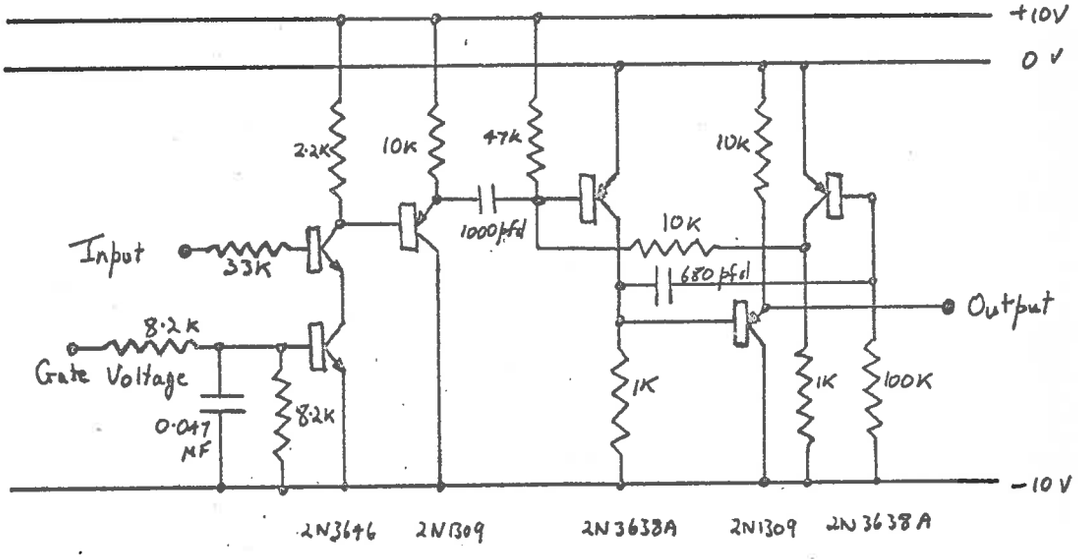

Figure B.1(c) The series gate and output monostable circuit.

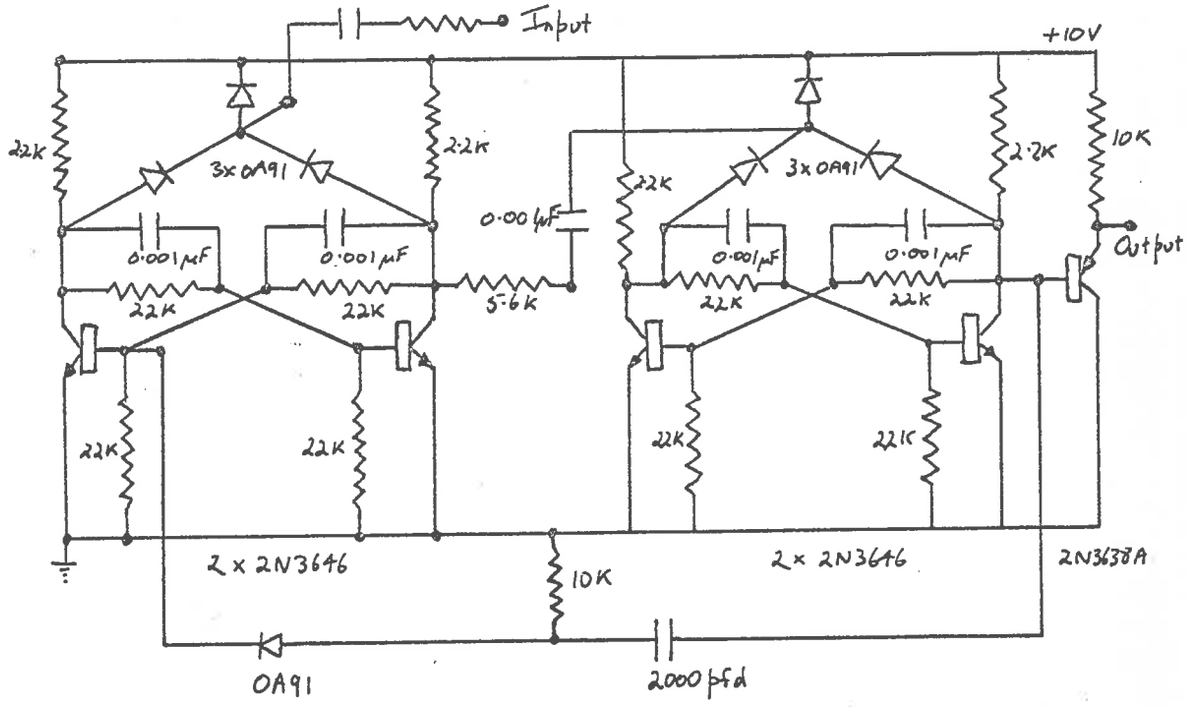

Figure B.1(d) The circuit for the divide by 3 "binary".

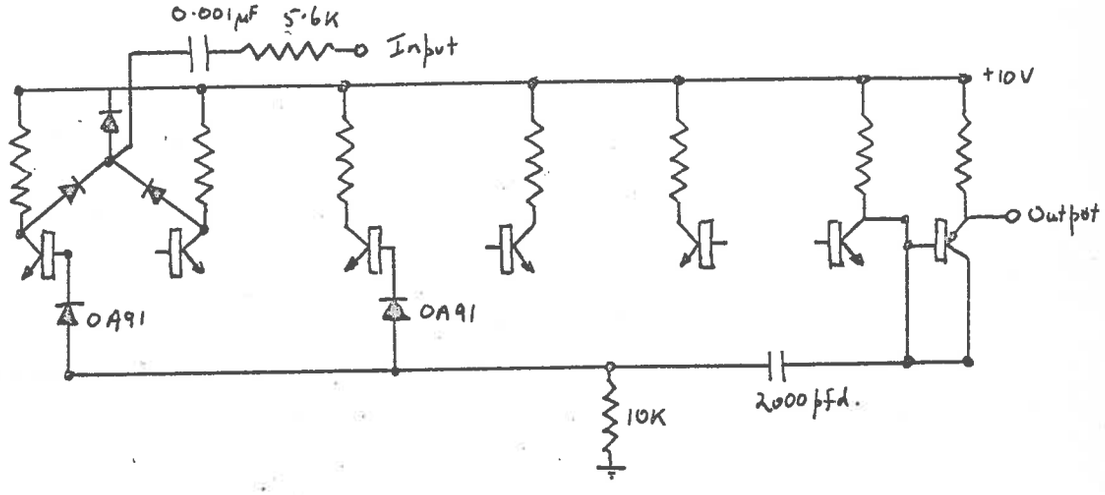

Figure B.1(e) The divide by 5 configuration.

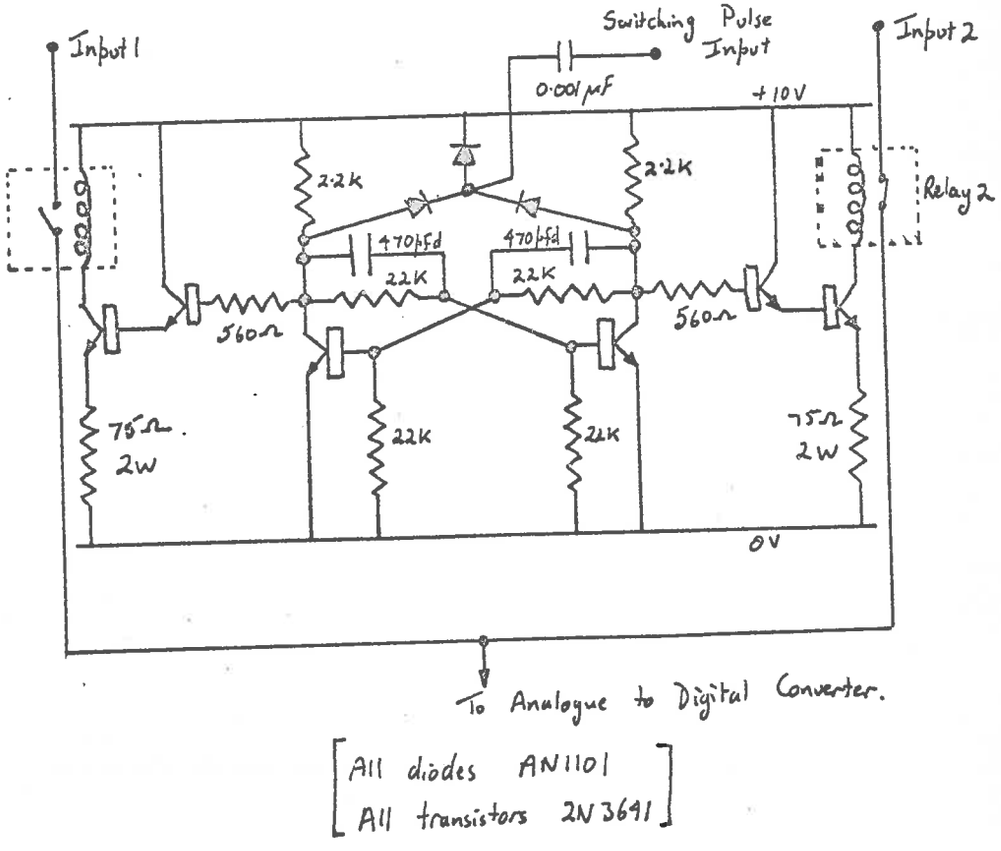

Figure B.2 The switching circuit for the inputs to the analogue to digital converter.

an inhibit voltage from the input to the multichannel analyser; the stop control prevents the scalar operating and restores the inhibit voltage. The reset control is used to clear all the binaries and set the switch S to a predetermined position.

Appendix C

Transfer of information from the multichannel analyser to punched cards

Information from the multichannel analyser can be read out in parallel; that is 8 binary coded decimal digits are presented at the output simultaneously and these represent the channel number, 3 digits, and the count in that channel, 5 digits. In the present system these 8 digits are decoded simultaneously with 8 relay decoders (see figure C.1) to provide a unique closure (one of ten) for each binary coded number. These 8 unique configurations are then scanned with a uniselector to operate one of the interposer magnets on the IBM card punch for each of the 8 numbers (see figure C.2). Thus each channel is punched out and the sequence is arranged so that 8 channels are punched onto each card. The contents of the multichannel analyser (400 Channels comprising numbers up to 99,999) can be punched out in approximately 5 minutes.

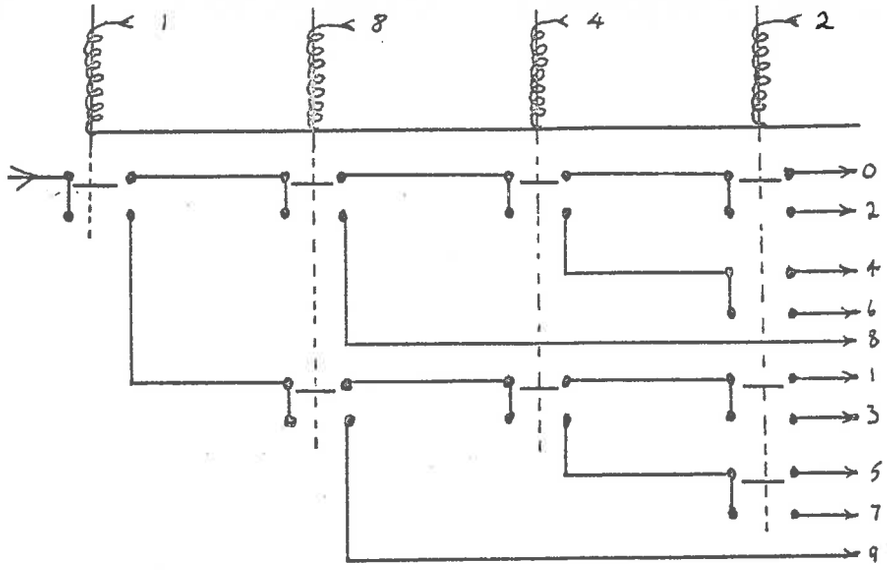

Figure C.1 Circuit for one of the relay decoders (schematic).

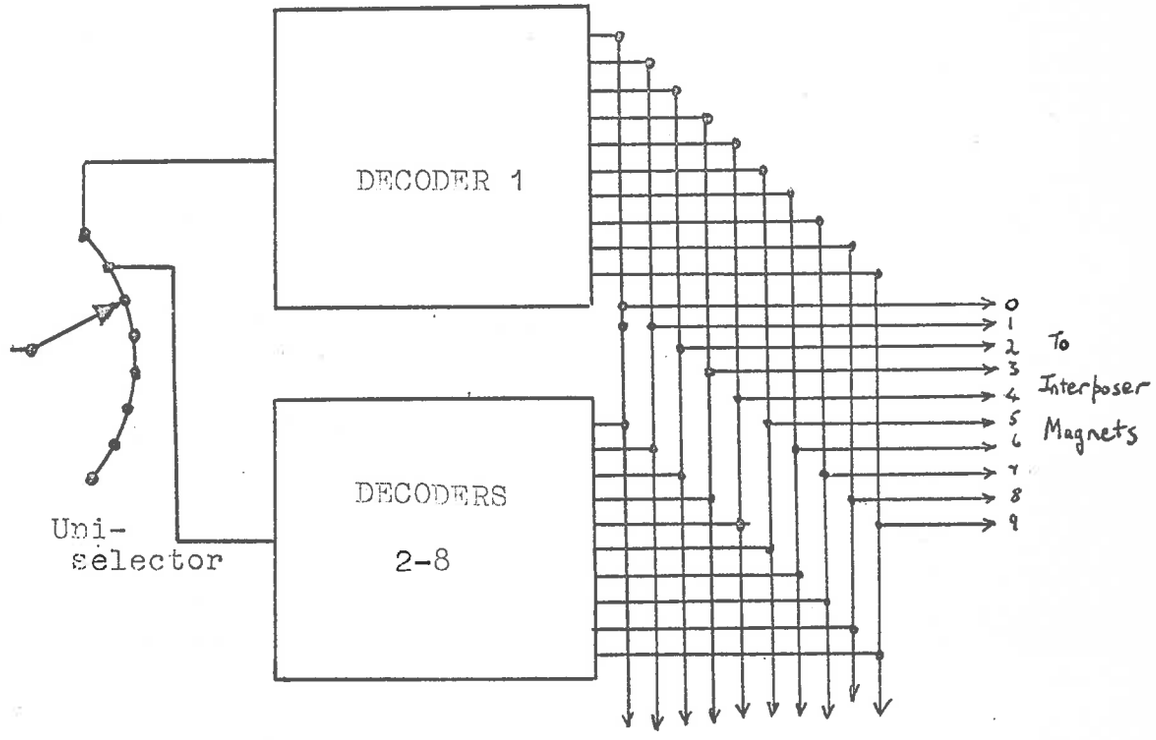

Figure C.2 The scanning circuit (schematic).

Appendix D

Publications

The following papers have been written on the work described in this thesis;

1. "Photo-absorption cross sections of molecular oxygen between 1250Å and 2350Å".
   A.J. Blake, J.H. Carver and G.N. Haddad.
   J. Quant. Spectrosc. Radiat. Transfer 6, 451 (1966).

2. "A digital data handling system for recording vacuum ultraviolet absorption spectra"
   K.H. Lokan, G.N. Haddad, A.J.D. Farmer, D.G. McCoy and B.R. Lewis.
   In Preparation.

BIBLIOGRAPHY

ABOUD, A.A., CURTIS, J.P., MERCURE, R., REINE, W.A.,
(1955) Astrophys. J. 130, 381.

ALLISON, R., BURNS, J., TUZZOLINO, A.J.,
(1964) J. Opt. Soc. Am. 54, 747.

BETHE, H.A. and SALPETER, E.E.,
(1957) Handbuch der Physik 35, 88. Ed. S. Flugge.

BETHKE, G.W.
(1959) J. Chem. Phys. 31, 669.

BEUTLER, H.,
(1934) Z. Phys. Chem. 27, 287.

BEUTLER, H.,
(1935) Z. Phys. Chem. 29, 315.

BEUTLER, H., DEUBNER, A., JÜNGER, H.O.,
(1936) Z. Phys. 98, 181.

BORN, M. and OPPENHEIMER, J.R.,
(1927) Ann. Phys. 34, 457.

BRIX, P. and HERZBERG, G.,
(1954) Can. J. Phys. 32, 110.

BROIDA, H.P. and GAYDON, A.G.,
(1954) Can. J. Phys. 32, 110.

BUNCH, S.M., COOK, G.R., OGAWA, M., EHLER, A.W.
(1958) J. Chem. Phys. 28, 740.

BYRAM, E.T., CHUBB, T.A., FRIEDMAN, H.,
(1955) Phys. Rev. 98, 1594.

BYRAM, E.T., CHUBB, T.A., FRIEDMAN, H. and KUPPERIAN, J.E.,
(1956) Astrophys. J. 124, 480.

CARVER, J.H. and MITCHELL, P.,
(1964) J. Scient. Instrum. 41, 555.

CARVER, J.H., MITCHELL, P., MURRAY, E.L., HUNT, B.G.,
(1964) J. Geophys. Res. 69, 3755.

CARVER, J.H., MITCHELL, P., MURRAY, E.L, ROFE, B.,
(1966) Space Research 6. To be published.

CHUBB, T.A., BYRAM, E.T., FRIEDMAN, H., KUPPERIAN, J.E.,
(1958) Annls. Geophys. 14, 109.

COOK, G.R., CHING, B.K.,
(1965) Report No. TDR-469 (9260-01)-4. (Aerospace Corporation).

COOK, G.R., METZGER, P.H.,
(1964) J. Opt. Soc. Am. 54, 968.

CURRY, J., HERZBERG, G.,
(1934) Ann. d. Phys. 19, 800.

CURTIS, J.P.,
(1954) Phys. Rev. 94, 908.

DALGARNO, A., LYNN, N.,
(1957) Proc. Phys. Soc. (Lond.) A70, 802.

DIEKE, G.H.,
(1958) J. Mol. Spectry. 2, 494.

DIEKE, G.H., HOPFIELD, J.J.,
(1920) Z. Phys. 40, 299.

DIEKE, G.H., HOPFIELD, J.J.,
(1927) Phys. Rev. 30, 400.

DITCHBURN, R.W.,
(1962) J. Quant. Spectrosc. Radiat. Transfer, 2, 361.

DITCHBURN, R.W., BRADLEY, J.E.S., CANNON, C.G., MUNDAY,G.,
(1954) Rocket Exploration of Upper Atmosphere.
(London Pergamon Press). Ed. R.L.F. Boyd and M.J. Seaton.

DITCHBURN, R.W. and HEDDLE, D.W.O.,
(1953) Proc. Roy. Soc. (London) A220, 61.

DITCHBURN, R.W., HEDDLE, D.W.O.,
(1954) Proc. Roy. Soc. (London)A226, 509.

DITCHBURN, R.W. and YOUNG, P.A.,
(1962) J. Atmos. Terr. Phys. 24, 127.

DORSCHNER, J., von, GÜNTLER, J., SCHMIDT, K.H.,
(1965) Astron. Nachr. 288, 149.

ELSASSER, W.M.,
(1942) Harvard Meteorological Studies No.6 (Harvard University Press).

FRIEDMAN, H.,
(1960) Physics of the Upper Atmosphere, Ed. J.A. Ratcliffe, (New York: Academic Press).

FRIEDMAN, H., LICHTMAN, S.W., BYRAM, E.T.,
(1951) Phys. Rev. 83, 1025.

FRIEDMAN, H., CHUBB, T.A., SIOMKAJLO, J.M.,
(1964) Sounding Rocket Research Techniques,
Instruction Manual no.9 (IQSY Secretariat, London).

GILMORE, F.R.,
(1965) J. Quant. Spectrosc Radiat. Transfer. 5, 369.

GOODY, R.M.,
(1952) Quant. J.R. Met. Soc. 78, 165.

GOODY, R.M., (1964)
Atmospheric Radiation I Theoretical Basis.
(Oxford; Clarendon press).

GOULD, R.J.,
(1964) Astrophys. J. 140, 638.

GOULD, R.J., GOLD, T., SALPETER, E.E.,
(1963) Astrophys. J., 138, 408.

GOULD, R.J., HARWIT, M.,
(1963) Astrophys. J. 137, 694.

GOULD, R.J., SALPETER, E.E.,
(1963) Astrophys. J., 138, 393.

HALL, L.A., DAMON, K.A., HINTEREGGER, H.E.,
(1963(a) Space Research 3, 745.

HERZBERG, G.,
(1932) Naturwissenschaften 20, 577.

HERZBERG, G.,
(1950) Molecular spectra and molecular structure
(I Spectra of diatomic molecules)
(Princeton: Van Nostrand)

HERZBERG, G.,
(1952) Can. J. Phys. 30, 185.

HERZBERG, G., HOWE, L.L.
(1959). Can. J. Phys. 37, 636.

HERZBERG, G. and MONFILS, A.,
(1960) J. Mol. Spectry 5, 482.

HESSER, J.E. and DRESSLER, K.,
(1966) J. Chem. Phys. 45, 3149.

HINTEREGGER, H.E.,
(1953) J. Opt. Soc. Am. 43, 328.

HINTEREGGER, H.E.,
(1962) J. Atmos. Sci., 19, 351.

HOPFIELD, J.J.,
(1930) Nature 125, 927.

HORI, T.,
(1927) Z. Phys. 44, 838.

HUFFMAN, R.E., LARRABEE, J.C., TANAKA, Y.,
(1965) Appl. Opt. 4, 1581.

HULST v.d., H.C.,
(1948) Harvard Obs. Monograph 7, 73.

HYMAN, H.H.,
(1930) Phys. Rev. 36, 187.

JEPPESEN, C.R.,
(1933) Phys. Rev. 44, 165.

JEPPESEN, C.R.,
(1938) Phys. Rev. 54, 68.

JOHNSON, F.S., PURCELL, J.D., TOUSEY, R.,
(1951) J. Geophys. Res. 56, 583.

JOHNSON, F.S., PURCELL, J.D., TOUSEY, R., WATANABE, K.,
(1952) J. Geophys. Res., 57, 157

JURSA, A.S., TANAKA, Y., LE BLANC, F.,
(1959) Planet Space Sci. 1, 161.

JURSA, A.S., NAKAMURA,M., TANAKA,Y.,
(1963) J. Geophys. Res. 68, 6145.

JURSA, A.S., NAKAMURA,M., TANAKA,Y.,
(1965) J. Geophys. Res. 70, 2699.

KAPLAN, L.D., EGGERS, D.F.,
(1956) J. Chem. Phys. 25, 876.

KNAPP, H.F.P., MEYDENBERG, v.d., C.J.N., BETNAKKER, J.J.M.,
and HULST, v.d. H.C.,
(1965) I.A.U. Colloq. Interstellar Grains
(New York:)

KNAPP, R.A. and SMITH,A.M.,
(1964) Appl. Opt. 3, 637.

KNAUSS, H.P., BALLARD, S.S.,
(1935) Phys. Rev. 48, 796.

KOLOS, W., and WOLNIEWICZ, L.,
(1965) J. Chem. Phys. 43, 2429.

KREUSLER, H.,
(1901) Ann. Phys. 6, 418.

KUIPERIAN, J.E., BYRAM, E.T., FRIEDMAN, H.,
(1959) J. Atmos. Terres. Phys. 16, 174.

LADENBERG, R., REICHE, F.,
(1913) Ann. Phys. 42, 181.

LADENBURG, R., and von VOORHIS, C.C.,
(1933) Phys. Rev. 43, 315.

LAMBRECHT, H., and SCHMIDT, K.H.,
(1964) Astron. Nachr. 288, 11.

LEE, P.,
(1955) J. Opt. Soc. Am. 45, 703.

LEE, P., WEISSLER, G.L.,
(1952) Astrophys. J., 115, 570.

LEIFSON, S.W.,
(1926) Astrophys. J. 63, 73.

LYMAN, T.,
(1928) The Spectroscopy of the extreme ultraviolet.
(Longmans, Green and Co.).

MADDEN, R.P., and CODLING, K.,
(1965) J. Appl. Phys., 36, 380.

METZGER, P.H., COOK, G.R.,
(1964) J. Quant. Spectrosc. Radiat. Transfer. 4, 107.

METZGER, P.H., COOK, G.R.,
(1965) J. Opt. Soc. Am. 55, 516.

MITCHELL, P.,
(1966) Thesis. University of Adelaide.

MONFILS, A.,
(1961)(a) Acad. Roy. Belg., Bull. Classe Sci.47, 585.

MONFILS, A.,

(1961)(b) Acad. Roy. Belg., Bull Classe Sci. 47, 816.

MONFILS, A.,

(1965) J. Mol. Spectry. 15, 265.

MORSE, P.M.,

(1929) Phys. Rev. 34, 57.

MORTON, D.C.

(1965) Astrophys. J. 141, 73.

MULLIKEN, R.S. and RIEKE, C.A.,

(1941) Rep. Progress in Physics 8, 231.

MCCREA, W.H. and MCNALLY, D.,

(1960) Mon. Not. R. Astron. Soc. 121, 238.

NAMIOKA, T.,

(1964)(a)

J. Chem. Phys. 40, 3154.

NAMIOKA, T.,

(1964)(b) J. Chem. Phys. 41, 2141.

NAMIOKA, T.,

(1965) J. Chem. Phys. 43, 1636.

NICHOLLS, R.W.,

(1965) Astrophys. J. 141, 819.

OORT, J.H.,

(1965) Trans. I.A.U. Vol. XIIA, 789.

OSTERBROCK, D.E.,

(1962) Astrophys. J. 136, 359.

PACKER, D.M., LOCK, C.,

(1951) J. Opt. Soc. Am. 41, 699.

PATCH, R.W.,

(1964) J. Chem. Phys. 41, 1881.

PEEK, J.M., LASSETTRE, E.N.,

(1963) J. Chem. Phys. 38, 2392.

PLASS, G.N., FIVEL, D.I.,

(1953) Astrophys. J. 117, 225.

PRESTON, G.,

(1961) Astrophys. J. 107, 141.

PRESTON, G.,

(1961) Astrophys. J. 134, 632.

PRESTON, W.M.,

(1940) Phys. Rev. 57, 887.

PRICE, W.C., COLLINS, G.,

(1935) Phys. Rev. 48, 714.

RAICH, J.C., GOOD, R.H.,

(1964) Astrophys. J. 139, 1004.

REICHE, F.,

(1956) J. Opt. Soc. Am. 46, 590.

ROGERSON, J.B.,

(1963) Space Sci. Rev. 2, 621.

SAMSON, J.A.R.,

(1964) J. Opt. Soc. Am. 54, 6.

SCHAAFSMA, A., DIEKE, G.H.,

(1929) Z. Phys. 55, 164.

SCHIFF, L.I.,

(1955) Quantum Mechanics (McGraw-Hill Book Co. Inc.).

SCHNAIDT, F.,

(1939) Beitr. Geophys. 54, 203.

SCHULTZ, E.D., HOLLAND, A.C., MARMO, F.F.,

(1962) CGA Tech. Rep. 62-15-N (NASA contract NASW-395).

SCHUMANN, V.,

(1901) Ann. Phys. 4, 642.

SMITH, L.G., WEEKS, L.,

(1965) G.C.A. Tech. Rep. 65-10-N.

SMITH, L.G., ACCARDO, C.A., WEEKS, L.H., MCKINNON, P.J.,

(1965) J. Atmos. Terres. Phys. 27, 803.

SPITZER, L., Jr.

(1949) Astrophys. J. 109, 337.

SPITZER, L.,Jr., DRESSLER, K. and UPSON, W.L. III.,

(1964) Publ. Astron. Soc. Pacific 76, 387.

STEWART, K.H.,

(1966) Private communication.

TANAKA, Y.,

(1944) Sci. Pap. Inst. Phys. Chem. Res. (Tokyo). 42, 49.

TANAKA, Y.,

(1952) J. Chem. Phys. 20, 1728.

TANAKA, Y., HUFFMAN, R.E. and LARRABEE, J.C.,

(1962) J. Quant. Spectrosc. Radiat. Transfer.

TANAKA, Y., JURSA, A.S., LE BLANC, F.J.,

(1958) J. Opt. Soc. Am. 48, 304.

THOMPSON, B.A., HARTECK, P., REEVES, R.R.,

(1963) J. Geophys. Res. 68, 6431.

TILFORD, S.G., VANDERSLICE, J.T., WILKINSON, P.G.,

(1965) Astrophys. J. 141, 1226.

TOUSEY, R.,

(1963) Space Science Rev. 2, 3.

UEHLING, E.A.,

(1934) Phys. Rev. 46, 917.

VARSAVSKY, C.M.,

(1966) Space Sci. Rev. 5, 419.

WAINFAN, N., WALKER, W.C., WEISSLER, G.L.,

(1955) Phys. Rev. 99, 542.

WATANABE, K.,
(1958) Adv. Geophys. 5, 157.

WATANABE, K., INN, E.C.Y.,
(1953) J. Opt. Soc. Am. 43, 32.

WATANABE, K., MARMO, F.F.,
(1956) J. Chem. Phys. 25, 965.

WATANABE, K., INN, E.C.Y., ZELIKOFF, M.,
(1953) J. Chem. Phys. 21, 1026.

WEISSLER, G.L.,
(1959) Handbuch der Physik, Vol. 21.
Ed. S. Flugge (Berlin-Springer-Verlag).

WERNER, S.,
(1926) Proc. Roy. Soc. (London) A113, 107.

WILKINSON, P.G., BYRAM, E.T.,
(1965) Appl. Opt. 4, 581.

WILKINSON, P.G., MULLIKEN, R.S.,
(1957) Astrophys. J. 125, 594.

WILLIAMS, S.E.,
(1940) Nature. 145, 68.

WITMER, E.E.,
(1926) Proc. Nat. Acad. Sci. 12, 338.

WOLNIEWICZ, L.,
(1966) J. Chem. Phys. 45, 515.

WOOLLEY, R, v.d.R., STIBBS, D.W.N.,

(1953)"The outer layers of a star" (Oxford: Univ. press).

WRUBEL, M.H.,

(1949) Astrophys. J. 109, 66,.

ZWICKY, F.,

(1959) Publ. Astron. Soc. Pacific 71, 468.